High Performance Fibre Reinforced Fluoropolymers

By Kingsley Kin Chee Ho

A thesis submitted in partial fulfilment for the requirements of the Doctor of Philosophy of the University of London and the Diploma of Imperial College London

Department of Chemical Engineering
Imperial College London
South Kensington
London, SW7 2AZ.
UK

Abstract

The aim of the research was to design and fabricate high performance fibre reinforced fluoropolymers that could deliver exceptional mechanical and chemical performance in the most severe environments.

The offshore oil and gas industry continues to develop deep-sea oilfields. The extreme conditions encountered in such operations require superior material performance and durability. Conventionally used engineering materials have exhausted their potential because of their poor chemical resistance and damage tolerance and/or the high costs involved in supporting their own weight. Polymer composites overcome such limitations, thus enabling new design strategies for cost effective, weight and energy saving materials. Spoolable reinforced thermoplastic pipes have been developed to transport highly corrosive fluids, including crude oil, brine and sour gases at high service pressures. For these reasons, industrial applications for thermoplastic composite materials are currently expanding rapidly.

This research summarises the development of a continuous process to manufacture unidirectional polyvinylidene fluoride (PVDF) composites. Specific objectives were highlighted to overcome the adhesion problem between PVDF and carbon fibres by designing a stable and durable fibre/matrix interface. These include the following:

- The development of an atmospheric plasma fluorination procedure which enables batch, continuous and inline treatment of carbon fibres,
- Characterise the impact of fluorination of carbon fibres on the surface and bulk properties,
- Investigate the interfacial behaviour of fluorinated carbon fibres and PVDF
- Manufacture continuously atmospheric plasma fluorinated unidirectional carbon fibre reinforced PVDF and examine the interface dominated mechanical properties of the carbon fibre/ PVDF composites.

The results show that atmospheric plasma fluorination of carbon fibres increases the surface hydrophobicity of the fibres, enhanced interfacial shear strength at the fibre/ matrix interface and improved the overall mechanical performance of the unidirectional fibre reinforced PVDF composite laminates.

Declaration

The work described in this thesis was carried out in the Department of Chemical Engineering and Chemical Technology, Imperial College London between October 2004 and April 2008. Except where acknowledged, the material is the original work of the author and includes nothing which is the outcome of work in collaboration, and no part of it, that has been submitted for a degree at any other university.



Acknowledgements

It is a pleasure to thank the many people who have helped make this thesis possible.

First I would like to start by thanking my supervisor Dr Alexander Bismarck for all of his help, suggestions, and support over the past and if it was not for him I would not have made such progress in my research. Also I would like to thank the Engineering and Physical Sciences Research Council (EPSRC) for providing the financial support for the project (GR/S75673/01).

It is an impossible task for me to thank everyone given the many people who have helped to design, implement, apply, criticise and support my work. I am going to try anyway and if your name is not listed, rest assured that my gratitude is not less than for those listed below.

I am indebted to my many student colleagues for providing a stimulating and fun environment in which to learn and to work. Mike Tran and Steven Lamoriniere started the design and building of the composite line facility before I arrived and they both have mentored me throughout my PhD research. Also I would like to thank other members in the PaCE group for their support and in particular: Angelika Menner, Anthony Abbott, Charnwit Tridech, Ivan Zadrazil, Jonny Blaker, Julasak Juntaro, Sherry Qian, Shu San Manley and Uros Vukicevic.

I would like to thank Patricia Carry, Pim Amrit, Richard Wallington, Sarah Payne and others in the Department of Chemical Engineering who had helped me during my PhD research.

Special thanks to my good friend Chris Fu. Thank you for everything: from being my guardian and my mentor since the age of 15, to looking after me throughout my University life.

I wish to thank my family, relatives and Qiujun Li for providing a loving environment for me. Lastly and most importantly I wish to thank my parents, Yeung Yuk Fung and Ho Kam Fat. They raised me, supported me, taught me and loved me. To them I dedicate this thesis.

Contents

Abstract 2

Declaration 3

Acknowledgements 4

Contents 5

List of figures 10

List of tables 17

Publications 19

Presentations at Conferences 20

Awards and Prizes 22

Chapter 1: Aims and Objectives 23

Chapter 2: Literature Review 27

2.1 Background in thermoplastic tubular pipes in the Oil and Gas industry 27

2.1.1 Pipe design 29

2.1.2 Coating system requirement for subsea pipelines 33

2.1.3 The outlook 34

2.2 Carbon fibre manufacture 35

2.2.1 Precursors for carbon fibre manufacturing 36

2.2.2 Thermal stabilisation of PAN fibres 39

2.2.3 Carbonisation of PAN fibres 41

2.2.4 Surface treatment of PAN carbon fibres 44

2.2.5 Sizing of carbon fibres 47

2.3 Fluoropolymers as matrices for carbon fibre reinforced composites 48

2.3.1 Background 48

2.3.2 Chemistry and market of fluoropolymers 49

2.3.3 PVDF in the chemical process industry 52

2.4 Background in wetting behaviour of solids 55

2.5 Composites 58

2.5.1 Background 58

2.5.2 Properties and applications of carbon fibre reinforced composites 58

2.5.3 The role of surface modification on carbon fibre and the adhesion to PVDF 61

2.5.4 Testing of unidirectional carbon fibre reinforced PVDF composites 64

2.5.4.1 Flexural properties 65

2.5.4.2 Short beam shear test 67

Chapter 3: Experimental 71

3.1 Materials 71

3.2 Atmospheric plasma modification of carbon fibres 73

3.2.1 Atmospheric plasma treatment of carbon fibres in batch 74

3.2.2 Continuous fluorination of carbon fibres in atmospheric plasma 75

3.3 Surface characterisation of carbon fibres 76

3.3.1 Dynamic contact angle measurements on carbon fibres 76

3.3.1.1 Determination of the fibre diameter using the modified Wilhelmy-method 77

3.3.1.2 Determination of the fibre wettability using the modified Wilhelmy-method 78

3.3.1.3 Determination of the fibre surface free energy by contact angle models 80

3.3.2 Zeta (ζ) –Potential measurements 83

3.3.3 Fibre surface composition: X-ray photoelectron spectroscopy 87

3.3.4 Fibre surface morphology: SEM 91

3.3.5 Fibre surface area: BET N_2 adsorption measurements 92

3.3.6 Characterisation of the wetting behaviour of single carbon fibres by fluoropolymer melts 93

3.4 Bulk characterisation of carbon fibres 95

3.4.1 Raman spectroscopy of carbon fibres 95

3.4.2 X-ray Diffraction (XRD) analysis of carbon fibres 97

3.4.3 Electrical conductivity of carbon fibres 99

3.4.4 Single fibre tensile strength measurements 100

3.4.5 PVDF crystallinity in the presence of atmospheric plasma fluorinated carbon fibres 103

3.5 Fabrication of carbon fibre reinforced PVDF Composites 105

3.5.1 Inline modification and manufacturing 105

3.5.2 Quality control of the produced carbon fibre/ PVDF composite tape 108

3.6 Mechanical properties of carbon fibre/ PVDF composites 111

3.6.1 Micromechanical characterisation of model composites: Single fibre pull-out test- Apparent interfacial shear strength as a measure of practical adhesion 111

3.6.2 Macromechanical characterisation of carbon fibre/ PVDF composites 113

3.6.2.1 Preparation of composite test specimen 113

3.6.2.2 Flexural testing of carbon fibre/ PVDF composites 115

3.6.2.3 Apparent short beam shear testing of carbon fibre/ PVDF composites 116

Chapter 4: Results and Discussion **118**

4.1 Surface characterisation of carbon fibres 118

4.1.1 Influence of atmospheric plasma modification on wetting behaviour, surface area and morphology of carbon fibres 118
4.1.1.1 Atmospheric plasma batch modified T700 carbon fibres 118
4.1.1.2 Continuously atmospheric plasma fluorinated AS4 carbon fibres 125
4.1.2 Influence of AP batch treated T700 fibres on ζ-potential 129
4.1.3 XPS surface analysis of atmospheric plasma fluorinated carbon fibres subjected to configurations 131
4.1.3.1 Atmospheric plasma batch fluorinated T700 carbon fibres 131
4.1.3.2 Continuously atmospheric plasma fluorinated AS4 carbon fibres 136
4.1.4 Influence of atmospheric plasma batch fluorination on wetting behaviour between T700 carbon fibres and PVDF melt 139
4.2 Bulk characterisation of carbon fibres 140
4.2.1 Raman spectroscopy 140
4.2.1.1 Atmospheric plasma batch fluorinated T700 carbon fibres 140
4.2.1.2 Continuous atmospheric plasma fluorinated AS4 carbon fibres 142
4.2.2 X-ray diffraction (XRD) and conductivity analysis of atmospheric plasma batch fluorinated T700 carbon fibres 144
4.2.3 Impact of atmospheric plasma fluorination on single fibre tensile properties of T700 carbon fibres 146
4.2.3.1 Atmospheric plasma batch fluorinated T700 carbon fibres 146
4.2.3.2 Continuous atmospheric plasma fluorinated AS4 carbon fibres 147
4.2.4 Effects on the PVDF matrix crystallinity in the presence of APF carbon fibres 153

4.3 Quality control of carbon fibre reinforced PVDF composite via powder impregnation 155

4.4 Mechanical properties of carbon fibre/ PVDF composites 158

4.4.1 Micromechanics: Single fibre pull-out test: Apparent interfacial shear strength as a measure of practical adhesion 158

4.4.2 Macromechanical properties 163

4.4.2.1 Impact of APF on flexural properties of carbon fibre reinforced PVDF 163

4.4.2.2 Impact of APF on apparent short beam shear strength of carbon fibre reinforced PVDF 165

Chapter 5: Conclusions **167**

5.1 Possible future work 171

5.1.1 Impact of plasma fluorination on the environment 171

5.1.2 Post manufacturing development of composite parts 172

References **175**

Glossary **191**

Symbols 191
Subscripts 194
Superscripts 195
Abbreviations 196

Appendix **199**

A 199
B 200
C 202
D 203
E 204

List of figures

Fig. 1.1: Overview of the sequence followed during the design, optimisation and fabrication of carbon fibre reinforced PVDF 25

Fig. 2.1: A side view of an oil well 27

Fig. 2.2: Schematic illustrations a) Steel pipe in steel pipe system, b) Steel pipe in thermoplastic fibre reinforced pipe system 30

Fig. 2.3: Schematic illustration of a thermoplastic composite flowline 31

Fig. 2.4: Schematic illustration of a typical multi-layer insulation system used in subsea pipelines. 33

Fig. 2.5: Schematic illustrations of a) PAN and rayon and b) pitch carbon fibre manufacturing process 35

Fig. 2.6: Structural formula of acrylonitrile (left) and PAN (right) 37

Fig. 2.7: Cyclisation of PAN, which takes place at 200 °C in the presence of oxygen 39

Fig. 2.8: Aromatisation during stabilisation of PAN fibres in the presence of oxygen 40

Fig. 2.9: Dehydrogenation: first stage of carbonisation at 400-600 °C 42

Fig. 2.10: Further denitrogenation: second stage of carbonisation at 600-1500 °C 42

Fig. 2.11: Intermolecular crosslinking of stabilised fibres through oxygen containing group 43

Fig. 2.12: Typical arrangement for electrochemical surface oxidation of carbon fibres 45

Fig. 2.13: Flow diagram of commercial process for polymerisation of VDF 54

Fig. 2.14: Schematic illustration of a liquid droplet resting on a flat horizontal solid surface 55

Fig. 2.15: Relationship between contact angle and good/ poor wetting behaviour 56

Fig. 2.16: Images showing the "filaments" in corona treatment and a smooth treat pattern from atmospheric plasma treatment 64

Fig. 2.17: A 3-point flexure bending arrangement for testing unreinforced and reinforced plastics 66

Fig. 2.18: Short beam shear test showing test configuration 69

Fig. 2.19: Effect of shear stress distribution in a laminated specimen 69

Fig. 3.1: Schematic illustrations of atmospheric plasma fluorination setup for: (a) batch setup, (b) continuous single sided setup, (c) continuous double sided setup 74

Fig. 3.2: Schematic illustrations (left) of the modified Wilhelmy setup and photograph of the actual setup used (right) 76

Fig. 3.3: Representative image of a typical weight change as function of time during fibre immersion and withdrawing from dodecane 77

Fig. 3.4a: Representative image of a typical weight change as function of time during fibre immersion and withdrawing from H_2O on a partially wetted ($\theta < 90^{\circ}$) carbon fibre surface 79

Fig. 3.4b: Representative image of a typical weight change as function of time during fibre immersion and withdrawing from H_2O on a hydrophobic ($\theta > 90^{\circ}$) carbon fibre surface 79

Fig. 3.5: Schematic illustration of an electrochemical double layer: Gouy-Chapman-Stern-Graham, GCSG Model 84

Fig. 3.6: Schematic illustration of a pH dependent ζ-potentials 86

Fig. 3.7: Schematic illustration of (a) the cylindrical glass cell setup and (b) its assembly for (c) ζ -potential measurements 87

Fig. 3.8: Schematic illustration of the interaction between an x-ray beam and a substrate in a XPS system 89

Fig. 3.9: Survey XP spectra (exemplary shown) of fluorinated carbon fibres 90

Fig. 3.10: A representative microscopic image showing a PVDF melt droplet on a carbon fibre at 205 °C 94

Fig. 3.11: Schematic representation of the potential energy of a diatomic molecule showing typical Raman and IR transitions 96

Fig. 3.12: Illustration of vibrational modes for single-crystal graphite. The B2g is predicted but not yet observed experimentally 97

Fig. 3.13: Schematic illustration of a X-ray incident beam diffracting from crystal planes, obeying the Bragg's Law 98

Fig. 3.14: Schematic illustration of the four point method (note: the schematic is not to scale) 99

Fig. 3.15: Schematic illustration of single fibre tensile test specimen 102

Fig. 3.16: A representative DSC curve of as received PVDF powder 104

Fig. 3.17: View of a) alpha-PVDF chain and b) beta-PVDF chain 105

Fig. 3.18: Schematic illustration of the laboratory scale line for the production of UD fibre reinforced thermoplastic polymers 106

Fig. 3.19: A representative example of photographic images of fibre pretension unit (left) and spreading pins to be immersed into the impregnation bath 107

Fig. 3.20: A representative example of photographic images of IR ovens (left), cartridge heaters and consolidator (right) 108

Fig. 3.21: Representative microscopic images of powder impregnated carbon fibre roving during a) drying and b) melting 109

Fig. 3.22: A photographic image of 1m long carbon fibre reinforced PVDF tape specimens 110

Fig. 3.23: A representative of photographic images of (a) the fibre embedding device, (b) pull-out device and (c) Side view of single fibre pull-out setup 112

Fig. 3.24: A photographic image of the steel mould used for hot pressing 114

Fig. 4.1: Advancing θ_a and receding θ_r contact angles of desized T700 carbon fibres APF in a 70:1 N_2:$CHClF_2$ plasma jet 120

Fig. 4.2: Representative SEM images of desized T700 carbon fibres APF in a N_2 + $CHClF_2$ plasma jet for a) 0 min, b) 2 min, c) 4 min and d) 8 min 121

Fig. 4.3: Effect of atmospheric plasma fluorination on T700 fibre (BET) surface area 125

Fig. 4.4: Representative SEM images of atmospheric plasma fluorinated AS4 carbon fibres a) original, b) batch, c) continuous straight, d) continuous double sided i) 0.75m/min, ii) 0.33m/min, iii) 0.15m/min 128

Fig. 4.5a: ζ-potential as function of pH of desized T700 carbon fibres and of carbon fibres AP treated in a nitrogen and N_2 + $CHClF_2$ plasma jet for 4 min 130

Fig. 4.5b: ζ-potential as function of pH of desized T700 carbon fibres and of carbon fibres AP treated for various times in a N_2 + $CHClF_2$ plasma jet 131

Fig. 4.6a: Carbon 1s XP spectra of T700 carbon fibres AP fluorinated in N_2 + $CHClF_2$ plasma jet 133

Fig. 4.6b: Fluorine 1s XP spectra of T700 carbon fibres AP fluorinated in N_2 + $CHClF_2$ plasma jet 134

Fig. 4.6c: Oxygen 1s XP spectra of carbon fibres AP fluorinated in N_2 + $CHClF_2$ plasma jet 134

Fig. 4.7: High resolution C 1s, F 1s, N 1s and O 1s XP spectra of AS4 PAN based carbon fibres exposed to either batch or double-sided continuous APF treatments (4 min total exposure) 138

Fig. 4.8: Contact angles between atmospheric plasma fluorinated T700 carbon fibres and PVDF melt as function of exposure time to atmospheric plasma fluorination 139

Fig. 4.9: Raman spectra of T700 carbon fibres AP fluorinated (APF) in a N_2 + $CHClF_2$ plasma jet 141

Fig. 4.10: Ratio of degenerate deformation mode and crystallite graphite mode of APF desized T700 carbon fibres in a N_2 + $CHClF_2$ plasma jet as function of treatment time 142

Fig. 4.11: Ratio of degenerate deformation mode (d) and crystallite mode (g) of original and continuous APF AS4 carbon fibres as function of residence time 143

Fig. 4.12: X-ray diffraction patterns of carbon fibres AP fluorinated (APF) in a N_2 + $CHClF_2$ plasma jet 144

Fig. 4.13: Variation in tensile strength of APF T700 carbon fibres as a function of exposure time 147

Fig. 4.14: Weibull plots of continuous double sided APF treated AS4 carbon fibres at a) original, b) 0.15 m/min, c) 0.33 m/min and d) 0.75 m/min 149

Fig. 4.15: Optical microscopic images of desized and original (T0) carbon fibres, images taken at a) 180 °C, b) 150 °C, c) 140 °C, d) 130 °C, e) 120 °C and f) 120 °C for 5 min 154

Fig. 4.16: Optical microscopic images of 1 min exposure (T1) to APF carbon fibres, images taken at a) 180 °C, b) 150 °C, c) 140 °C, d) 130 °C, e) 120 °C and f) 120 °C for 5 min 155

Fig. 4.17: Fibre volume content of as produced carbon fibre/PVDF tape as function of PVDF powder concentration in the impregnation bath 156

Fig. 4.18: Fibre volume content of as produced carbon fibre/PVDF composite tape as function of manufacturing time 157

Fig. 4.19: Representative optical microscopic images of as produced laminated unidirectional carbon fibre reinforced PVDF composites after consolidation and compression moulding 158

Fig. 4.20: A graph (exemplary shown) of pull-out force as function of displacement of a single fibre pull-out test 159

Fig. 4.21: Apparent interfacial shear strength between APF T700 carbon fibres and PVDF as function of exposure time to atmospheric plasma fluorination 160

Fig. 4.22: Apparent interfacial shear strength between APF T700 fibres and PVDF as function of the embedded fibre length 160

Fig. 4.23: Representative SEM images showing 2 min a), b) and 4 min c), d) APF T700 carbon fibres pull-out from PVDF droplets 161

Fig. 4.24: Apparent interfacial shear strength as function of contact angles between APF T700 carbon fibres and PVDF melt 162

Fig. 4.25: Flexural load as function of flexural extension during flexural testing 163

Fig. 4.26: Flexural strength and modulus of laminated carbon fibre/PVDF composites as function of fluorine content of the fibres fluorinated in atmospheric plasma 165

Fig. 4.27: Short beam shear strength of laminated carbon fibre/PVDF composites as function of surface fluorine content of the carbon fibres 166

Fig. 5.1: Examples of possible sources of delamination initiation caused by through-thickness stresses 172

Fig. 5.2: Schematic of the basic modes of crack loading, a) mode I (opening), b) mode II (shear) and c) mode III (tearing) 173



List of Tables

Table 2.1: Benefits of composites in flowline applications 32

Table 2.2: Application areas of fluoropolymers and its copolymers 50

Table 2.3: Effect of fluorine substitution in polyolefins 51

Table 2.4: Potential advantages of composite materials and areas in which composites are used 60

Table 2.5: The effect of plasma treatment on the interfacial shear strength of Hercules PAN-based carbon fibres 63

Table 3.1: Summary of relevant properties of the carbon fibre used for this study 71

Table 4.1: Dynamic contact angles of 4 min atmospheric plasma fluorinated (APF) desized T700 carbon fibres against water (W), diiodomethane (DIM) and formamide (FA) 119

Table 4.2: Fibre diameters (d_f) and surface free energies γ_s(EoS) calculated using the Equation-of-State approach of desized T700 carbon fibres APF for various times in a N_2 + $CHClF_2$ plasma jet 122

Table 4.3: Surface free energies calculated using both the Equation-of-State (γ_s(EoS)) and acid-base approach (γ_s(AB)) of 4 min AP treated desized T700 carbon fibres 123

Table 4.4: Dynamic contact angles of APF AS4 carbon fibres against water (W), diiodomethane (DIM) and formamide (FA) 126

Table 4.5: Fibre diameters (d_f), BET surface area and surface free energies ((γ_s(EoS)) of APF AS4 carbon fibre 127

Table 4.6: Surface composition (in at.-%) of AP batch fluorinated T700 carbon fibres in a N_2 + $CHClF_2$ plasma jet determined by XPS 132

Table 4.7: Surface composition (in at.%) of atmospheric plasma fluorinated AS4 carbon fibres determined by XPS 136

Table 4.8: 2θ values, half width at half maximum ($\Delta\theta_{1/2}$) and calculated interlayer distance (d) of APF T700 carbon fibres in a N_2 + $CHClF_2$ plasma jet 144

Table 4.9: Resistance (R), conductivity (κ) and resistivity (ρ) of APF T700 carbon fibres in a N_2 + $CHClF_2$ plasma jet 145

Table 4.10: Tensile strength, Weibull modulus and scale parameter at different gauge lengths of APF AS4 carbon fibres as function of residence time 148

Table 4.11: Predicted tensile strength of continuous double sided plasma fluorinated AS4 carbon fibres at a) 40mm and b) 50mm gauge length 152

Table 4.12: Melting points (T_m), heat of melting (H_m) and degree of crystallinity (X_c) of pure PVDF powder, desized and original (T0) carbon fibres/ PVDF and 1 min exposure (T1) to APF carbon fibres/ PVDF 155

Publications

1. **K. K. C. Ho**, M. Laffan, S. Lamoriniere, M. Q. Tran, A. Bismarck , *Composites A*, Submitted.

2. M. Q. Tran, **K. K. C. Ho**, G. Kalinka, M. S. P. Shaffer, A. Bismarck, *Comp. Sci. Tech.* 2008, **68**, 1766.

3. A. Bismarck, W. Brostow, R. Chiu, H. E. H. Lobland, **K. K. C. Ho,** *Polym. Eng. Sci.* 2008, **48**, 1971.

4. **K. K. C. Ho**, A. F. Lee, S. Lamoriniere, A. Bismarck, *Composites A*, 2008, **39**, 364.

5. **K. K. C. Ho**, G. Beamson, G. Shia, N. V. Polyakova, A. Bismarck, *J. Fluorine Chem.* 2007, **128**, 1359.

6. **K. K. C. Ho**, G. Kalinka, M. Q. Tran, N. V. Polyakova, A. Bismarck, *Comp. Sci. Tech.* 2007, **67**, 2699.

7. **K. K. C. Ho**, S. Lamoriniere, G. Kalinka, E. Schulz, A. Bismarck, *J. Colloid Interface Sci.* 2007, **313**, 476.

8. **K. K. C. Ho**, A. F. Lee, A. Bismarck, *Carbon*, 2007, **45**, 775.

Presentations at Conferences

Invited presentation:

1. **K. K. C. Ho** and A. Bismarck. "Continuous Modification and Processing of High Performance Fibre Reinforced Fluoropolymer Composites" at the International Conference on Polymer Processing 2007, 18th – 20th May 2007, Beijing, China. (partially supported by a SCI Richardson Travel Award).

Presentations at Conferences:

1. **K. K. C. Ho** and A. Bismarck. "Fluorination of Carbon Fibres: Will such Fibres Adhere to Fluoropolymers" at PolyCHAR-14 World Forum of Advanced Materials, 17th – 22nd April 2006, Nara, Japan.

2. **K. K. C. Ho** and A. Bismarck. "Characterisation of Plasma Fluorinated Carbon Fibres" at PolyCHAR-14 World Forum of Advanced Materials, 17th – 22nd. April 2006, Nara, Japan. (Awarded the Carl Klason Second Prize for a Student Presentation, in fierce competition with students from 35 countries") (Session Chair Opening Session 1: Characterisation).

3. **K. K. C. Ho** and A. Bismarck. "No Crack under Pressure": Towards Fibre Reinforced Fluoropolymers for Applications in Extreme Environments" at the 3rd International Conference on Materials for Advanced Technologies (ICMAT) and International Union of Materials Research Societies 9th International Conference on Advanced Materials, Symposium B: Chemical and Molecular Modification of Interfaces, 3rd – 8th July 2005, Singapore. (partially supported by a Royal Academy of Engineering Travel Award).

Poster Presentations:

- M. Q. Tran, **K. K. C. Ho** and A. Bismarck. "Development of Ultra-inert Thermoplastic Composites" at PolyCHAR-14 World Forum of Advanced Materials, $17^{th} - 22^{nd}$ April 2006, Nara, Japan.

Awards and Prizes

- Society of Chemical Industry: SCI Honours- Richardson Travel Award 2007
- Carl Klason Second Prize for Best Student Paper 2006
- The Royal Academy of Engineering: Scheme for Engineers in Research and Development, International Travel Grants 2005



Chapter 1

Aims and Objectives

The aim of the project was to design and fabricate high performance carbon fibre reinforced fluoropolymers that can deliver exceptional mechanical and chemical performance in the most severe environments, for instance those encountered in the oil and gas industry. The oil and gas industry continues to explore and develop deep-sea oilfields in which materials encounter extreme conditions in such operations that require superior material performance and durability. The materials have to withstand combined severe service conditions, aggressive media (sweet and sour well fluids), high abrasion, high but fluctuating temperatures, pressure differences and mechanical load. Conventional engineering materials, such as steel, have reached their limits because of their poor chemical resistance and damage tolerance and/ or the high costs involved in supporting their own weight [1]. Polymer composites might have the potential to overcome such limitations thus enabling new design strategies for cost effective, weight and energy saving materials [2,3]. Metal pipes, which are heavy and require corrosion protection, used as risers, flowlines and choke and kill lines, will have to be replaced by non-corroding and lighter alternative materials if deeper sea reservoirs are to be explored. Spoolable reinforced thermoplastic pipes have been developed to transport highly corrosive fluids including crude oil, brine and various gases at high service pressures [4,5]. For these reasons, industrial applications for thermoplastic composite materials are currently expanding rapidly.

A major topic in the field of materials and chemical engineering has been the search for high performance structural materials. The desired materials should be lightweight,

possess increased strength, toughness and greater resistance to combined conditions of severe chemical or environmental attack and significant mechanical loadings as compared to conventional engineering materials. Fibre reinforced polymers are able to provide a beneficial balance between the traditional properties of a polymer (light weight and processability) and selective properties of metals (high strength, modulus and toughness). Fibre reinforced polymers allow tailoring of unique combinations of such properties to meet practical and design requirements.

The overall aim of this research was to develop a continuous process with integrated surface modification technology to manufacture unidirectional carbon fibre reinforced PVDF composites. Such composites should have a stable and durable fibre/ matrix interface and good mechanical properties. The following approach was adopted (Fig. 1.1):

- Develop an atmospheric plasma fluorination (APF) procedure that enables batch, continuous and inline modification of carbon fibres,
- Characterise the impact of APF on the fibres surface and bulk properties,
- Fabrication of APF carbon fibre reinforced PVDF composites,
- Examine the micro- and macromechnical properties of APF carbon fibre reinforced PVDF composites.

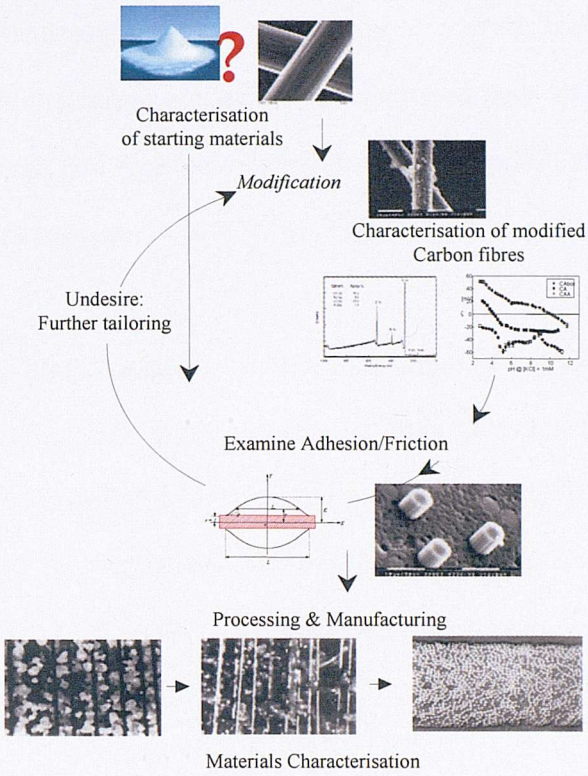


Fig. 1.1: Overview of the sequence followed during the design, optimisation and fabrication of carbon fibre reinforced PVDF

This thesis is structured in a standard style with an Introduction, Literature Review, Experimental, Results and Discussion and Conclusions.

Chapter 1, which is the Introduction chapter, provides an overview of the research area, motivation, aims and objectives. Also chapter 1 provides an overview of the sequential approach of the work undertaken during this research.

Chapter 2 reviews the background literature focusing on thermoplastic tubular pipes in oil and gas industry, carbon fibre manufacturing, PVDF as a matrix, fundamentals of wetting, an overview of carbon fibre reinforced composites, the importance of fibre/ matrix interface modification in carbon fibre reinforced PVDF composites and relevant mechanical tests for this study.

Chapter 3, the Experimental chapter, describes in detail the materials used, the atmospheric plasma modification procedures, surface and bulk characterisation tools for carbon fibres and micro- and macromechanical tests for carbon fibre reinforced PVDF composites used in this research work.

Chapter 4, the Results and Discussion chapter, presents all the findings of this research including the influence on APF to the surface and bulk properties of carbon fibres, how quality measures are important in fabrication of carbon fibre reinforced PVDF composite via powder impregnation. The results of interface dominated mechanical properties of single fibre composite and laminated composites are also presented and discussed.

Chapter 5 summarises the main conclusions drawn and highlights possible further work which could be considered when continuing this research.

Chapter 2

Literature Review

2.1 Background in thermoplastic tubular pipes in the Oil & Gas industry

In October 2004 when this research began, a barrel of Brent Crude Oil was $55 USD and by the time this thesis was written, a barrel of Brent Crude Oil has reached over $130 USD*. There is common fear that the oil price will increase in the long term. The demand is increasing but the supply is dwindling with present day oil production technology. Therefore, oil companies are under pressure to be more efficient in how they extract crude oil. There are many possibilities to improve production and one of which was the development of Enhanced Oil Recovery (EOR) systems.

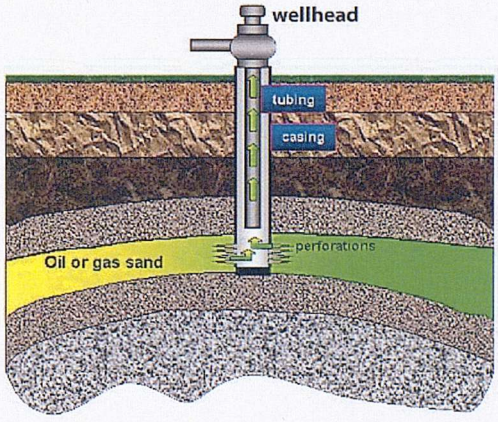


Fig. 2.1: A side view of an oil well †

* Market data. Link in: http://www.bloomberg.com/energy/ accessed 02.2008

† Rolls-Royce Energy. Link in: http://www.rolls-royce.com/energy/overview/oilgas/apps_typ.jsp accessed on 13.08.08.

Most oil reserves possess a certain amount of natural gas pressure and so when a well is drilled through impermeable rocks, the hydrostatic pressure therefore propels the oil to the surface. This typically recovers up to 15% of the total oil in the reservoir and the process is known as primary recovery [6]. In secondary oil recovery the pressure difference between the surface and the reservoir is maintained by injecting fluids or gases into the oil reservoir [7]. After secondary oil recovery, typically up to two thirds of the oil remains in the reservoir. Tertiary oil recovery utilises gases, chemical or thermal energy to extract oil after the secondary recovery has become unsustainable [7]. EOR is often defined as secondary or tertiary methods that do not entail pressure maintenance of the oil well [8]. EOR techniques include the reduction of capillary forces by the addition of surfactants to water that is used for displacement of oil [6]. Thermal recovery processes, including steam and CO_2 injections, are also used [7,9].

Although ensuring that more oil is extracted from the well is important; what also plays an important role are the cost, corrosion resistance, weight and installation ability of equipment and materials. This, therefore, leads to the research and development of new materials, such as thermoplastic materials, to be used in pipes for the oil and gas industry [10,11]. Non-metallic materials have been used as structural components, fluid barriers, armouring, mechanical and corrosion protection and thermal insulation for oil and gas pipelines, flexible pipes, control lines and hydraulic tubes [10,11].

The term "spoolable pipeline structures" is a concept that encompasses a wide range of technologies, from narrow-bore control fluid lines through coiled tubing, flexible pipes, coated flowline, etc. [12,13]. Often a non-metallic element, such as a polymeric material, is used as the containment layer of an exclusion layer. Typically, these spoolable pipeline structures have a diameter between 115-245 mm, tensile load ratings up to 68 tonnes and must withstand internal pressures of up to 20 MPa and external

collapse pressures of up to 45 MPa. The application of such structures has undergone dramatic growth due to the ability to manufacture each structural component. Reeling on a drum, reel or cassette and installation or deployment of the structure in a continuous process avoids the need for offshore welding and fabrication, reducing risk and improving the economics. The benefits of using thermoplastics have outweigh the higher direct product cost and are becoming more universally accepted and practiced [10].

2.1.1 Pipe design

The limitations on a pipe to be used in subsea pipelines and risers is highly dependent on the amount of longitudinal force and pressure loads. In each case, products are individually tailored to meet the specific requirements of the application. This is mainly due to that the deformation of the pipes caused by the additional excessive or accidental loads, such as collision with adjacent risers in deepwater floating production systems [14], may lead to the bending deformation. During operation, the pipe wall of pipelines is constantly subjected to various loads such as [15]:

- pure external/ internal pressure
- pure bending/ tension/ compression
- combined pressure, axial force and bending

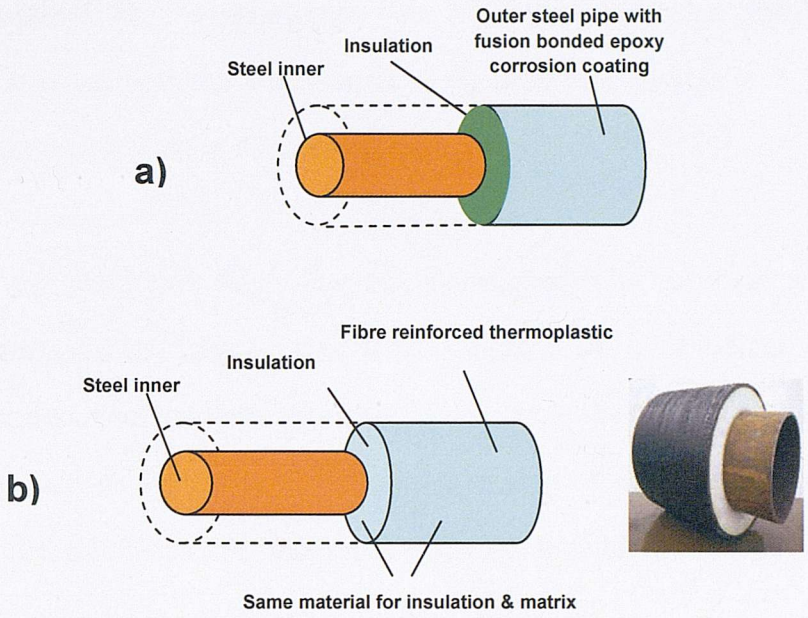


Fig. 2.2: Schematic illustrations of a) Steel pipe in steel pipe system, b) Steel pipe in thermoplastic fibre reinforced pipe system

The details of each design requirement for the individual sections of subsea pipelines and risers are however beyond the scope of this thesis. For a complete study please refer to Ref. [15]. An example would be the common pipe in pipe system (Fig. 2.2a) used in offshore subsea production systems.

Subsea pipelines generally have limitations in terms of maximum length in which the pipe can be deployed. This is due to the high temperature of untreated well fluids together with pipes that are poorly insulated, which limits the flow through the pipe. Today pipe in pipe systems typically have an overall heat transfer coefficient between 2-8 W/m^2K and nowadays pipe length is into the 60 km range (as compared to 20 years ago when the pipe length was 20 km in range) and the effect from high temperature well fluids is becoming more critical. This is because as the pipe length increases, the amount of heat energy stored in the system also increases and this induces the risk of pipe wall buckling and leads to additional measures being required to maintain seabed stability [16]. A lower overall heat transfer coefficient (0.5-1 W/m^2K) could be achieved

when a thermoplastic fibre-reinforced outer layer (with better heat insulating properties) is applied together with the same matrix as the liner insulation (Fig. 2.2b), which would allow longer transportation distances [17].

Currently the maximum depth that can be reached with common steel pipe in pipe systems is about 2000-2500 m. Due to the weight of the total system, the steel starts to yield when deployed to depths in excess of this range [18]. Instead, when the outer layer of the pipe in pipe system is replaced by a reinforced plastic pipe, the overall weight would be much reduced and, therefore, allow the pipe to be deployed to deeper depths without the inner steel yielding (Fig. 2.2b).

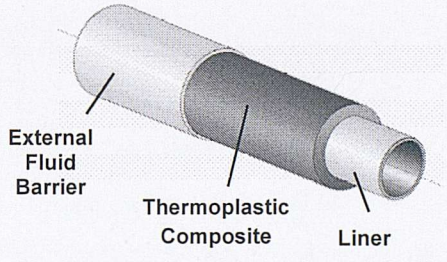


Fig. 2.3: Schematic illustration of a thermoplastic composite flowline [19]

Another example would be subsea pipes that consist of reinforcing layers made of thin layers of plastic sandwiched between reinforcing layers (Fig. 2.3). These pipes consist of three layers. The inside layer is a conventional polyethylene pipe surrounded by carbon fibre reinforced composites to withstand stress. These reinforced carbon fibre composites are in turn surrounded by an outer polyethylene coating. Each individual layer has a different function to perform. The polyethylene inner pipe supports the carbon fibre reinforced composite layer and provides the rigidity required to withstand external stress. The support provided by the inner pipe is absolutely essential as the reinforced composite can only withstand longitudinal stress. The carbon fibre

constitutes is the main structural element of the pipe, absorbing the stress caused by internal pressure and is wrapped around the inner pipe in several layers in alternating directions with an angle of approximately 55°. The number of layers required depends on the internal pressure in each case. The outer external fluid barrier layer is applied to provide mechanical protection against damages. The advantages of using thermoplastic composites are extended and are summarised Table 2.1.

Table 2.1: Benefits of composites in flowline applications*

Benefit	**Description**	**Applications**
Chemical/ corrosion resistance	Composites have high chemical resistance, depending on the matrix chosen.	Rough environments that are difficult for inspection. Environments with H_2S, CO_2
Ease of installation	1) Spoolability, composites flowlines are less stiff as compared to steel flowlines and thereby increase installation rate significantly. 2) Composite flowlines are much lighter in weight and therefore simplifying the equipment required for installation. 3) High flexibility for installation around corners or obstacles.	Onshore.
Insulation	Composites provide insulation because of their low heat transfer coefficient.	Cold environments.
Re-usability	Quick installation but also de-installation, thereby opening a new application of reusability.	Short usage, small reservoirs.

* Thermoplastic Composite Flowline Solutions. Link in: http://www.airbornedevelopment.com/act/composites.phtml?p=Flowline1 accessed 13.08.08.

2.1.2 Coating system requirement for subsea pipelines

The vast majority of material used in the offshore oil and gas industry is steel based. This can vary from carbon steels (taken from American Petroleum Institute standards, Grade B to Grade X70 and higher) to exotic steels, such as duplex [15]. Depending on the product being transported in the pipeline and the location where the pipeline is installed, the pipeline is prone to corrosion both internally and externally. In order to protect the pipeline from corrosion in a marine environment, polypropylene is commonly used to act as an outer shield to minimise defects and damage by handling during transportation and installation (Fig. 2.4) [15]. Beneath the high electrical resistivity coating, polypropylene foams are used as insulating layers before fusion bonded epoxy (FBE) is applied as an external coating barrier for the inner steel against moisture reaching the steel surface. FBE which is most commonly used for offshore pipelines [20,21] as thin film coatings, 0.5-0.6 mm thick and consists of thermosetting powders which are applied to the preheated metal base by electrostatic spray and subsequently cured.

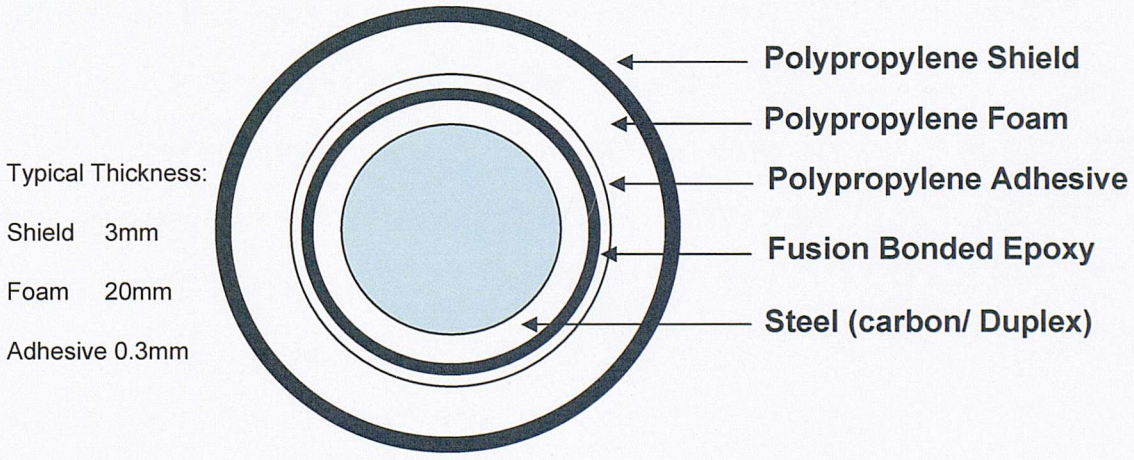


Fig. 2.4: Schematic illustration of a typical multi-layer insulation system used in subsea pipelines. Redrawn from Ref. [22]

Internal coatings to pipelines are applied primarily to reduce the friction between transporting goods within the pipe and, therefore, enhance flow efficiency. Since the first field application by Tennessee Gas Pipeline Co. in 1955 [23,24,25], internal coatings has been used to improve corrosion protection, pre-commissioning operations and pigging operations. This is when a device called the "pig" is inserted into a flowing pipeline to scrape off deposits such as wax or paraffin from the inside of the pipeline or to push liquids through a multi-phase pipeline [26,27]. The majority of internal coated linings used are epoxies, urethanes and phenolic, with epoxies being the most common material due to their broad range of desirable properties such as hardness, water resistance, excellent adhesion, etc.

2.1.3 The outlook

The use of reinforced thermoplastic pipes opens up possibilities when exploring natural gas and oil from deep sea fields. These materials have the potential to replace steel pipes in oil and gas systems at least to a certain extent in a certain diameter range. Depending on the soil conditions on site, fibre reinforced thermoplastic pipes can be laid inexpensively in one length using ploughs or wheel ditchers. This is a method which is widely used on land pipes for gas distribution systems. With the equipment currently available, it would even be possible to increase the depth of cover at relatively low additional cost. For example in a fibre reinforced composite pipe, a join would only be required approximately every 280 m along the pipeline route, whereas in contrast, joints are needed every 12 to 18 m along a steel pipeline [28]. An initial cost estimate indicates that the cost of using reinforced thermoplastic composites may be 30% lower than that of steel (based on a pipeline with a diameter of 150 mm and a length of 4 km) [28].

Reinforced thermoplastic composites are made up of at least a matrix and reinforcement. In the remaining sections of the literature review, carbon fibre as a reinforcement and PVDF as the matrix will be introduced. In addition, the adhesion and adhesive properties as well as the characterisation of interface dominated mechanical properties of unidirectional carbon fibre reinforced PVDF will be presented.

2.2 Carbon fibre manufacture

The history and the science of carbon fibres are reviewed in order to understand the impact of carbon fibres on fibre reinforced polymer technology. The main processing steps involved in the manufacturing of carbon fibre are shown below:

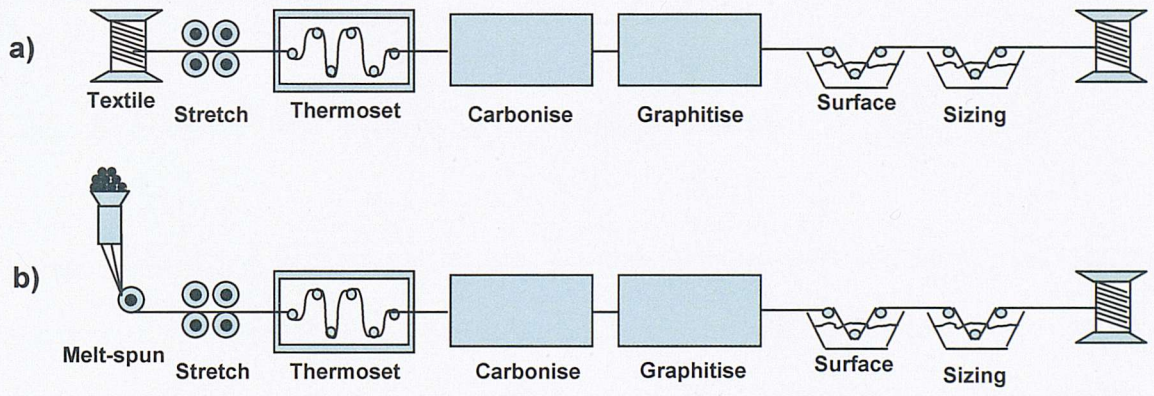


Fig. 2.5: Schematic illustrations of a) PAN and rayon and b) pitch carbon fibre manufacturing process [29]

Carbon fibres were first developed by Thomas Edison in 1879 for use as filaments for early light bulbs. He took cellulose based materials, such as cotton or bamboo, and carbonised them at high temperature and in a controlled atmosphere*. This process is known as pyrolysis, which is still used today for manufacturing carbon fibres [30,31].

* Bacon's breakthrough, National Historic Landmark, American Chemical Society. Link in: http://acswebcontent.acs.org/landmarks/landmarks/carbon/car3.html accessed on: 18.02.08

Starting from the late 1950s, carbon fibres were produced for high temperature missile applications and were finally commercially available in the 1960s* [32,29]. This represented a breakthrough in materials with low densities which are both strong and stiff. For a perfect graphite, the Young's modulus is approximately 1000 GPa and, consequently, the tensile strength should be about 100 GPa. However due of defects, the practical strength is always an order of magnitude lower than the theoretical strength, thus, in the most perfect form of fibrous carbon up until the mid 1980s, the graphite whisker, the Young's modulus is about 680 GPa and tensile strength is about 20 GPa [33,34,35]. Carbon fibres in the world market offered a practically attainable form of reinforcement material which could be produced in volume at reasonable cost (In 1993, a pound weight of commercial grade carbon fibre cost approximately £60, by 2003 a pound weight of commercial grade carbon fibres cost approximately £3*) for use in fibre reinforced composites.

2.2.1 Precursors for carbon fibre manufacturing

Carbon fibres are commercially manufactured from three different precursors; rayon (regenerated cellulosic fibres), polyacrylonitrile (PAN) and petroleum pitch. Carbon fibres were initially made from rayon by hot stretching during graphitisation. An early commercial available rayon-based carbon fibre (Thornel 50) achieved strength and modulus values of 2.76 GPa and 345 GPa respectively in the mid 1960s [26,27,28,29,36], but the yield of the process was only about 15 % w/w of the precursor rayon. On the other hand the use of PAN as a precursor allowed the stretching to be carried out at lower temperature and increased the process yield to 50 % [37]. The

* Lewis R. Carbon Fibre: Transforming F1. Link in: http://www.carkeys.co.uk/features/technical/632.asp accessed on 01.10.08

Consortium Developing Carbon-Fiber Composites from Renewable Resources. Link in: http://www.greencarcongress.com/2006/03/consortium_deve.html accessed on 01.10.08

starting point of the manufacturing process of both rayon and PAN based carbon fibres are textile fibres (Fig. 2.5a). For pitch carbon fibres, the petroleum pitch is converted into a meso phase pitch by a refining operation before spinning (Fig. 2.5b). As PAN based carbon fibres are adopted in the work of this thesis, therefore only the structure of PAN based carbon fibres are presented.

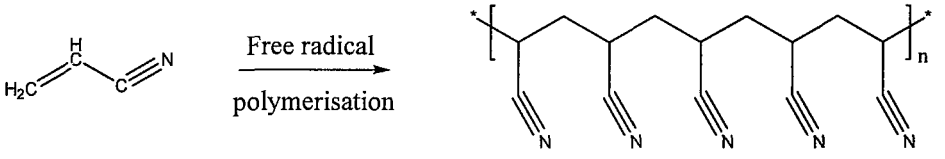


Fig. 2.6: Structural formula of acrylonitrile (left) and PAN (right)

The mechanical properties of the resulting carbon fibres depend, to a large extent, on the mechanical properties of the PAN precursor fibres, and are commonly used as reinforcement in composites and find applications in sporting goods, aerospace, automobile industry etc. PAN was the original precursor for high strength, i.e. high performance, carbon fibres [38] and PAN based carbon fibre still holds the largest market for carbon fibres [39]. This is mainly because of the following reasons [40]:

- The structure of PAN permits a faster rate of pyrolysis and allows molecular chains to be aligned in the preferred orientation along the fibre axis.
- PAN decomposes before melting.
- PAN precursors can be stretched to up to 800 % strain and further improvement in the orientation is also possible during thermal stabilisation at around 180 °C, and through various post spinning modifications
- As mentioned before, it has a high carbon yield of up to 50 % when pyrolysed at 1000 °C and above.

The development of special grade PAN fibres holds a key to the whole carbon fibre industry. The first step in preparing a spool of the textile PAN fibre precursor is to polymerise acrylonitrile and to spin it. PAN has highly polar nitrile groups and as a result, strong dipole-dipole forces exist between adjacent chains. These polar forces create a hindrance effect in the molecular alignment during spinning. A comonomer of 2-5 % is often added to acrylonitrile to give a copolymer of PAN [41,42]. Two most commonly used comonomers are methylacrylate and itaconic acid and they have specific roles. The methylacrylate reduces the glass transition temperature so that the fibre can be stretched in a steam environment as opposed to a glycol environment. On the other hand itaconic acid, which was a traditional dye site for the original Courtelle textile fibre, acts as an initiator for the formation of a ladder polymer. Other comonomers such as acrylamide are also used, for further details please see Ref. [**Error! Bookmark not defined.**,43,44,45]. Once the homopolymer and the copolymer has been selected, they are then polymerised in aqueous sodium thiocyanate solution and carefully filtered.

The PAN is spun into fibres. There are four types of spinning techniques and among those the most widely used technique for the spinning of acrylic fibres is wet spinning. The acrylic precursor fibres are spun into a coagulation bath having a higher percentage of solvent (such as dimethyl sulfoxide or dimethylformamide) at low temperature [46]. The fibre diameter depends upon the spinneret's orifice diameter, the let off rate and the take up velocity. A schematic of a spinning setup can found in Ref. [47,48]. The fibres are stretched during spinning, where the trapped solvent decreases the cohesive force among the nitrile groups of the polymer chain, i.e. reducing the dipole-dipole interaction [49] and in return allows for better orientation and mechanical properties of the carbon fibres produced from this precursor. The stretching of fibres also results in the uncoiling of polymer chains and, therefore, enable a ladder polymer to be formed [50]. In general,

the higher the spin-stretch factor (defined as the ratio of windup speed to the filament speed at the spinneret hole [51]), the higher the tensile modulus of the resulting carbon fibres [52].

2.2.2 Thermal stabilisation of PAN fibres

The second step in the processing of PAN fibres into carbon fibres is to thermally stabilise the PAN fibres by oxidizing them in air at a temperature of approximately 220 °C. Stabilisation involves cyclisation, dehydrogenation and oxidation. Cyclisation (Fig. 2.7) is one of the critical steps in processing of carbon fibres, and takes place around 200 °C [53] via radical reaction for PAN homopolymer and ionic mechanism for copolymer of PAN [54]. During the oxidation, the fibres are kept in tension while cyclisation takes place, so that the molecular orientation induced during stretching is maintained [55,56].

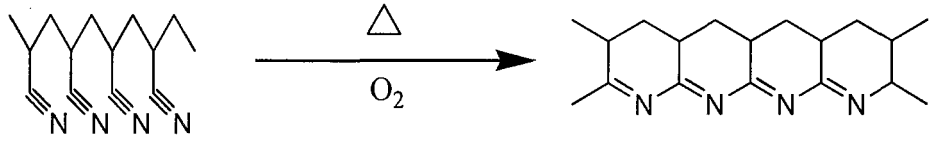


Fig. 2.7: Cyclisation of PAN, which takes place at 200 °C in the presence of oxygen

During thermal stabilisation, the colour of the precursor fibres changes from white to yellow, brown and ultimately black fibres. Berlin et al. [57] and Fester [58] believe the colour change is due to the development of a polyene structure during heat treatment of PAN whilst others [59,60,61] suggested that it is because of the formation of a condensed ring structure containing carbon-nitrogen double bonds (Fig. 2.8).

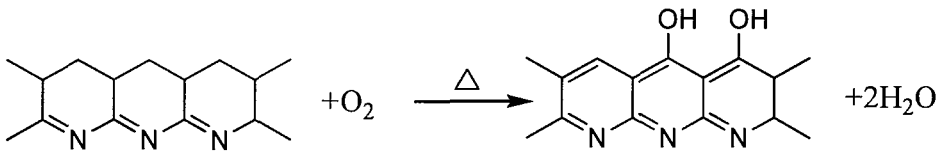


Fig. 2.8: Aromatisation during stabilisation of PAN fibres in the presence of oxygen

The application of tension to the fibres, the heating temperature during stabilisation as well as the medium (i.e. in oxygen) are important parameters which affect the final structure of the fibre and hence its ultimate mechanical properties. During stabilisation, if no load is applied to the spin-stretched PAN fibres, shrinkage to the fibres was reported to occur [62,63,64,65]. It is believed that there are two types of shrinkage: physical and chemical. Physical shrinkage is attributed to the entropy recovery of a drawn and quenched material [66]. This is due to the randomly-coiled conformation of the PAN molecule with intermolecular repulsive forces between the neighbouring nitriles group dipoles. By stretching the fibres during the precursor preparation, conformational change is developed which elongates the tactic regions to allow ladder polymer formation to occur. It is the length of the isotactic regions which determines the graphitic nuclei which form. Chemical shrinkage on the other hand occurs as a result of chemical reactions during stabilisation. This is due to the formation of cyclised ladder polymer [67,68] and maybe considered as a measure of cyclisation reaction [69]. An optimum heating rate of 1-3 °C/ min until up to 260-280 °C were reported for the acrylic precursors to result in a maximum tensile strength of the resulting carbon fibres [70]. The stabilisation of the precursor fibre has been studied in various media [71] and it was found that precursor fibres stabilised in an oxidising medium produce better carbon fibres than ones stabilised in an inert atmosphere [72,73]. Fitzer et al. [74] have demonstrated that oxygen initiates the formation of active centres for cyclisation but it also retards the stabilisation by increasing the activation energy. Nevertheless, stabilisation in an oxidizing medium is preferred because it forms oxygen containing groups such as -OH, C=O, -COOH which helps generate crosslinks during

carbonisation [75]. Fitzer el al. [74] also pointed out that PAN fibres can be stabilised at higher temperatures of 300-400 °C at a very fast heating rate, in the order of 200-300 °C/ min. This leads to formation of a highly ordered and compact structural arrangement in the stabilised fibres [76]. The resulting mechanical properties of the resulting carbon fibres show significant improvement over ones prepared by stabilisation at temperatures of 200-300 °C [76], which has considerably improved the economics of carbon fibre production.

2.2.3 Carbonisation of PAN fibres

Stabilised precursor fibres are converted into carbon fibres in the process of carbonisation, which involves heat treatment of PAN fibres in an inert atmosphere [40]. This process further eliminates impurities by removing all elements other than carbon and leads to the formation of a graphite like structure. The carbonisation temperature directly affects the graphitic structure of produced carbon fibres. This finding dates back to the work in the 1960s by Watt and co-workers at the Royal Aircraft Establishment (RAE) [76,77]. They discovered that the application of tension during the initial oxidation step at 220 °C was important for maintaining or even enhancing molecular alignment during carbon fibre processing to 2500 °C [77,78]. Heat treatments in excess of 2500 °C were found to result in high modulus fibres and was subsequently designated as Type I fibres (Structural models of high modulus PAN based carbon fibres can be found in Ref. [34]). The RAE workers also established that an optimum treatment of 1000-1500 °C yields high strength type carbon fibres and these high strength fibres were designated as Type II carbon fibres.

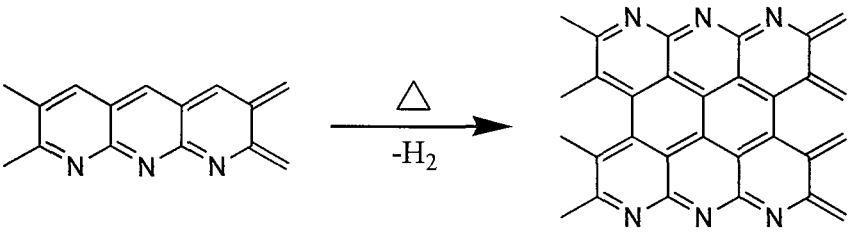


Fig. 2.9: Dehydrogenation: first stage of carbonisation at 400-600 °C [79]

In the cabonisation process of Type II fibres, the heating rates in the two temperature zones are crucial. The first zone (Fig. 2.9) with a temperature of up to 600 °C requires a relatively low heating rate of less than 5 °C/ min to remove water and maybe some volatiles. This slows down the mass transfer; if the heating rate is too high it causes surface irregularities in the form of pores because of the diffusion of evolved gases [41].

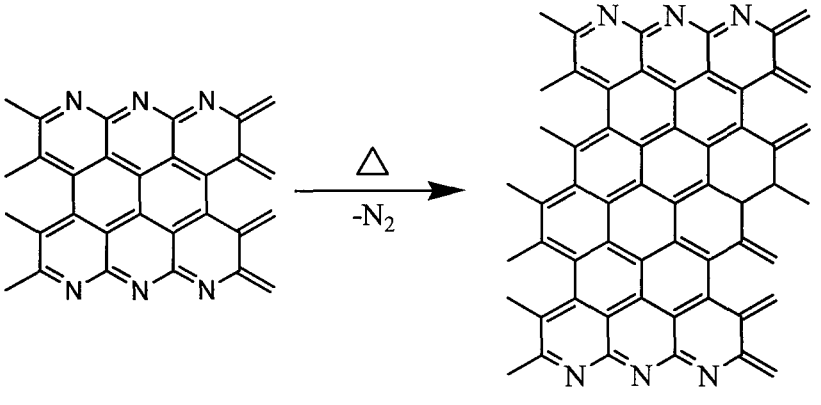


Fig. 2.10: Further denitrogenation: second stage of carbonisation at 600-1500 °C [79]

In the second heating zone (Fig. 2.10) between 600-1500 °C, a higher heating rate is used because of the damage caused by exothermic reactions or the evolution of by-products already took place in zone 1. However, other gases such as nitrogen and hydrogen cyanide (Fig. 2.10) as well as hydrogen and water (Fig. 2.11) are produced by intermolecular crosslinking of the polymer chains.

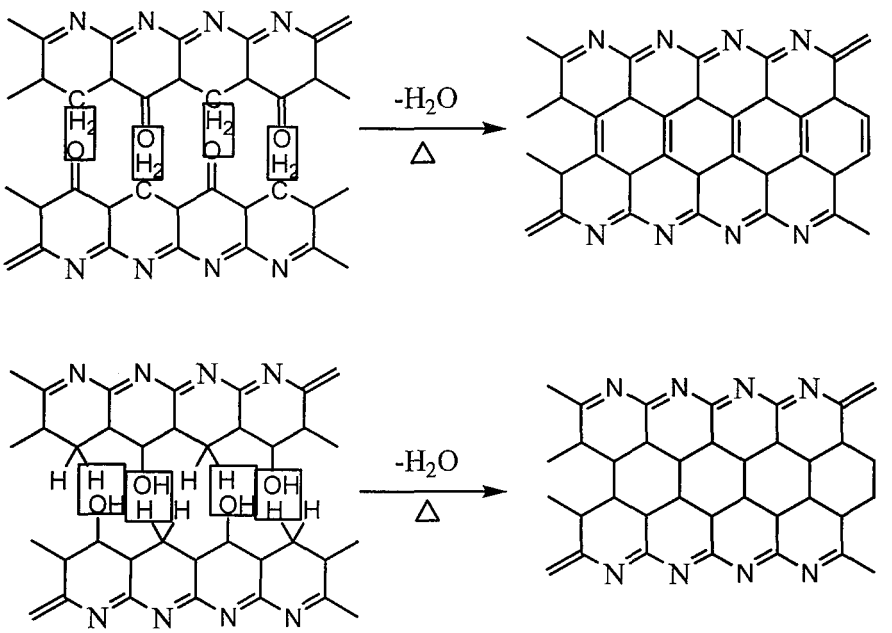


Fig. 2.11: Intermolecular crosslinking of stabilised fibres through oxygen containing group [69]

During crosslinking, the carbon atoms of one cyclised sequence fit in to the spaces left by the nitrogen of the adjacent sequence [80]. This helps the growth of a graphite structure in the lateral direction. An inert atmosphere is needed to avoid oxidation of the fibres at such high temperature and common gases such as nitrogen, argon, or other non-oxidizing media, such as HCl [81] and ZnO [82] have also been used.

The strength of the carbon fibre is largely associated with defects in the structure, many of them in the bulk of the fibre arising from catalysed graphitisation of impurities present within the original polyacrylonitrile dope. These impurities can be dust particles or maybe gel polymers which has not been filtered out of the dope. A decrease of the tensile strength of the carbon fibres has been reported for heat treatments above 1500 °C [83,84]. However, the tensile modulus keeps increasing at a slow rate of up to 3000 °C [85], which results in fibres having crystallite orientation mainly parallel to the fibre axis over a long distance order (Details of *Characterisation parameters of typical PAN based carbon fibres* can be found in Ref. [39]). It was noted that nitrogen can no longer

be used as a medium because above 2000 °C, nitrogen becomes active and forms cyanogen (CN_2) by reacting with carbon fibres [69].

2.2.4 Surface treatment of PAN carbon fibres

Kaelble et al. [86], Larsen et al. [87] and Daukeys [88] have shown that when carbon fibres without any surface treatment are used to produce carbon fibre-epoxy composites, a low interlaminar shear strength (ILSS) is observed. They have also observed that the ILSS is directly related to the fibre-matrix adhesion and, therefore, hence that the adhesion between the original carbon fibres and the epoxy matrix is weak. It was also observed that as the temperature of graphitisation increases, the ILSS decreases although the Young's Modulus of the carbon fibres increased. This has prompted the development of a number of surface treatments in order to improve the fibre-matrix interfacial bonding. As produced PAN based carbon fibres contain many graphitic edge planes exposed at its surface (a schematic of high tensile strength PAN based carbon fibres can be found in Ref. [89]) and it is at these less ordered edge plane regions where surface reactions can take place preferentially. The surface exposed edge sites of the treated PAN based carbon fibre-epoxy composites typically exhibit much better adhesion possibly as a result of higher chemical reactivity of the graphitic edge planes. It should be noted that the strong anodic treatments of fibres are also able to induce degradation and/ or fibre modulus decreases with a decreasingly graphitic structure. PAN based carbon fibres had to be used as starting material for this work, therefore the industrially used electrochemical oxidation process (Fig. 2.12) will be discussed in detail.

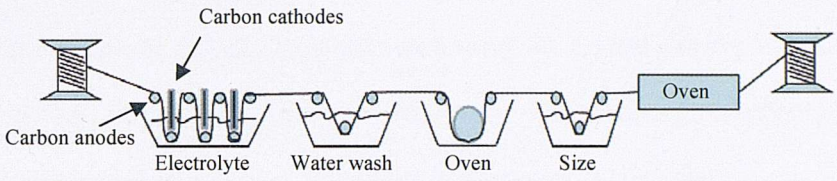


Fig. 2.12: Typical arrangement for electrochemical surface oxidation of carbon fibres. Redrawn from Jones [39]

Ammonium bicarbonate NH_4HCO_3 and ammonium bisulphate NH_4HSO_4 are commonly used electrolytes for electrochemical oxidation of PAN-based carbon fibres [90] to introduce oxygen containing functional groups, such as carboxyl and phenolic, to the carbon fibre surface [91]. This is because electrochemical oxidation treatment offers more control over the surface chemistry as compared to gas-phase or acid oxidation [55]. In addition, it also allows continuous modification of carbon fibres [92,93,94]. The work by Donnet et al. [95,96] in the mid 1970s showed that the oxygen content of Type II fibre carbon fibres increased considerably when oxidised anodically in a solution of nitric acid containing potassium dichromate and sodium hydroxide together with a weight loss due to the evolution of CO_2 [95,96]. In acid solutions, O_2 is produced at the anode surface by the decomposition of water [97]:

$$2H_2O \rightleftharpoons 4H^+ + 2O^{2-} \tag{2.1}$$

In alkaline solutions, the O_2 is viewed as being produced by the discharge of OH^- ions [97]:

At the anode, $$4OH^- \rightarrow 2H_2O + 4e^- + O_2$$

At the cathode, $$4e^- + 4H_2O \rightarrow 4OH^- + 2H_2 \tag{2.2}$$

The concentration of the electrolyte in water must be sufficient to enable the electrolytic process to take place and further electrolytes must be added during the run in order to allow for depletion in the bath due to fibre take-up. The choice of electrolyte however is very dependent on practical issues. Processing parameters include:

1) Circulation of electrolyte,
2) Heating the bath to 50 °C to enhance ionic mobility and reduce surface tension,
3) Multistage treatment process to provide fresh surface for treatment,
4) Addition of surfactant to reduce surface wetting and improve fibre wetting,
5) AC/ DC current supply for various treatment times

The processing parameters need to be adjusted to ensure the level of surface treatments are sufficient for a given fibre type which also shows influence to the matrix adhesion.

Mahy and co-workers [98] found that the surface area of Type II fibres did not increase significantly as a result of electrochemical surface treatment. Nakao et al. [99] found that by processing electrochemically oxidised carbon fibre into epoxy based composites, an improvement in composite ILSS was observed. However, there is a negative effect on the transverse flexural strength of the composites. Sherwood and his group [100] has studied the surface chemistry of electrochemically treated carbon fibres extensively using XPS and confirmed that the increase in ILSS with surface treatment is not dependent upon the surface concentration of chemical groups (such as O-1s/ C-1s or the amount of carbonyl, carboxyl functionalities). Therefore, they suggested that micro-mechanical keying of the resin to the fibre surface might play a role in the adhesion increase of composites [101]. Jones [102] claims that the electrolytic surface treatment process produces a surface on which the known concentration of chemical

functionalities cannot be accommodated on the surface of a smooth cylinder. Details of atomic percentages of surface concentrations of elements determined on a range of commercially available carbon fibres by Jones et al. are summarised by Wright [103] and can be found in Ref. [104]. At the moment no consensus has been reached on the roles of physical absorption and chemical bonding when investigating the surface chemistry of carbon fibres and this is made more difficult by the buried interface [104].

2.2.5 Sizing of carbon fibres

In the last stage of carbon fibres manufacturing (Fig. 2.5 and 2.12), a thin layer of epoxy resin is usually coated onto the fibres to a) protect the fibres from possible damage during transportation and handling and b) to improve inter-filamentary adhesion and to aid in wetting out the fibre in resin matrices because most carbon fibres are intended for epoxy resin-based composites [105,106,107,108,109]. Normally around 0.5-2 wt-% is added to the fibre which corresponds to a coating thickness of approximately 0.03 μm. Drzal et al. [110] measured the adhesion of sized carbon fibres and epoxy resin using the embedded single fibre critical length test (single fibre pull-out test) and found that the interfacial shear strength increased by about 25%. The authors proposed that the sizing layer interacts with the bulk matrix and causes a change in local properties at the fibre-matrix interphase. The properties of this sizing layer itself are imparted to the interphase and can affect adhesion. A similar conclusion was reached by Jones et al. [111] on studies of carbon fibre reinforced thermoplastic (polyethersulfone) composites using the single fibre fragmentation test. They suggested from the analysis of time-of-flight secondary ion mass spectrometry that the adhesion enhancement arises from a strong interaction, via penetration of the sizing resin into the PES matrix, between the resin used for the sizing, the fibre and the matrix. This is due to the fact that solvent deposition leads to a strongly bound deposit [111]. A schematic of the interphase region

between fibre and matrix can be found in Ref. [112]. Sherwood et al. [113] studied the effect of the size compound on the effect of adhesion using XPS and X-ray wavelength dispersive microscopy. They claimed that the surface chemistry of the sized fibres was dominated by the sizing and also more sizing compounds were found on fibres that had received greater surface treatment in the surface modification step, which led to greater stability of the size on the fibre surface.

2.3 Fluoropolymers as matrices for carbon fibre reinforced composites

2.3.1 Background

Fluoropolymers are essentially polyolefins in which some or all of the hydrogen atoms have been replaced by fluorine atoms. They were first discovered in 1938 by Dr R. J. Plunkett when he was working as a chemist for *DuPont*[*]. He and his assistant J. Rebok had accidentally polymerised a refrigerant gas tetrafluoroethylene (TFE) when they filled a pressurised cylinder with TFE. After some time when they opened up the tank, they were surprised to find a waxy white powder which was later on commercialized as Teflon® polytetrafluoroethylene (PTFE)[†]. This new fluoropolymer was found to be rather inert towards strong acids, bases and heat. It was also insoluble in any common solvent.

[*] History of Teflon®.Link in: http://www.teflon.com/NASApp/Teflon/TeflonPageServlet?pageId=/consumer/na/eng/news/news_detail.teflon_history.html accessed on 18.11.04

[†] Encyclopaedia of fluoropolymers. Link in: www.freedictionary.com accessed on 18.11.06

During the Second World War, the US army was looking for a material that was resistant to uranium hexafluoride, which is an extremely corrosive gas. It was then that PTFE was recognised and used to make gaskets for atomic bombs [114]*. After the war, it was not until 1960 that PTFE was first introduced to the public as Teflon-coated muffin and frying pans. Since then, other fluoropolymers have become available and subsequently there has been a great expansion in the areas of application [115] (Table 2.2).

2.3.2 Chemistry and market of fluoropolymers

The volume of commercial fluorine containing polymers is not large when compared with other polymers, such as polyvinyl chloride. It is estimated that the demand for fluoropolymers will rise by 5.7 % per year until 2011 in the USA, approaching a total of $2 billion USD [116]. Fluoropolymers are required in many important applications (Table 2.2) [115].

Thermoplastic fluoropolymers are held together by weak secondary bonds, such as van der Waals and hydrogen bondings. In general, when thermoplastics are subjected to heat and pressure, these intermolecular bonds can be temporarily broken and flow freely. Upon cooling, the molecules relocate into new positions and it is this mechanism that allows thermoplastics to be melted and reshaped [117]. One of the reasons for fluoropolymers to have a high melting point is the restricted rotation about the C-C bonds along the chain, which results primarily from the repulsion between the highly electronegative fluorine atoms [118]. Secondly, when hydrogen atoms are partially substituted, this results in very strong intermolecular forces from the C-F dipole which

* Nichias cooperation. Annual report 2005 p8. Link in: http://www.nichias.co.jp/nichias-E/investors/pdf3/08.PDF access 30.10.2006.

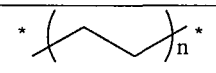
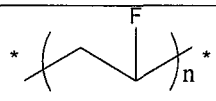
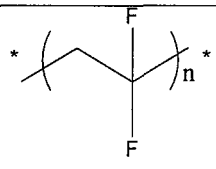
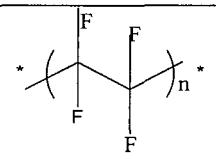
give rise to a very high yield strength, such as in PVF and PVDF, as compared to the aliphatic analogs such as polyethylene (Table 2.3). When all the hydrogens were substituted by fluorine, such as for PTFE, there are strong repulsion forces between fluorine atoms from different chains, which resulted in low surface free energy (which typically lie between 18.5-35 mJ/m^2 (Table 2.3)) and cause the material to yield at low stresses (Table 2.3).

Table 2.2: Application areas of fluoropolymers and its copolymers*

Fluoropolymers	**Application areas**
ETFE, FEP, PCTFE, PFA, PFE, PTFE, PVDF	Aerospace
PCTFE, PVDF	Aircraft
ETFE, FEP, PCTFE, PFA, PTFE, PVDF	Automotive
PCTFE, PFA	Bottles
ETFE, FEP, PFA, PFE, PTFE, PVDF	Cable jacketing
FEP, PFA, PTFE, PVDF	Coating
PFE, PTFE, PVDF	Gaskets
ETFE, FEP, PCTFE, PFA, PTFE, PVDF	Insulations
ETFE, FEP, PFA, PFE, PTFE, PVDF	Piping
ETFE, FEP, PCTFE, PFA, PFE, PTFE	Seals
ETFE, FEP, PFA, PTFE, PVDF	Tubings
ETFE, FEP, PCTFE, PFA, PTFE, PVDF	Valves

* Fluoropolymer Applications. The Plastic Web. Link in: http://www.ides.com/generics/Fluoropolymer/Fluoropolymer_applications.htm accessed 18th Feb 2008.

Table 2.3: Effect of fluorine substitution in polyolefins [119]

Polymer	Structure	Melting temperature/ °C	Density/ gcm^{-3}	Yield strength/ MPa	Surface energy/ γ_s
Linear Polyethylene (PE)		135	0.94	28	31
Polyvinyl fluoride (PVF)		175	1.4	56	28
Polyvinylidene fluoride (PVDF)		164	1.75	52	25
Polytetrafluoroethylene (PTFE)		327	2.2	13	18.5

The copolymers of fluoropolymers such as the random copolymer of TFE and hexafluoropropylene copolymer have achieved significant commercial importance within the fluorocarbon polymer family. These copolymers were developed to lower the melting point and melt viscosity so that they can be processed by conventional processing methods, which is not possible for the case of TFE homopolymers (pre-treatments of TFE homopolymers such as etching in metallic sodium dissolved in a solution of naphthalene are required if TFE homopolymers are to be processed [120]).

The weaknesses of common fluoropolymers are for example, their low creep performance and low resistance towards ionising radiation. PVDF in particular has a relatively low resistance to ketones* (such as methyl ethyl ketone and methyl isobutyl ketone) and strong alkaline media. Fluorinated ethylene propylene copolymer (FEP) has

* A full list of Kynar® PVDF chemical chart can be found in: http://www.arkema-inc.com/literature/pdf/681.pdf

low fatigue resistance and a lack of stability towards radiation and tetrafluoroethylene-perfluoro alkoxy vinyl ether copolymer (PFA) has a low heat deflection temperature. For example PTFE can be used as sealant tapes whereas PFA can be used in high pressure/ temperature tubing. Blends of fluoropolymers are not common because of the combination of their high melting points and the chemical nature. However they do exist. For example, PTFE powders are sometimes added to other polymers in order to enhance lubrication and chemical resistance, PVDF is blended with other polymers, such as acrylates and methacrylates and are used as coatings to increase weather resistance [121,122,123].

2.3.3 PVDF in the chemical process industry

Polyvinylidene fluoride (PVDF) was first commercially introduced in 1961 by the Pennwalt Chemical Company (later known as Pennwalt Corporation, followed by Elf Atochem North America, Inc. and from 2004 known as Arkema Inc.). The polymer was originally to be used as piping and moulded parts for plutonium recovery applications in nuclear facilities, abrasion resistant insulation for computer back panel wire and as a long life finish on metal panels used in the construction industry. By 1970s, the demand for PVDF and PVDF-copolymers expanded and was seeing strong growth in architectural finishes and plastic-lined steel for chemical plants. By the early 1980s, there was a worldwide shortage of PVDF-type polymer due to a new regulation introduced by the United States National Electrical Code (NEC) for low-smoke, low-flame polymers to be used in plenum areas of buildings (This had been slowly phased out since 1990 and replaced by polyvinylchloride, PVC and FEP). This also coincided with the blooming of the high purity semiconductor chip industry where manufacturers discovered that polymer outperform metals in the transport of high purity washing chemicals [124]. PVDF has become the material of choice compared to other cheaper

polymers, due to the fact that it could be easily processed into high purity components, such as piping [125], tank linings, pumps, filtration products, fittings, flexible tubings etc. In addition, PVDF is the least expensive fluoropolymer on a cost per volume ratio, therefore, it is often the first such material considered for new arising applications [126]. The PVDF grade used in this research study is was Kynar® by Arkema. The United States Department of Agriculture (USDA) and the National Sanitation Foundation Standard 61 have recognised Kynar to be used in storage areas in contact with meat and poultry as well as water containers.

PVDF is manufactured by polymerisation of 1,1-difluoroethene (CH_2=CF_2), also known as vinylidene fluoride (VDF) (The details of the synthesis of vinylidene fluoride can be found in Ref. [127,128,129,130,131,132]).While there are other methods of producing PVDF homopolymers, emulsion and suspension polymerisation remain the two most common methods used [132].

Although manufacturers keep the details of the commercial processes of emulsion polymerisation (Fig. 2.13) of VDF confidential, it is known to take place inside a high pressure reactor (2.8-4.8 MPa) equipped with a stirrer, heater (at 60-90 °C) and cooling devices [132]. Inside the reactor the reactants include a fluoroalkyl surfactant, such as ammonium salt of a fluorotelomer acid, paraffin wax to stabilise the emulsion, a chain transfer agent, such as isopropyl alcohol, and initiators and chain terminators [132]. Upon completion of polymerisation, the product is recovered as latex. Further processing, such as flash evaporation and creaming (separation of small latex particle from the dispersed latex), allows the latex to be concentrated. This is followed by washing, which helps to eliminate any residual impurities such as polymerisation initiator and surfactant. Concentrated latex is then coagulated into a powder form, which is ideal for the powder impregnation process used in this research. The untreated/

agglomerated spherical PVDF particles have a diameter as small as 0.2 μm [126]. Further processing of the powder into other forms such as pellets and films, etc is possible.

Suspension polymerisation of VDF in general takes place in batch form (typically in 5 litres batches), constantly stirred in a reactor that consists of 3.3 litres of water and 1.1 kg of VDF, initiators (such as an organic peroxide), colloidal dispersants and chain transfer agents to control the molecular weight. In addition, about 1 g of water soluble polymer (such as cellulose derivatives or polyvinyl alcohol) is added to reduce coagulation. The preferred polymerisation takes around 0.25-6 h at a temperature and pressure between 30-110 °C and 6.9-21 MPa, respectively [133,134]. This results in a slurry of spherical particles of PVDF, which then need to be recovered by filtration, washing and drying. Intensive studies on the effects of the different initiators, molecular weight and yield of suspension polymerisation can be found in [135,136,137,138].

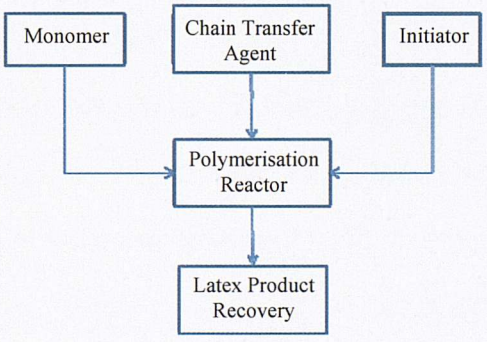


Fig. 2.13: Flow diagram of commercial process for polymerisation of VDF [139]

PVDF is a semi-crystalline polymer with a degree of crystallinity between 45-70 %. The degree of crystallinity depends on the processing conditions and methods used. PVDF is commercially available as pellets, powder or liquid dispersion. Depending on the molecular weight, PVDF is available in a range of melt flow indices and viscosities. Like any other thermoplastics in general, low molecular weight grades with high melt

flow rates are used for injection moulding at a processing temperature between 180-240 °C. High molecular weight grades offer better melt strength and are used for extrusions at a processing temperature range between 210-290 °C. Even higher molecular weight PVDF are used in casting applications such as membranes. The PVDF Kynar® 711 produced by Arkema used in this research has a molecular weight of ~84,000 g mol^{-1} and a glass transition temperature (Tg) between -41 to -37 °C. It should be noted that the melt of PVDF should never exceed 315 °C because PVDF decomposes at temperature above 315 °C and highly corrosive and toxic HF gas is evolved. Compared to other commercial fluoropolymers, PVDF has the lowest melting point, but actually has the highest heat deflection temperature under load [140]. PVDF is the least permeable of all fluoropolymers. The combination of PVDF homopolymer and other copolymers of VF_2/ HFP would even make them the highest abrasion resistant polymer in the fluoropolymer family.

2.4 Background in wetting behaviour of solids

When a liquid drop is placed on a solid substrate, it either spreads as a thin continuous film or beads up [141]. It is the displacement of a liquid that a solid is in contact with that is known as wetting. Wetting can be quantified by contact angle (θ) measurements. θ is defined as the angle at which a liquid vapour interface meets the solid surface (Fig. 2.14).

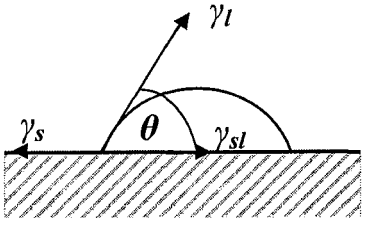


Fig. 2.14: Schematic illustration of a liquid droplet resting on a flat horizontal solid surface

For an ideal smooth and energetically homogeneous solid, θ is specific for any given system and is determined by the three-phase contact line from the solid-liquid interface to the liquid-vapour interface that can be described by the Young's equation [142]:

$$\gamma_l \cos\theta = \gamma_s - \gamma_{sl} \tag{2.3}$$

where γ_l, γ_s and γ_{sl} are the surface and interfacial free energies of the liquid, solid and solid-liquid interfaces, respectively.

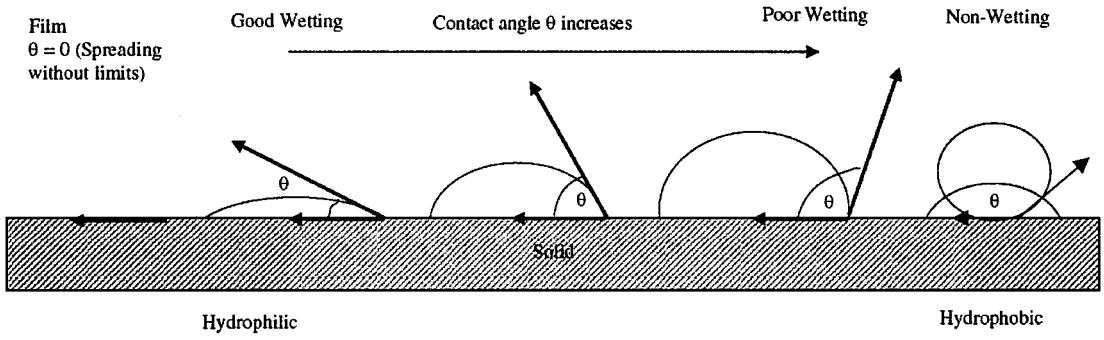


Fig. 2.15: Relationship between contact angle and good/poor wetting behaviour [143]

Under most circumstances, when a liquid has a high surface tension (e.g. H_2O; γ_l= 72.8 mN/m) and is sitting on a low surface energy surface (e.g. polyethylene; γ_s= 31 mN/m) [144], a droplet is formed (Fig. 2.15); whereas when the same high surface tension liquid is sitting on a high surface energy substrate (e.g. clean glass; γ_s= 300-1500 mN/m) [145] the droplet spreads and wets the surface (Fig. 2.15). On the other hand a low surface tension liquid (e.g. dodecane; γ_l= 25.4 mN/m) will spread without limits and wet all surfaces with $\gamma_s > 25.4$ mN/m regardless whether they are high surface energy substrates or low energy substrates. The measurement of a single static contact angle to characterise the interaction is not adequate for any interaction study between any given solid/ liquid. This is due to the fact that static contact angles are

dependent on the recent history of the interaction. If the three phase (Fig. 2.14) boundary is in actual motion the angles produced are called Dynamic Contact Angles. Dynamic contact angle measurements always provide two limiting contact angles the advancing contact angle θ_a, which is characteristic for the low-energy parts of the investigated surface, and the receding angle θ_r, which reflects the high-energy portion of the surface and are referred to as advancing and receding angles.

In reality, surfaces are not 100 % smooth and homogeneous but heterogeneous, which leads to the formation of contact angle hysteresis. This is the difference between the maximum (advancing) and the minimum (receding) contact angle and can be caused by chemical heterogeneity or surface roughness. For the case of chemical heterogeneity, different chemical functionalities represent areas with different contact angles compared to the surrounding surface. For example when wetting with water, hydrophobic functionalities will pin the motion of the contact line as the liquid advances thus increasing the contact angles. When the water recedes the hydrophilic functionalities will hold back the draining motion of the contact line thus decreasing the contact angle. From this analysis it can be seen that, when testing with water, advancing angles will be sensitive to the hydrophobic functionalities and receding angles will characterise the hydrophilic functionalities on the surface. For situations in which surface roughness generates hysteresis, the actual microscopic variations of slope in the surface create the barriers which pin the motion of the contact line and alter the macroscopic contact angles [146,147].

2.5 Composites

2.5.1 Background

Ever since the history of human kind began, people have used composites, such as wood (cellulose reinforced lignin), straw and branch reinforced clays for building shelters. After the Stone Age, the development of metal-working skills strongly dominated most "engineering" and in particular steel has been of major importance since the 19th century [148,149]. Metals and steel continued to dominate the materials world until 1960s when there was a rise in natural and synthetic polymers, composites and ceramics engineering materials. More recent developments in fibre reinforced composite materials opened up exciting new opportunities to enhance the design and the manufacturing for applications in the automotive [150,151] and aerospace/ spacecraft industry [152,153].

2.5.2 Properties and applications of carbon fibre reinforced composites

A composite is a structural product that consist of two (or more) distinctive materials combined together in which the overall performance exceeds those of any individual component. The principle constituent in carbon fibre reinforced composite material is carbon fibres. Although a number of fibres are commercially available for use as the reinforcement in fibre reinforced composites, this thesis focused on PAN based type II carbon fibres.

Carbon fibre occupies the largest volume fraction in a carbon fibre reinforced composite and share the major portion of the load acting on a composite structure, depending on

the direction of the load. The other component that makes up the continuous portion of fibre reinforced composites is the matrix. The matrix material (in this case PVDF) is responsible to 1) transfer stresses between the fibres, 2) provide a barrier against an adverse environment and 3) protect the fibres from wear and abrasive damage [154]. The performance of composites is determined mainly by the composition and arrangement of the constituents, i.e. the matrix and the fibre. This involves parameters such as fibre volume fraction, fibre aspect ratio, fibre orientation, as well as strength and moduli of matrix and fibres, respectively. When a load acts upon a composite, it is transferred from the matrix to the fibres via the interface/ interphase, which directly affects the shear and delamination resistance of a composite. If the fibre to matrix interaction is weak, the composite will have poor mechanical performance [155]. Performance of fibre reinforced composites can only be maximised if effective load transfer from the matrix to the fibres is guaranteed. This is made possible by ensuring adhesion or compatibility between the fibre and the matrix by enhanced mechanical interlocking and/ or chemical bonding [156].

Fibre reinforced composites are commonly used in a form of laminates where individual thin layers of continuous fibres and matrix are consolidated into a material with the desired thicknesses. By controlling the fibre orientation in each layer as well as the stacking sequence of the layers, a wide range of physical and mechanical properties of composite laminates can be obtained. A unidirectional fibre reinforced composite shows exceptional stiffness and strength properties in the fibre longitudinal direction because of the structural arrangement. Continuous fibre reinforced composites are widely used in the aerospace, defence and oil and gas industries [157,158] because they offer a combination of strength and modulus that are either comparable to or better than many traditional metallic materials. This is because of their low specific gravities, the strength-weight ratio and modulus-weight ratio, of fibre reinforced composite materials are known to be superior to those of metallic materials.

Table 2.4: Potential advantages of composite materials and areas in which composites are used [148]

Potential advantage of composite materials	**Typical applications or application areas**
Very high specific strength and stiffness	all applications where weight is a premium, in particular aerospace defence, sporting goods, industrial machinery, bridges
Very good fatigue properties	aircraft brakes, fan blades, tail plane (A320 & B777)
Corrosive resistance	marine and off-shore applications, bridges
Thermal insulation	refrigerated containers, building panels, fire walls and doors
Electrical insulation	electrical housings, transformer spacers, cable trays, ladders
Biological inertness	replacement joints, tendons
Energy absorption	helmets, bullet-proof partitions, armour, crash barriers
Fire and smoke properties	fire walls and doors, aircraft interiors
Geometrical complexity/ parts integration	all applications, in particular automobiles and aircrafts
Shape Flexibility	used to achieve shapes that cannot be made with metals (at similar cost)
Thermal expansion	used to eliminate thermal expansion
Tooling and manufacturing cost	all applications, in particular automobiles and aircrafts

Table 2.4 shows a variety of applications where composite materials are advantageous for a range of markets and applications [159]. An ideal hexagonal arrangement for circular fibres could give a maximum fibre volume fraction greater than 90% whereas a square packing array results in more than 75%. In practice volume fractions of 60% are commonly used as surface tension forces and natural viscosity of the liquid matrix wetting the fibres limits the packing density [160]. In any event, it would not be desirable to have the fibres touching as the point of contact would weaken the

composite. Unidirectional and continuous fibre reinforced composites have been dominated by thermoset matrix materials until about 15 years ago when thermoplastic matrices were combined with continuous fibres as reinforcement to produce unidirectional fibre reinforced thermoplastic composite materials [161]. Despite the excellent properties of thermoplastics, including high environmental resistance, high impact strength and recyclability [162,163,164], thermosets are more commonly used as matrix systems than thermoplastics in composite materials because manufacturing fibre reinforced thermoplastic composite material is difficult [104]. The melt viscosity of thermoplastic resins is extremely high compared to that of thermosetting resins [165,166], which makes it difficult to impregnate fibre bundles by thermoplastic melts [167]. To overcome these difficulties, various thermoplastic composite manufacturing processes have been developed, such as comingled yarns and powder-coated yarns [168,169,170,171,172].

2.5.3 The role of surface modification on carbon fibre and the adhesion to PVDF

When considering the development of carbon fibre reinforced thermoplastic polymers, and more specifically PVDF, the lack of compatibility between the polymer and carbon fibres is due to the inert nature of the matrix and the lack of reactive groups as compared to thermosetting systems (and indeed, other engineering thermoplastics). Therefore, the primary function of a fibre surface modification is to improve the fibre wettability by the matrix and to create optimum adhesion at the fibre-matrix interface. Conventional surface oxidation and sizing of carbon fibres during manufacturing are designed to enhance adhesion to epoxy matrices but not for fluoropolymers (Please see section 2.2.4 and 2.2.5). The introduction of fluorine functional groups to the fibre surface has been proven to enhance interfacial compatibility [173,174]. The introduction

of fluorine to the surface of carbon fibres is commonly carried out using direct fluorination [175,176,177,178]. This is where a dilute form of F_2 gas is passed over a batch of carbon fibres placed inside a specially designed reactor for a given period of time [179] and which in most cases does not exceed 60 min in order to limit fluorination only to the fibre surface [180]. However, this is only a batch process and, therefore, alternative fluorination procedures are required to introduce surface functional groups continuously and in return promotes better interfacial adhesion between the fibre and the matrix. Many reviews have given details of the common surface treatment on carbon fibres in order to improve or optimise adhesion. One of them is plasma modification, the theory of which is reviewed here.

A plasma is an excited gas, which consists of atoms, ions, free radicals and free electrons. Plasma treatment has been extensively applied for processing semiconductors and other materials for about 30 years [181,182,183,184,185]. A plasma can be generated in air, termed a corona discharge, or under reduced pressure, termed a glow discharge. It is commonly used to modify the physical and chemical state of material surfaces without significantly altering the bulk properties such as: cleaning, degradation and ablation [186,187], crosslinking, oxidation [188,189], polymerisation and grafting [190,191] and ion implantation. For further general information about the capability of plasma, please see the review by Kinloch [120]. As plasma treatment has been used to modify the carbon fibres for this work, therefore the area will be discussed in detail.

Although low-pressure plasma treatments is applied to modify carbon fibres, the disadvantages of low-pressure plasma treatments [192,193,194] are that they require a well designed system including vacuum pumps, sealed and contained handling equipment*. Typical low-pressure plasma systems with a RF generator operates at

* Low pressure plasma, Plasma Treat. Link in:
http://www.plasmatreat.de/GB/html/glossary/l.html accessed on 08.08.08

13.5 MHz, 100 W at 2-50 Pa, gas flow rate of 8-40 cm^{-1} min^{-1} and 20 s – 20 min exposure time [104]. Low pressure plasma treatments are, therefore, often only used in batch processes given the size of the reactor chamber is limited by capital and operational costs. However, this does not restrict investigations of low pressure plasma treatment of carbon fibres to the research level. Donnet et al. [195,196] found that grooves on original M40 carbon fibres can be completely removed by exposing the fibres to a microwave-generated plasma using air for as little as 12 s. Later, Edie and co-workers [197] found that a 143% increase in interfacial shear strength, as determined by short beam shear strength test, over an original Hercules AU-4 fibres using ultra high vacuum (Ar/O_2, O_2) plasma. Using a similar plasma system, Peng and Rebouillat [198] only found a 66% increase in interfacial shear strength over a commercially treated AS4 fibre (Table 2.5).

Table 2.5: The effect of plasma treatment on the interfacial shear strength of Hercules PAN-based carbon fibres [55]

Hercules PAN-based carbon fibre	Interfacial shear strength rating (%)
AU4 original fibre (Control sample index 100%)	100
AU4 plasma treated fibre (Ar/O_2, O_2)	243
AS4 commercially treated fibre	166

For continuous modification processes, corona treatment and atmospheric plasma (AP) are the alternative techniques. A corona discharge plasma species does not require a vacuum system, and may be use continuously and industrially, however, the plasma species are not uniform, as shown in Fig. 2.16. Alternatively, an AP can be generated at a stable and uniform plasma environment at atmospheric pressure in a way that permits a uniform and continuous surface treatment (Fig. 2.16) [199,200,201]. Like other plasma treatments, AP treatments can generate various active species depending on the feed gas composition [202]. Given continuous plasma modification (functionalising,

Advantages of fluorination, Air Products. Link in:
http://www.airproducts.co.uk/fluorination/advantages.htm accessed on 08.08.08

etching, polymer grafting, etc.) of fibres have been proven feasible to promote interfacial adhesion between the fibre and the matrix [203,204], if continuous plasma fluorination of carbon fibres can be carried out, the compatibility between PVDF and such fluorinated fibres could be tailored directly during the manufacturing process of the composites. Consequently, no intermediate offline surface treatment steps are required. Therefore, the aim of this project was the development of a continuous inline atmospheric plasma fluorination process of carbon fibres to tailor the fibre/ matrix interface while manufacturing unidirectional fibre reinforced PVDF composites.

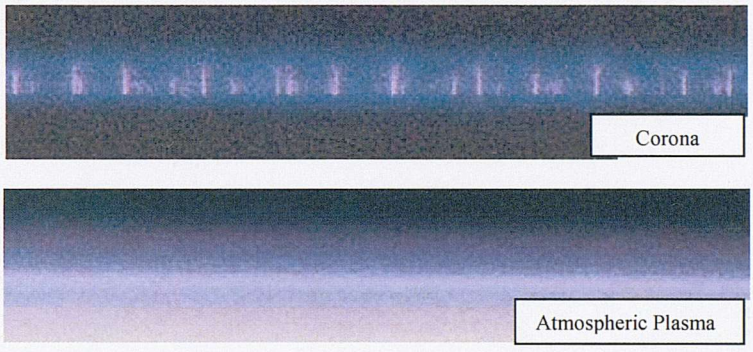


Fig. 2.16: Images showing the "filaments" in corona treatment and a smooth treat pattern from atmospheric plasma treatment*

2.5.4 Testing of unidirectional carbon fibre reinforced PVDF composites

There are three distinct uses for a mechanical test [205]. It may be used a) to obtain design data, b) for quality control and c) for specification purposes. In this thesis, the specific purpose of carrying out mechanical testing was to examine the effect of the surface modification of fibres on the interface dominated properties of carbon fibre reinforced PVDF. Two techniques were selected based on the fact that they are

* Enercon surface treating system. Link in: http://www.enerconind.com/treating/products/plasma3.html accessed on 08.08.2008

routinely used and easy to use [104] and mainly because they only require a small amount of material, which was limited because of carbon fibre supply problems.

2.5.4.1 Flexural properties

Flexural properties can be determined through flexural testing which is a simple bend test of a beam based on a small deformation elastic theory, however, it is only valid on light, thin, narrow, linearly elastic (Hookean) materials [205]. For Hookean materials, when a stress is applied, the strain is instantaneously and reversibly proportional to the stress. It is common knowledge that polymers do not behave precisely in this way. Therefore, the ranges of strains and strain rates where linear elasticity occurs is only an approximation in flexural testing which depends on the test specimen, the temperature and the accuracy required [205]. The advantages of flexural testing are that the test requires only small specimens and the relative simplicity of the test. There are three common standards for determining the flexural strength and modulus of reinforced plastic materials: ASTM D790, BSI 2782 method 1005 and CRAG [104] but all three of them use a 3-point test arrangement (Fig. 2.17). The different standards offer a range of choices in terms of specimen dimensions, support and loading rollers, e.g. ASTM allows for a series of span-thickness (S/h) ratios, BSI just one and CRAG requires the laminate to be 2 mm thick.

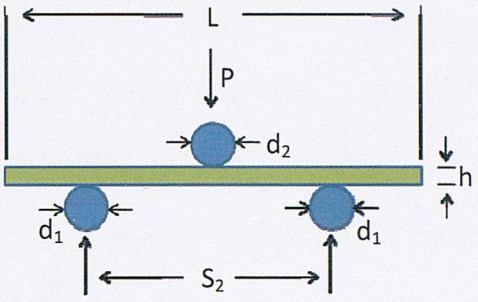


Fig. 2.17: A 3-point flexure bending arrangement for testing unreinforced and reinforced plastics. Redrawn from MSc Composite Materials Course on Mechanical testing of Advanced Fibre Composites, Imperial College London, Sept 1995.

Flexural behaviour of laminated unidirectional carbon fibre reinforced PVDF can be determined when an external load is applied perpendicular to the axis of the composite. When a rectangular beam is bent a continuous change occurs from maximum compressive stress on the loaded surface through the thickness to maximum tensile stress on the opposite side. Three failure modes can occur during flexural testing: compression failure along the top of the composite sample, shear failure in the middle of the composite sample and tensile failure along the bottom of the composite sample (Fig. 2.18). Ideally, if the beam is subjected to pure bending, the compressive stress on the loaded surface is equal to the tensile stress load on bottom surface, therefore, at the midpoint of thickness the shear stress is at a minimum. However, because carbon fibre reinforced composites are anisotropic, to ensure that the primary failure comes from tensile or compression stress and not shear stress, the span to thickness ratio (S/h) must be controlled. Span to thickness ratio is the length of the outer span divided by the thickness of the specimen. For most materials S/h= 16 is acceptable. Some materials require S/h= 32 to 64 to keep the shear stress low enough. Compression failure beneath the central roller in a flexural test is of particularly of interest in this research because compression on the top of the composite leads to microbuckling which is very sensitive to the fibre/ matrix interface or adhesion strength. In addition, flexural test is also dependent on the fibre strength. If the fibres are degraded as result of atmospheric plasma fluorination (APF), the tensile strength drops, which then dominates the flexural

failure [206]. In this research, APF was carried out to modify carbon fibres and processed into carbon fibre/ PVDF composite laminates, therefore, if there was improvement in flexural properties that would mean that the fibre / matrix interface strength was improved. A decrease in flexural properties would mean that the fibres were damaged as a result of APF.

Chambers and McGarry [207] conducted flexural tests on a thin beam of pure polymer and found that the deformation due to shear was negligible. On the other hand, if the polymer was reinforced by unidirectional glass fibres, then shear deformation occurs at mid-thickness of the specimen. The authors observed that shear deformation gives rise to an increase in the flexural modulus whilst the flexural strength decreases. These authors also conducted a range of tests on two different types of glass fibre reinforced plastics with different ductilities (polyester and epoxy) with spans of 5.08 cm (2 in) to 43.18 cm (17 in) on a 0.635cm (0.25 in) thick composite and found a decrease of about 25% in the flexural strength for the composite containing a less ductile matrix whilst for the more ductile matrix, the strength remained essentially constant. A lack of ductility in a resin caused the laminate to fail at maximum fibre stress (often known as modulus of rupture, MOR) even at fairly low strains which leads to a decrease of tensile modulus with increasing stress. The equations to calculate the flexural strength and modulus can be found in Section 3.6.2. It is beyond the scope of this thesis to review all the work on flexural testing. In general, the span and span-to-thickness ratio should be chosen depending on the characteristic of the investigated material [208].

2.5.4.2 Short beam shear test

The short beam shear test (SBS) is a testing method used to determine the interlaminar shear strength (ILSS) of composites by maximising the shear stress component and

minimising any other forms of induced stresses such as tensile and compression in a specimen. When the generalised plane stresses are applied to a laminate, different layers tend to slide over each other because of the difference in the elastic constants. Since the layers are elastically connected through the faces, shear stresses are developed on the faces of each layer. The SBS test is very similar to the flexural test described in the previous section as the same bending mode applies but the test requires even less material, specimen preparation is minimal and the test is very simple to perform. ILSS is a common mechanical test used by many researchers (Section 2.2.4) to examine fibre/ matrix interaction. In this research, the objective of APF of carbon fibres is to enhance the bonding to PVDF, therefore, by using the short beam shear test, the fibre/ matrix strength of APF carbon fibre reinforced PVDF laminated can be examined. The disadvantages for the SBS test, however, is the sample size; because the sample size is so small it is widely accepted that the SBS test does not give material properties due to the free edge effects. When a load is applied to the beam, the transverse stresses that are produced are negligible in the region away from the laminate boundaries, therefore, making the SBS analysis on composite laminates adequate. However, the state of stress near a free boundary is not a plane stress state but a three-dimensional stress state. In many cases the transverse stresses, especially the transverse shear stress, may be quite large near the edge and influence the failure mechanism, such as matrix cracking at the free edge. These cracks then propagate into the laminate and initiate rupture causing premature failure of the laminate [209]. Cui et al. [210] stated that edge effects in unidirectional fibrous composites are negligible and, therefore, the influence of width is not thought to be important. Please see Ref. [211,212,213,214,215] for studies on interlaminar stresses at the free edge on finite-width angle-ply laminates. Other disadvantages of the SBS test are that the specimen is not loaded uniformly in shear and that there is no way to reliably measure strain and hence determine the shear modulus [216]. This is because the shear stiffness in fibre composites relative to the stiffness in

tension or compression along the fibre directions in polymer matrix composites is so small, which maximises the consequences of spurious tensile or compressive loads. In addition the fibre orientation must be precisely controlled and specimens must be aligned perfectly so to ensure non-shear stresses are kept to a minimum. The equations to calculate ILSS can be found in Section 3.6.2.

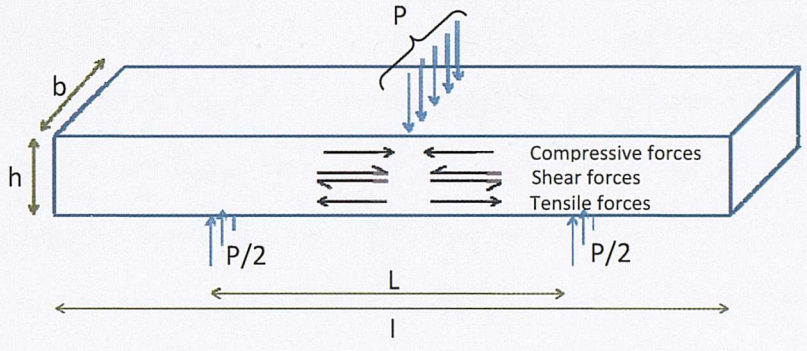


Fig. 2.18: Short beam shear test showing test configuration. Redrawn from MSc Composite Materials Course on Mechanical testing of Advanced Fibre Composites, Imperial College London, Sept 1995.

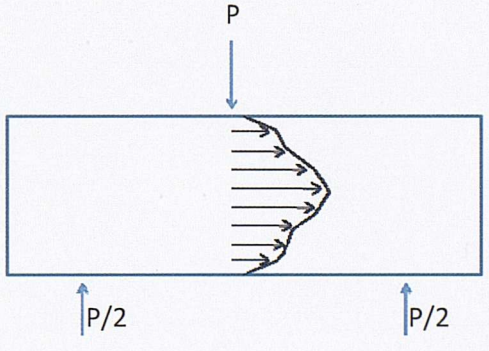


Fig. 2.19: Effect of shear stress distribution in a laminated specimen. Redrawn from MSc Composite Materials Course on Mechanical testing of Advanced Fibre Composites, Imperial College London, Sept 1995.

There are four possible failure mechanisms involved in a short beam shear test: tensile fracture, interlaminar shear, compressive/ fibre buckling or a mixed mode failure. Shear failure will take place in the midplane in the form of delamination (Fig. 2.18 and 2.19) due to the shear stress distribution. In order to maximise the probability of an

interlaminar shear failure, the S/h ratio is an important factor. This is because shear failure should arise before tensile or compressive failure occurs. With ductile thermoplastic matrices, because of their large ultimate strains to failure it may be impossible to obtain a shear failure. The recommendation in this case is that the smaller the span-to-thickness ratio, the greater the likelihood that the failure mode will be interlaminar shear. It should be noted that a continuous reduction of the S/h ratio is not a solution because the rollers would eventually impinge and specimens would then jam in the loading jig. Additionally, the shorter the beam, the greater the lateral forces that are applied to attain a particular skin strain and, consequentially, the greater the local indentation at the loading points and the greater the distortion of the longitudinal stress field. It should also be noted that due to the non-uniform stress state the shear strength obtained does not provide meaningful shear properties for design purposes and are often referred to as apparent interlaminar shear strength. However, it is still a useful tool for quality control of a particular composite manufacturing technique.

Chapter 3

Experimental

3.1 Materials

Two different types of commercially available continuous, high strength* and high strain* polyacrylonitrile (PAN) based carbon fibres were used for this research namely AS4 and T700. The properties of these fibres are summarised in Table 3.1.

Table 3.1: Summary of relevant properties of the carbon fibre used for this study*

Fibre type	Torayca® T700SC	HexTow™ AS4
Typical Fibre properties		
Filament	12000	12000
Tensile strength (MPa)	4900	4480
Tensile modulus (GPa)	230	231
Elongation (%)	2.1	1.8
Density (g/mm^3)	1.8	1.79
Typical epoxy composite properties (measured at room temperature)		
Tensile strength (MPa)	2550	2211
Tensile modulus (GPa)	135	141
Short Beam Shear Strength (MPa)	90	124

* HexTow AS4 carbon fibres product data sheet. Link in: http://www.hexcel.com/NR/rdonlyres/5659C134-6C31-463F-B86B-4B62DA0930EB/0/HexTow_AS4.pdf. Accessed on Dec 2007

Quaility of Torayca cabon fibres, commercial documentation – N°AQ.866 – 9. Sept 2003

The T700 carbon fibres were kindly supplied by Torayca® (Toray Industries, Tokyo, Japan) and the AS4 fibres by Hexcel Corporation (Duxford, Cambridge, UK). Although both carbon fibres were industrially oxidised, the Hexcel AS4 fibres were available in unsized form whereas the Torayca T700 fibres were only available with an applied sizing. The sizing, as discussed earlier (Section 2.2.5), allows easier handling and is commonly designed to give better compatibility to epoxy matrices. For the aim of the study, namely to provide adhesion to fluoropolymers, the sizing actually inhibits the interaction with fluoropolymers and was, therefore, removed. For the desizing process, 5 g batches of T700 carbon fibres were cut into three portions of approximately 2 m in length and packed into a cellulose extraction thimble (Single thickness, 33 mm*100 mm, Whatman International Ltd, Maidstone, UK) placed inside a Soxhlet apparatus and refluxed in acetone (VWR International Ltd, Lutterworth, UK) at 60 °C for 48 h. Fibres were then carefully removed using clean tweezers to prevent oil contamination from human skin, and was placed on a glass petri dish and dried in a vacuum oven for 24 h at 800 mbar and 60 °C in order to remove residual solvent.

The fluoropolymer matrix used for this research was the semi-crystalline melt processable fluorinated resin poly vinylidene fluoride (PVDF Kynar® 711, T_m= 170 °C), kindly supplied by Arkema (Serquigny, France). The surfactant used to stabilise an aqueous suspension of PVDF powder required for the continuously manufacturing of carbon fibre reinforced PVDF composites was Cremophor® A25 (BASF, Ludwigshafen, Germany). Gases used for the plasma modification were sulphur hexafluoride (SF_6), chlorodifluoromethane (CFC-Freon 22) and nitrogen- oxygen free (N_2). They were supplied by BOC (Surrey, UK).

3.2 Atmospheric plasma modification of carbon fibres

Atmospheric plasma treatments were performed in an Openair-Plasma-Technology system (single rotating FLUME Jet RD1004*, Plasmatreat, Steinhagen, Germany). The plasma jet was generated by ionising a feed gas mixture of N_2 and SF_6 (T700 fibres only) or chlorodifluoromethane (both T700 and AS4 fibres) in a 1:70 ratio and at a flow rate of 35 L / min creating a pressure drop of 2.3 bar at the jet nozzle. All atmospheric plasma treatments were operated with a power of 2.1 kW ($V = 296 \pm 3$ V, $I = 7 \pm 0.2$ A).

There are minimum requirements for the feed gas in terms of flow rate, pressure and density of the gas mixture, in order to sustain a stable plasma jet under atmospheric conditions. The fact that the sole density of SF_6 and CFC-Freon 22 are too high, nitrogen was used as a carrier gas. Trials with other inert gases, such as Helium and Argon, for use as a carrier gas were conducted and were found to be unstable with the atmospheric plasma device. Therefore, nitrogen was used as a carrier gas and since three different feed gases with different molecular weights are used, calibration factors set by the flow meter manufacturer† were taken into account to operate the plasma device. The actual flow rate of N_2+CFC that passed through the flow meter was to be multiplied by a correction factor of 0.1. For other gases, a table of correction factors can be found in the flow meter manufacturer's website‡‡‡‡.

* Please note the setup used in this research consists of a single plasma jet, multiple jet systems are commercially available.

† Gas Correlation Factors. Link in: http://www.keyinstruments.com/gas-correction-formulas.html. Accessed Nov 2004. **Please note according to the flow meter manufacturer that this correction factor is only accurate within ±10%.**

3.2.1 Atmospheric plasma treatment of carbon fibres in batch

Desized T700 and AS4 carbon fibres were atmospheric plasma treated in a batch process using the configuration shown in Fig. 3.1a. This configuration allows the fibres to be modified for any given length of time inside the 20 cm long borosilicate glass 3.3 unequal tee piece (PTU50/25, QVF Process System Ltd, Stafford, UK). The carbon fibre roving was positioned in tension using double sided tape onto a homemade aluminium frame and positioned at a distance of 15 mm from the plasma nozzle. From previous trial experiments, it was found that the most efficient distance between the plasma jet and the substrate for atmospheric pressure plasma treatment was between 12-15 mm. Also it was found that fluorinating carbon fibres in a semi-enclosed system generated a more confined environment and in turn was found to maximise the effectiveness of atmospheric plasma modification. A treatment duration of 4 min was chosen for batch treatment of T700 with N_2+SF_6 and T700 and AS4 with N_2+CFC. At the mean time three different treatment durations 0 (T0), 1 (T1), 2 (T2), 4 (T4), 8 (T8) min were chosen for batch treatment of T700 with N_2+CFC feed gas.

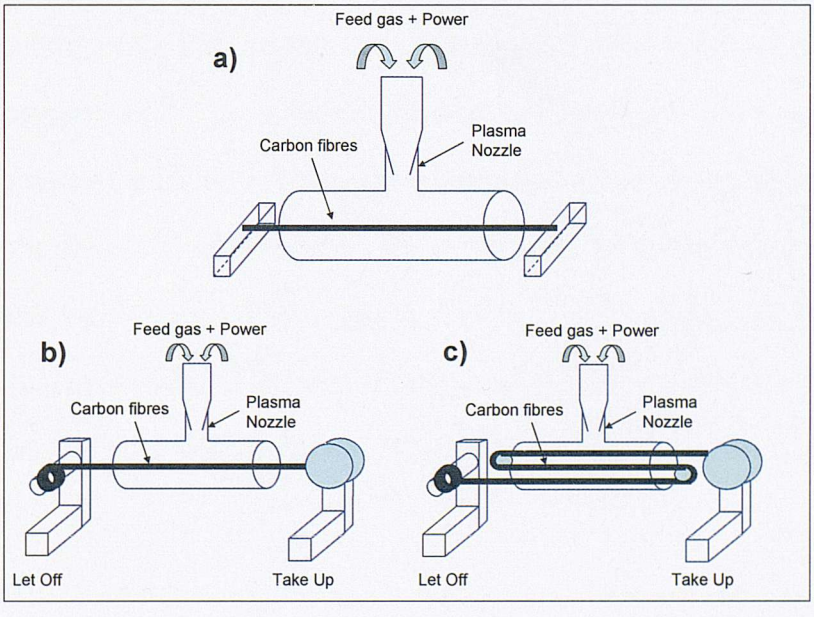


Fig. 3.1: Schematic illustrations of atmospheric plasma fluorination setup for: (a) batch setup, (b) continuous single sided setup, (c) continuous double sided setup

3.2.2 Continuous fluorination of carbon fibres in atmospheric plasma

Continuous atmospheric plasma fluorination (APF) was only performed on AS4 carbon fibres because, as discussed earlier, the sizing applied to the T700 fibres would have had to be removed prior to treatment, which was not feasible. AS4 is the only commercially available continuous unsized carbon fibres. Continuous desizing of T700 carbon fibres (and later on continuous fluorination and processing) at laboratory scale requires special attention, such as solvents, waste, quality control etc. Therefore, sized T700 fibres were not used for the continuous fluorination process.

Two different configurations were investigated for continuous APF of carbon fibres; among these the simplest configuration (Fig. 3.1b) was passing the fibres straight through the plasma jet at the slowest speed the take up device could be operated at, i.e. 0.15 m/min. In theory this should allow the maximum degree of fluorination. The fibres were being continuously treated but only one side of the roving was exposed to the jet. The corresponding residence time of the single sided APF treated carbon fibres within the glass chamber was 1.3 min. The configuration shown in Fig. 3.1c allows the fibres to be continuously fluorinated but now both sides of the carbon fibre roving were exposed to the plasma jet. The carbon fibres were redirected by means of phenolic resin roller pins allowing the fibres to be looped 3 times through the glass chamber, therefore, maximising the fibre exposure to APF. Three different treatment speeds of 0.15, 0.33 and 0.75 m/min were chosen. These speeds, other than 0.15 m/min, are used later on in Section 3.5 as processing speed to process carbon fibre reinforced PVDF. This corresponds to residence times within the glass chamber of 4 min, 1.8 min and 0.8 min, respectively.

3.3 Surface characterisation of carbon fibres

3.3.1 Dynamic contact angle measurements on carbon fibres

The modified Wilhelmy method (Fig. 3.2) [217,218] is a gravimetric method for the determination of dynamic contact angles between liquids and solids of any geometry.

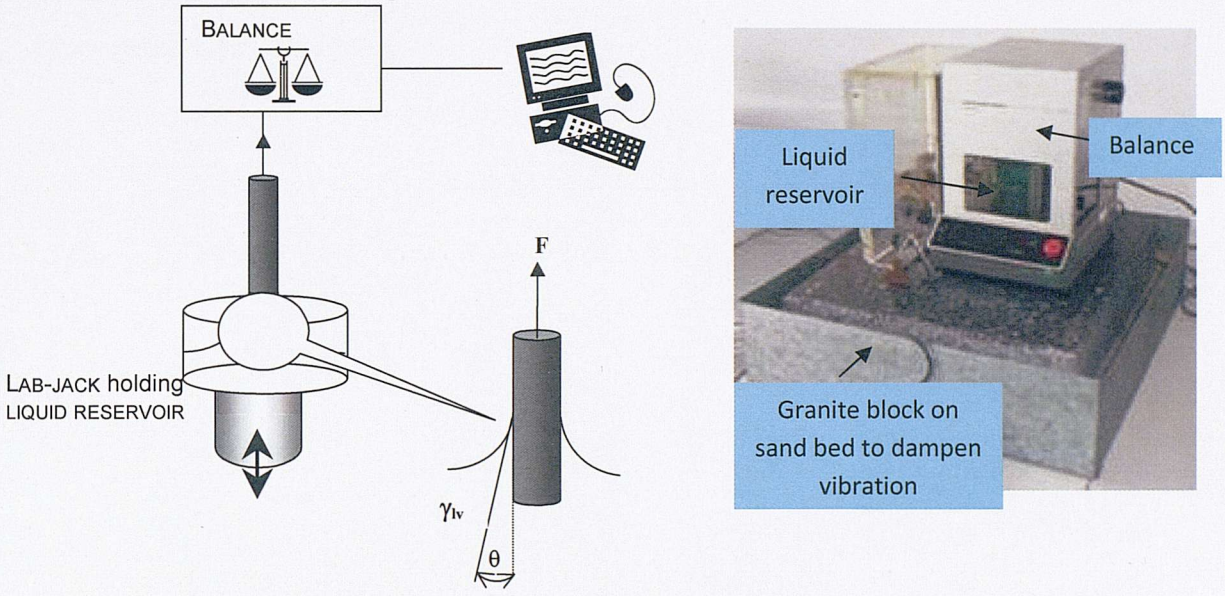


Fig. 3.2: Schematic illustrations [219] (left) of the modified Wilhelmy setup and photograph of the actual setup used (right)

The wetting force (mg) exerted on the fibre is measured as the fibre is immersed in or withdrawn from a liquid of a known surface tension. The advancing (θ_a) which corresponds to wetting a dry surface and the receding (θ_r) contact angles which corresponds to dewetting a wet surface are calculated from the mass change m measured during immersion and emersion of the fibres into and from each test liquid using the following equation:

$$\cos\theta = \frac{mg}{\pi d_f \gamma_l} \tag{3.1}$$

where d_f is the fibre diameter which is to be determined independently, g is the acceleration due to gravity and γ_l is the surface tension of the test liquid used.

3.3.1.1 Determination of the fibre diameter using the modified Wilhelmy-method

In order to determine the wettability of carbon fibres using the modified Wilhelmy-technique, the fibre diameter d_f must be known. The fibre diameter was also determined using the modified Wilhelmy technique using a liquid which spreads onto, i.e. completely wets, the fibres.

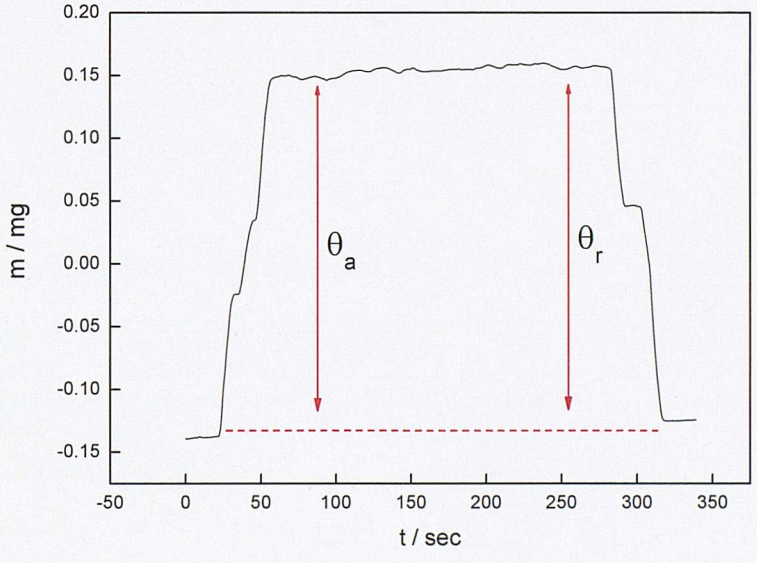


Fig. 3.3: Representative image of a typical weight change as function of time during fibre immersion and withdrawing from dodecane

n-Dodecane (γ_l = 25.4 mN/m, 99% purity, Fisher Scientific) was chosen as the liquid which wets the fibres completely i.e. cos θ = 1 (Eq. 3.3), and has a low evaporation rate. The absence of any contact angle hysteresis (exemplarily shown in Fig. 3.3) during the measurements with low surface tension liquids is a good indication of complete wetting. For each measurement 5 single fibres of equal length were attached to an aluminium carrier which was then placed into an ultramicrobalance (4504 MP8, Sartorius,

Göttingen, Germany; accuracy = 0.1 μg). A reservoir of test liquid was placed on an elevator underneath the fibres. The elevator was capable of ascending and descending at 0.1 mm/min. Readings from the ultramicrobalance were recorded continuously in real-time whilst the test liquid was being raised up towards the fibres. Once the fibres came into contact with the test liquid i.e. the fibres were wetted by the solvent, a mass change m was observed. The fibres were continued to be immersed, after the mass change had stabilised (typically for around 3 min) the motor was then reversed which lowered the elevator. The test liquid was then moved away from the fibres i.e. dewetting of the fibres occurred. The fibre diameter d_f was calculated using Eq. 3.2 (an example of the calculation can be found in Appendix A):

$$\cos\theta = \frac{mg}{nd\pi\gamma_l} \tag{3.2}$$

where g is the acceleration due to gravity, n is the number of fibres used and γ_l is the surface tension of the test liquid used. At least 25 single fibre samples were measured to obtain a statistical significant average. Values presented were averaged and errors are presented as standard deviations.

3.3.1.2 Determination of the fibre wettability using the modified Wilhelmy-method

Once the fibre diameter has been determined, the wetting behaviour of the fibres against different test liquids can then be quantified gravimetrically and the contact angles calculated using equation 3.1. A range of test liquids with different surface tensions were used in order to allow the determination of the surface tension γ of the modified carbon fibres. The test liquids used were deionised water (γ_l = 72.8 mN/m), formamide

(γ_l = 58.2 mN / m, 99 % purity, Fisher Scientific) and diiodomethane (γ_l = 50.8 mN / m, 99 % purity, Fisher Scientific).

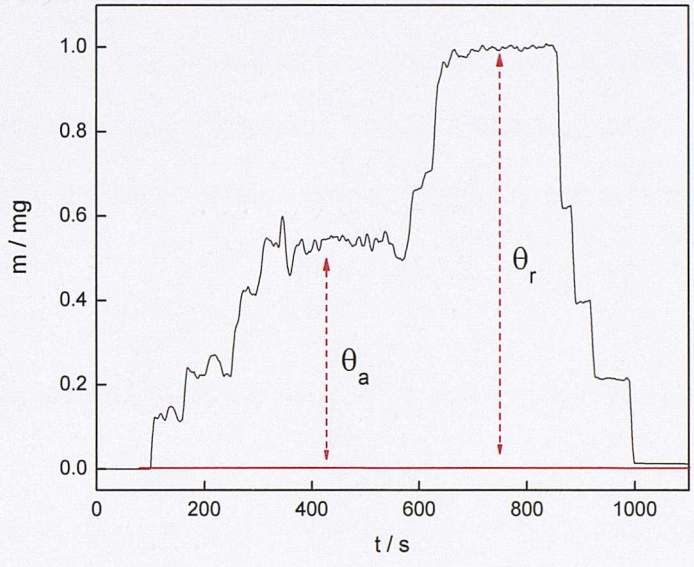


Fig. 3.4a: Representative image of a typical weight change as function of time during fibre immersion and withdrawing from H_2O on a partially wetted ($\theta < 90^o$) carbon fibre surface

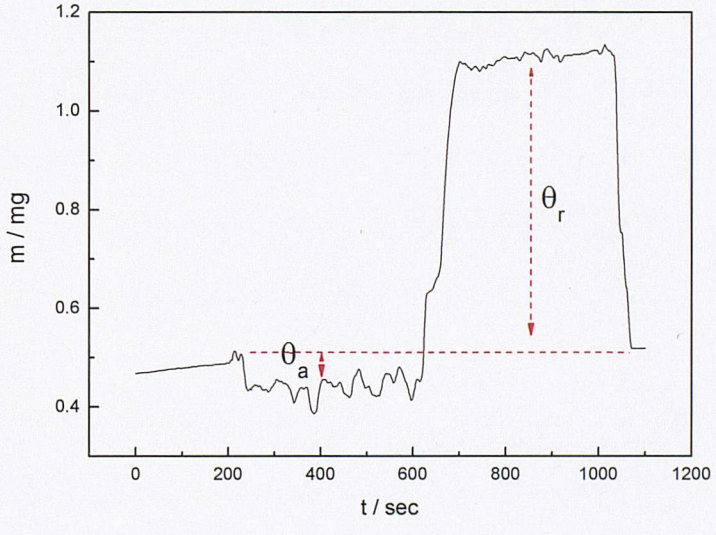


Fig. 3.4b: Representative image of a typical weight change as function of time during fibre immersion and withdrawing from H_2O on a hydrophobic ($\theta > 90^o$) carbon fibre surface

If the investigated carbon fibre is more hydrophilic ($\theta < 90°$), a positive mass change can be detected as the fibres immerse into water. A typical measurement is illustrated in Fig. 3.4a. On the other hand a negative mass change is detected when hydrophobic ($\theta > 90°$) carbon fibres are immersed into the water (Fig. 3.4b). Since an increase in C-F fluorine functionalities with a covalent bond character would result in an increase in the fibres surface hydrophobicity [220] and each measurement only requires 20 min, this technique has been the most useful technique to quickly assess whether fluorination has been successful.

3.3.1.3 Determination of the fibre surface free energy by contact angle models

The wetting properties of solid materials are of both fundamental and practical importance in the performance of materials and are governed by the solid surface energy. Although numerous techniques have been employed to characterise the surface tension of solids, the indirectly wetting technique, i.e. contact angle measurements, has remained one of the most commonly used. However there are limitations with the wetting technique especially for materials, such as natural fibres, that have high water absorption rates. In those circumstances, other techniques such as Inverse Gas Chromatography (IGC), are much better suited to determine the surface energetic properties [221]. Since carbon fibres do not fall into that category, it is possible to determine the surface energy of carbon fibres indirectly using wetting techniques.

The Young-Dupré equation links the thermodynamic work of adhesion W_a [222], i.e. the reversible work required to separate a unit area of interface of two different phases at equilibrium, with the wettability, i.e. the contact angle θ, and the surface tension of the wetting phase γ_l:

$$W_a = \gamma_l (1 + \cos\theta) \tag{3.3}$$

A range of comprehensive solid surface energy models have been developed, all of which focus on the estimation of the solid surface energy γ_s via physically acceptable combining rules in order to express the solid/ liquid interfacial tension γ_{sl}, defined as:

$$\gamma_{sl} = \gamma_s + \gamma_l - W_a \tag{3.4}$$

The theory of surface tension components originally initiated by the work of two scientists: 1) The Fowkes approach [223,224,225,226,227] and 2) The Neumann's equation-of-state (EoS) approach [228,229]. A more recent version of the surface tension component approach, the acid/base *AB* approach, was developed by van Oss et al. [230,231,232,233,234,235]. This approach separates physical from chemical interactions. It assumes that the overall surface tension of a compound is the sum of the physical interaction components of the surface tension γ^{LW} (Lifshitz/ van der Waals) and the chemical interaction or acid/base component γ^{AB} of the surface tension:

$$\gamma_s = \gamma_s^{LW} + \gamma_s^{AB} \qquad \text{or} \qquad \gamma_l = \gamma_l^{LW} + \gamma_l^{AB} \tag{3.5}$$

Since acid/ base interactions are intrinsically specific and depend on the complementary availability of corresponding sites at the interface, the *AB*-term is subdivided into an acid or electron acceptor γ^+ and a base or electron donor γ^- parameter of the surface tension:

$$\gamma_s^{AB} = 2\sqrt{\gamma_s^+ \gamma_s^-} \qquad \text{or} \qquad \gamma_l^{AB} = 2\sqrt{\gamma_l^+ \gamma_l^-} \tag{3.6}$$

The *LW*-component of the solid surface energy can be determined by measuring the contact angle of completely non-polar (or dispersive) liquids, such as diiodomethane, using:

$$\gamma_s^{LW} = \frac{\gamma_l(1+\cos\theta)^2}{4} \tag{3.7}$$

The acid/base approach combines all symmetrically and non-specifically forces in the *LW*-component and separates specifically and complementarily acting forces in the *AB*-component. Therefore, the total surface energy can be determined by measuring the contact angles of at least three test liquids with known surface tension components and parameters using:

$$\gamma_L(1+\cos\theta) = 2(\sqrt{\gamma_s^{LW}+\gamma_l^{LW}} + \sqrt{\gamma_s^{+}+\gamma_l^{-}} + \sqrt{\gamma_s^{-}+\gamma_l^{+}}) \tag{3.8}$$

However due to the presence of covalent C-F bonds in fluorinated carbon fibres where the water contact angle exceeds 90°, the *AB* approach does not provide valid results; negative acid γ^+ parameters are calculated. Therefore the Wu's and the Neumann's EoS approaches were used to determine the surface energy γ_s of fluorinated carbon fibres. Both tension models are based on the total surface interaction between two phases which has contribution from the dispersion and non-dispersion components [236]. This requires contact angles to be measured between a solid and at least two test liquids with known surface tensions and surface components.

The EoS approach assumes that the relationship between cos θ and γ_l is universal, i.e. the contact angle θ is solely determined by the solid γ_s and the liquid surface tension γ_l and is independent of the type and strength of the molecular interaction across the

liquid/ solid interface. The surface energy of a solid γ_s can be calculated by measuring the contact angle of any liquid with a known surface tension on a solid by combining the Young-Dupré equation (Eq. 3.3) with Neumann's (semi-empirical) EoS for the work of adhesion:

$$W_a = 2\sqrt{\gamma_l \gamma_s}\, e^{-\beta(\gamma_l - \gamma_s)^2} \tag{3.9}$$

where β is a constant, $\beta = 0.000115$ $(m^2/mJ)^2$.

The Wu's surface tension model [237] for estimating the surface free energy of fluorinated carbon fibres (γ_s) was calculated using the harmonic mean equation:

$$\gamma_l(1+\cos\theta) = \frac{4\gamma^d{}_s\gamma^d{}_l}{\gamma^d{}_s + \gamma^d{}_l} + \frac{4\gamma^p{}_s\gamma^p{}_l}{\gamma^p{}_s + \gamma^p{}_l} \tag{3.10}$$

where γ_l and γ_s are the surface tension of the liquids and the surface free energy of the solid, respectively. This approach is widely used to characterise the surface free energy of low-energy samples. The sum of γ^d and γ^p gives a good approximation of the total surface free energy γ_s:

$$\gamma_s = \gamma_s{}^d + \gamma_s{}^p \tag{3.11}$$

3.3.2 Zeta (ζ) –Potential measurements

Interfacial phenomena are important in almost every industrial process, from heterogeneous catalysis to the manufacturing of composite materials and from

environmental protection to medical technology. Therefore, knowledge about the presence of reactive functional surface groups is of general interest and measuring the zeta (ζ)-potential allow such information to be obtained. The method of measuring the electrokinetic or ζ-potential is dependent on the nature of the material and the knowledge of the ζ-potential can reduce the time needed to produce trial formulations and it is an aid in predicting long-term stability. For solid substrates, such as carbon fibres, the streaming potential technique is the most suitable method. If a solid is brought into contact with an aqueous electrolyte, the formation of an interfacial charge causes a rearrangement of the local free ions in the solution to produce a thin region of non-zero net charge density near the interface. The arrangement of the charges at the solid–liquid interface and the balancing counter ions in the liquid is usually referred to as the formation of an electrical double layer (EDL). The electric double layer is generally viewed as consisting of two layers: an immobile layer of ions opposite in sign to that of the surface (Helmholtz layer) and a diffuse layer stretching out into solution (Gouy Layer) [238,239]. The formation of the EDL (Fig. 3.5) due to the presence of a net charge on a surface, which affects the distribution of ions near that surface, resulting in an increase in concentration of counter ions [240,241].

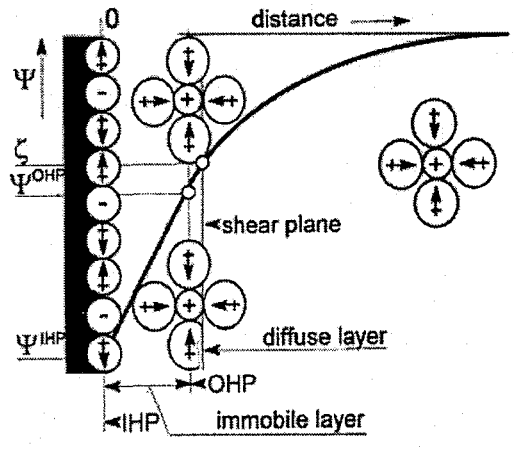


Fig. 3.5: Schematic illustration of an electrochemical double layer: Gouy-Chapman-Stern-Graham, GCSG Model [242]

ζ-potential is the electrical potential at the hydrodynamic plane of shear between the solid and the aqueous electrolyte. If a relative movement between the solid and the electrolyte solution is induced (in case of the streaming potential methods that is achieved by pumping a liquid through the packed fibre bed), the ions in diffusive part of the EDL is removed resulting in a shear plane at the border between the Helmholtz immobile layer and the diffusive layer as a result of a streaming potential. This gives rise to an electrical potential difference across the sample which can be measured. [243]. For a detailed theoretical description of the theory of EDL and ζ-potential please refer to Helmholtz-Smoluchowski equation [244,245].

The acid and basic surface character of a surface can be identified based on the shape of ζ = f(pH), (Fig. 3.6). For a solid containing acidic functional groups, at low pH the dissociation of acidic surface groups is suppressed. When pH increases, the increased dissociation of acidic surface groups causes an increase in the negative ζ- potential. In the case of basic groups, at high pH the dissociation of basic groups are suppressed. When pH decreases, the number of positively charged groups increases. A complete dissociation of acidic or basic functional groups is related to a plateau in the ζ-f(pH) curve. Non-polar solids have ζ=f(pH) shape without plateau due to the lack of acidic and basic dissociable groups and the increase in negative/positive ζ-potential with increasing/ decreasing pH is solely caused by the increasing adsorption of H^+/ OH^- ions, respectively [246]. The isoelectric point (iep) is the pH at which ζ=0 mV and therefore, allows the acidity or basicity of a solid surface to be measured [247]. The iep is determined by the function of the pKa concentration of all functional groups; the position of an iep at low pH indicates an acidic character of the solid surface and an iep at high pH signifies the surface contains dissociable basic surface groups [8].

ζ-Potential measurements allow the state, type and amount of dissociable surface functional groups on solid surfaces of interest to be estimated as well the dispersion forces proceeding from solid surfaces to be characterised [248]. It has been shown that the difference in the adsorption-free energies of electrolyte ions at the solid surface corresponds to the dispersive forces occurring at the solid/electrolyte interface [249]. ζ-potential measurements are a straight forward and reliable tool to predict the adhesive properties [250]; Bismarck et al. [251] has shown that an increasing difference of the ζ-potential plateau values obtained from $\zeta = f(pH)$ measurements, between both components i.e. reinforcement and matrix, means the measured adhesion strength also increases [17,251,252].

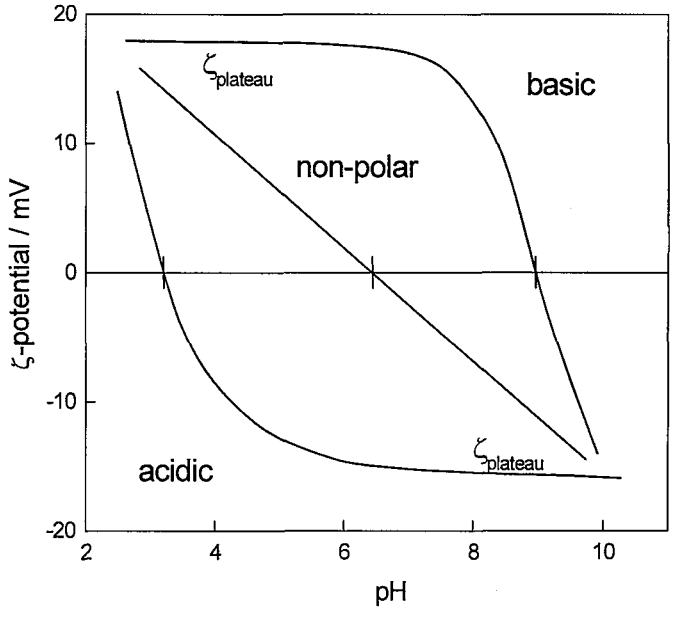


Fig. 3.6: Schematic illustration of a pH dependent ζ-potentials

The ζ-potential of carbon fibres was determined using the Electrokinetic Analyser (EKA, Anton Paar KG, Graz, Austria) based on the streaming potential method. A batch of carbon fibres (1.5 ± 0.2 g, approximately 1.5 m in length) was placed into a cylindrical glass cell (Fig. 3.7), where it was tightly sandwiched between two perforated

PMMA caps to separate the conducting fibres from the two perforated Ag/AgCl electrodes. The system was filled and rinsed with 1 mM KCl electrolyte solution. All entrapped air bubbles were removed from the cell at this stage. A pressure drop across the sample (increasing from 30 mbar to 150 mbar) was generated whilst the electrolyte was pumped through the cylindrical cell. The streaming potential that arose was first measured as a function of time to establish equilibrium using the two perforated Ag/AgCl electrodes. The pH-dependence of the ζ-potential was then measured starting from natural pH 5.7 to pH 3 and pH 10, respectively. The pH of the electrolyte was changed by adding 0.1 M HCl or 0.1 M KOH by means of an auto-titrating unit (RTU, Anton Paar KG, Graz, Austria) while the pH was measured using an in-situ pH probe and logged using a computer. The ζ-potential measurements were performed at 20 °C.

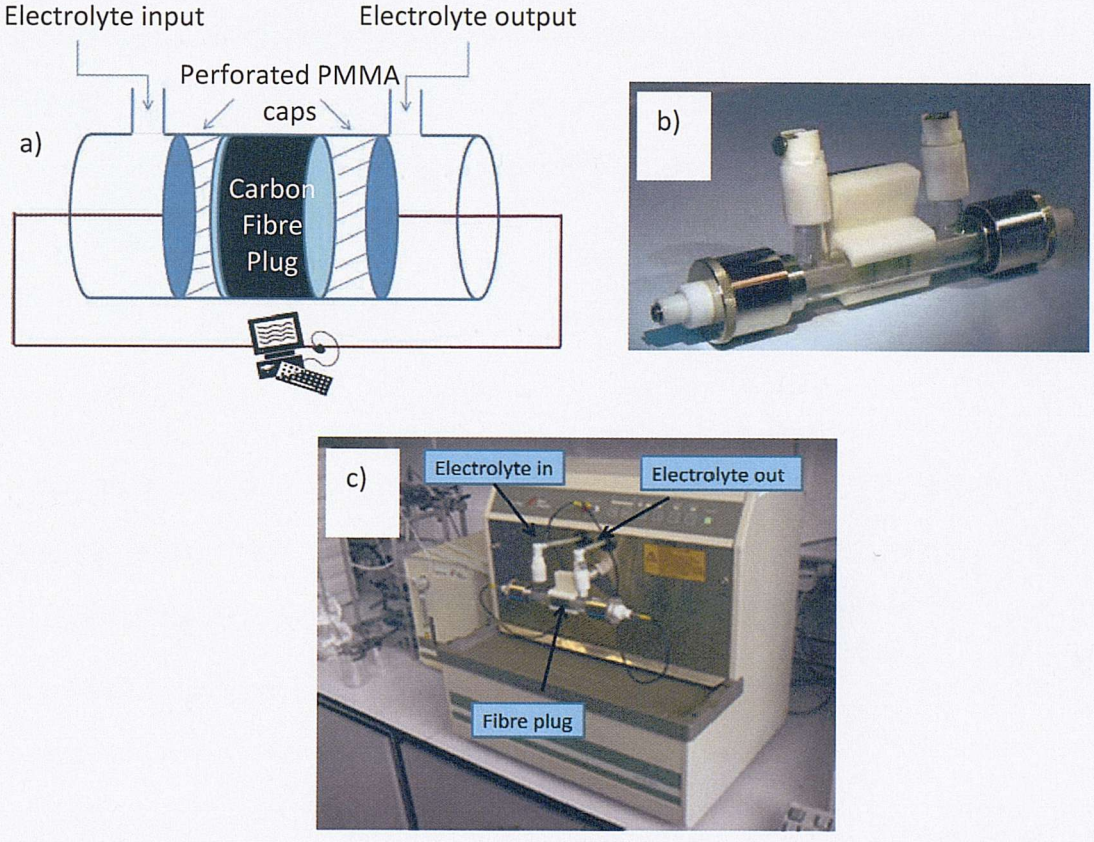


Fig. 3.7: Schematic illustrations of (a) the cylindrical glass cell setup and (b) its assembly for (c) ζ-potential measurements

3.3.3 Fibre surface composition: X-ray photoelectron spectroscopy

(The experimental work of the following section was conducted by Dr Adam F. Lee, Department of Chemistry, University of York as part of a research collaboration)

X-ray photoelectron spectroscopy, commonly known as XPS, is a technique that allows the composition of the outermost few atomic layers of solid surfaces to be analysed and, therefore, has been used to characterise the surface composition of carbon fibres within nanometres of the fibre surface [253,254]. XPS was judged by Seah and Briggs [255] as the most useful technique for modern surface analysis with a detection limit of about 0.5%. An extensive discussion of the basic principles involving XPS is beyond the scope of this chapter, for a more detailed explanation please refer to Ref. [255,256,257,258,259,260]. In general, XPS is a surface specific, non-destructive and surface sensitive technique to determine the chemical composition of solids by measuring the kinetic energy (KE) distribution of emitted photoelectrons.

$$A + h\nu \rightarrow A^+ + e^- \tag{3.12}$$

$$h\nu = BE + KE = BE + \frac{1}{2}mv^2 \tag{3.13}$$

where A is a atom within the material, $h\nu$ is the energy of the x-ray beam, A^+ is the ionised atom and e^- is the emitted photoelectron; m is the mass of the electron, v is the velocity of the electron and BE is the binding energy or also known as ionisation energy. Electrons may be ionised from any orbital with a binding energy less than the photo-energy of the x-ray beam.

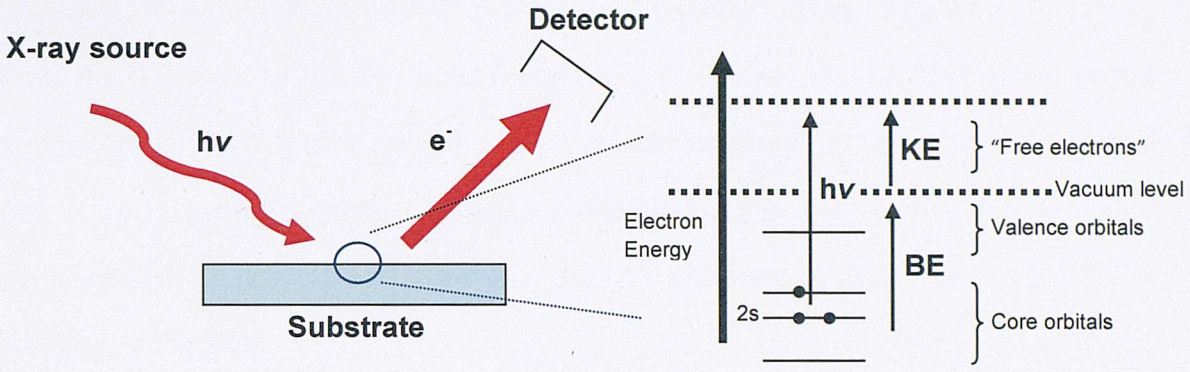


Fig. 3.8: Schematic illustration of the interaction between an x-ray beam and a substrate in a XPS system. Redrawn from BSc Chemistry Course, Queen Mary and Westfield College, University of London, Sept 2002.

During a measurement, a surface is exposed to a monochromatic x-ray beam under vacuum (Fig. 3.8 left, Eq. 3.12), which results in excited valence or core electrons ejected from an atom. The electrons are ejected within nanometres to the surface via an inelastic mean free path (IEMP) of about 0.5nm to 3nm. The IEMP is defined as the average distance that an electron will have to travel before it undergoes an inelastic collision with another of the matrix constituent atoms (Fig. 3.8, right) [261,262,263]. Therefore, very few electrons from depth greater than 2-3 times the IEMP will leave the bulk.

Complications due to charging in insulating samples is not an issue with virgin carbon fibres because they are conducting and the surface does not become positively charged. Charging effect is only common when the nature of samples are insulating because in that case more electrons are leaving the surface region than are replaced by those from the bulk. Therefore, in the case of virgin carbon fibres, it is uncommon to observe any of the usual effects due to charging such as the peak shifting to lower kinetic energies in XPS spectra [264].

During a measurement, all of the electrons were collected by the detector and analysed from the KE scale to the BE scale using Eq. 3.13 (More detailed information on the science behind how a XPS machine functions can be found in Ref. [265,266,267]). A plot of the intensity (counts/s (CPS)) of emitted photoelectrons of a given KE versus the associated BE gives a XP spectrum. A typical XP spectrum of fluorinated carbon fibres is shown is Fig. 3.9.

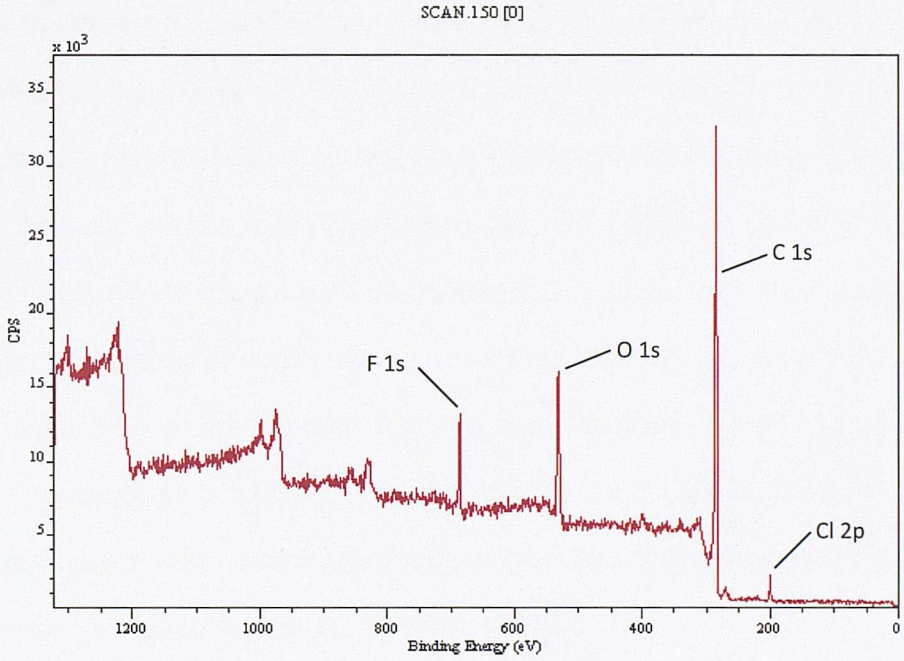


Fig. 3.9: Survey XP spectra (exemplary shown) of fluorinated carbon fibres

From the peak positions, the elemental composition of carbon fibre surfaces can be determined. From the area under the peak (normalised using appropriate sensitivity factors) the concentration of the element can be determined in at.-%. This allows for semi-quantitative analysis of the surface compositions of solids [268]. Furthermore, high resolution XP-spectra studies of the individual elements of interest from the survey XP spectra allow the chemical state and the bonding of the species to be investigated.

X-ray photoelectron spectra of atmospheric plasma fluorinated carbon fibres were recorded using a Kratos AXIS HSi instrument (Department of Chemistry, University of York, Heslington, York YO10 5DD, UK) at normal emission and at a take off angle of 90°. The device is equipped with a Mg K_α anode ($h\nu$ = 1253.6 eV), charge neutraliser relative to the sample surface. An analyser pass energy of 20 eV was used for the high resolution scans and 160 eV for wide scans, both with an X-ray power of 160 W. The elemental compositions of the fluorinated carbon fibres were determined using the response factors determined for the instrument by the manufacturer (C 1s = 0.318, Cl 2p= 0.964, F 1s = 1, Na 1s= 1.378, N 1s = 0.505, O 1s = 0.736, Si 2p= 0.371) from the wide scans and high resolution spectra. The instrument has not been recalibrated since new, but periodic checks have been conducted with standard samples. Spectral peak fitting was undertaken using CasaXPS Version 2.3.5 on Shirley background-subtracted spectra prior to fitting. In every case the minimum number of components was fitted using a common Gaussian-Lorentzian (70:30 mix) line shape for all elements. For each element a common peak width: C 1s = 1.4 eV, F 1s = 2.1 eV and O 1s = 2.3 eV was used. Comparative reference values for functional group binding energies were taken from the NIST Standard Reference Database [269].

3.3.4 Fibre surface morphology: SEM

Scanning electron microscopy, commonly known as SEM, was used to image the fibre surfaces to allow the surface morphology of fluorinated carbon fibres to be investigated [270]. A high energy beam of primary electrons was scanned across the sample in a raster scan by scan coils. The resulting raster scanning pattern is similar to that used in cathode-ray tube (CRT) television set in which the electron beam is 1) swept across the surface linearly in the *x* direction, 2) return to its starting position and 3) shift downward in the *y* direction by a standard increment. This process is repeated until a desired area of

the surface has been scanned. Signals are received above the surface, z direction, and stored digitally where it is ultimately converted to three-dimensional depth profile images that are ideal for surface structural studies. Several types of signals are produced from a surface in this process such as back scattered, secondary and Auger electrons [271,272].

A gold or chromium layer of coating is often required for the analysis of non-conductive samples. However, since carbon fibres are electrically conducting it is not necessary to coat them. Instead carbon fibres were prepared for SEM simply by cutting a small batch of carbon fibres (approximately 1 cm long of a 12k tow) and fixing them onto aluminium stubs using carbon tapes. They were examined using a LEO Gemini FEG-Scanning Electron Microscope (Oberkochen, Germany) at the Department of Materials, Imperial College London with backward-scattered primary electrons (SE2) mode of either 5 or 7 kV.

3.3.5 Fibre surface area: BET N_2 adsorption measurements

Brunauer-Emmett-Teller (BET) N_2 adsorption is a commonly used analytical technique used for determining the specific surface area of solids [273]. It has been used for the characterisation of fluorinated carbon fibres [274,275]. By measuring the BET specific surface area, A_s of fluorinated carbon fibres, it was able to assess the influence of atmospheric plasma fluorination on surface rougheness of the fibres. During the measurement, N_2 molecules are weakly adsorbed onto the fibre surface until saturation and the overall surface area A_s is determined from the total number of gas molecules that are adsorbed to the surface at a given pressure using the following equation:

$$\frac{\frac{P}{P_0}}{n_a(1-\frac{P}{P_0})} = \frac{1}{n_m C} + \frac{C-1}{n_m C}\frac{P}{P_0} \tag{3.14}$$

where $\frac{P}{P_0}$ is the relative pressure, n_a and n_m are the number of gas adsorbed and specific monolayer capacity, respectively [276].

Up to 2 g of carbon fibres with a length of approximately 2.5 m were packed into a glass vessel and degassed at 120 °C for 8 h. Measurements were conducted using a Micromeritics ASAP 2010 analyser (Micromeritics UK Ltd., Bedfordshire, England) using oxygen free N_2. The surface area of the carbon fibres A_s was determined according to the industrial standard ISO 9277 [277]. This was done by calculating the gradient $b = \frac{\Delta y}{\Delta x} = \frac{C-1}{n_m C}$ and the y-intercept $a = \frac{1}{n_m C}$ by plotting $\frac{\frac{P}{P_0}}{n_a(1-\frac{P}{P_0})} vs \frac{P}{P_0}$ which gives a straight line $y = a + bx$ within the relative pressure range $\frac{P}{P_0}$ from 0.05 to 0.3.

3.3.6 Characterisation of the wetting behaviour of single carbon fibres by fluoropolymer melts

An understanding of the wetting phenomena of polymers on reinforcing fibres allows prediction of the interfacial behaviour [278,279]. Although the wettability of carbon fibres can be measured gravimetrically using the modified Wilhelmy method (as described previously) against test liquids, the Wilhelmy method is not really that suited to determine the wettability of very thin fibres by polymer melts. This is because of the

viscosity and temperatures involved. A method that used a drop on fibre system was reported by Bucher and Hinkley [280] and Mayer et al. [281] as a direct measurement of fibre-resin interfacial properties. Also the authors correlated findings on interfacial properties findings to the mechanical properties of continuous fibre composites. However, for a drop on fibre system, the better the wettability of the polymer melts on the fibre, the more difficult the determination of the droplet perimeter using direct observation of microscopic images [282]. This is because the contact angle determined from droplets on the fibres is very sensitive to the errors made from determining the drop dimensions. A solution to maximise the accuracy over the conventional maximum drop length-height method was proposed by Song et al. [276]. The authors developed the generalised drop length-height method based on a drop-on-fibre system to measure the contact angle of liquids on single carbon fibres. The advantage of the generalised drop length-height method (based on the principle of the Laplace-Young equation, neglecting the effect of gravity) is that contact angle is calculated from the extracted drop profile of the entire droplet without the requirement to determine the maximum drop length. As a result, the accuracy of the method to determine the contact angle of liquid on fibres was increased by reducing the statistical error and improved the reliability and accuracy of the measurement.

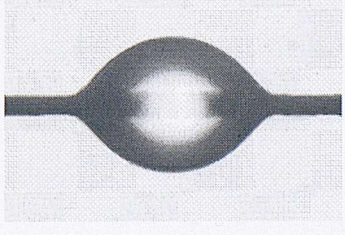


Fig. 3.10: A representative microscopic image showing a PVDF melt droplet on a carbon fibre at 205 °C

Three single fibres were fixed under tension on a stainless steel washer which was used as a supporting frame using an epoxy adhesive (Adhesive weld, J-B Weld, Slough, UK) and cured for 24 h. The fixed carbon fibres were dipped into a pool of PVDF powder and

the excess polymer was shaken off. For easier handling, the powder impregnated fibres were then heated to 200 °C on a hotplate to pre-melt the PVDF before cooling to room temperature. To examine polymer melt droplets on the fibres, the impregnated fibres were placed in a hot stage (THM600, Linkam Scientific Instruments, Surrey, UK), heated to 205 °C and held for at least 15 min to allow the droplets to reach equilibrium. The hot stage was placed under an optical microscope (BH2, Olympus, Tokyo, Japan) and digital images of melted fluoroplymer droplets on the carbon fibre were captured (DP70, Olympus, Tokyo, Japan)(Fig. 3.10). The contact angles were determined from at least 40 captured images in order to obtain a statistically significant average.

3.4 Bulk characterisation of carbon fibres

3.4.1 Raman spectroscopy of carbon fibres

Raman spectroscopy is a vibrational spectroscopic technique which is defined by a non-zero change in polarisability during a vibration. When photons are shone upon a molecule, the photons can be absorbed or scattered. The process of photon absorption requires that the energy of the incident photon is equal to the energy difference between the two states of the molecule. The two states are accompanied by a change in the dipole moment of the molecule. This leads to the molecule being excited from the vibrational state to a virtual state (Fig. 3.11). The virtual state system is very short lived and relaxes from this virtual state by the emission of photons. The Raman Effect is the exchange in energy between the incident and emitted radiation caused by the inelastic scattering of photons [283].

Two prominent Raman-active modes can be observed in Raman spectra of carbon fibres. The Raman band at 1580 cm^{-1} corresponds to E_{2g} mode (Fig. 3.12). This band had been

identified as the deformation (D) mode of the hexagonal C_6 carbon ring structure with E_{2g} symmetry, commonly observed in graphite crystal layers [284]. Polycrystalline graphitic mode (G) exhibits an additional peak at 1355 cm^{-1}, corresponding to the A_{1g} mode and is related to the graphitic mode. The ratio of the intensities of the two observed bands at around 1355 cm^{-1} (G) and 1580 cm^{-1} (D) is directly related to the amount of defective and crystalline modes in the carbon fibre sample. The ratio between the defective (d) and the graphitic band (g) also measures quantities including edge dislocations, vacancies and crystal edges. More simply stated, it is proportional to the number of atoms of a graphitic plane having one non-graphitic bond [285].

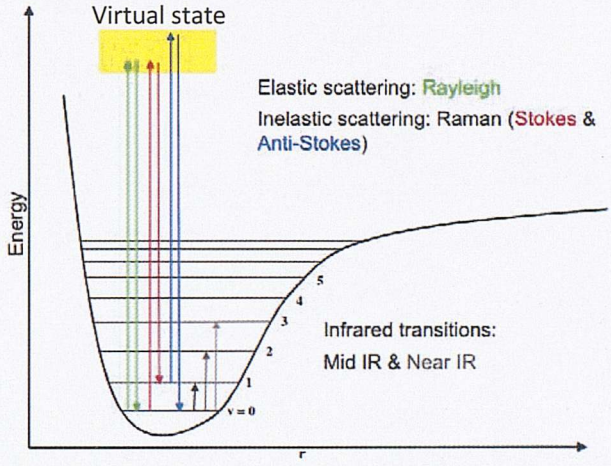


Fig. 3.11: Schematic representation of the potential energy of a diatomic molecule showing typical Raman and IR transitions [286]

Raman spectra of carbon fibres were acquired using a He-Ne laser at 634 nm with a LabRam Infinity Analytical Raman Spectrometer (Jobin Yvon Horiba, Middlesex, UK in the Department of Chemistry, Imperial College London). The laser spot size was reduced to a minimum while the laser power was at its maximum. At least 5 spectra were recorded at different spots of the same sample and averaged. Aperture at 50 μm with an acquisition time of 20 s and a diffraction gradient of 60 mm^{-1} were kept constant throughout the measurements at room temperature whilst scanning over a spectra ranging from 100-3000 cm^{-1}. The experimental results of Raman spectra were peak fitted

using a mixed Gaussian-Lorentzian (G/L ratio of 30:70, the fitting procedures as well as an example of a typically fitted spectrum can be found in Appendix B) curve in order to determine the peak intensities and Raman shifts. All measurements were performed at room temperature.

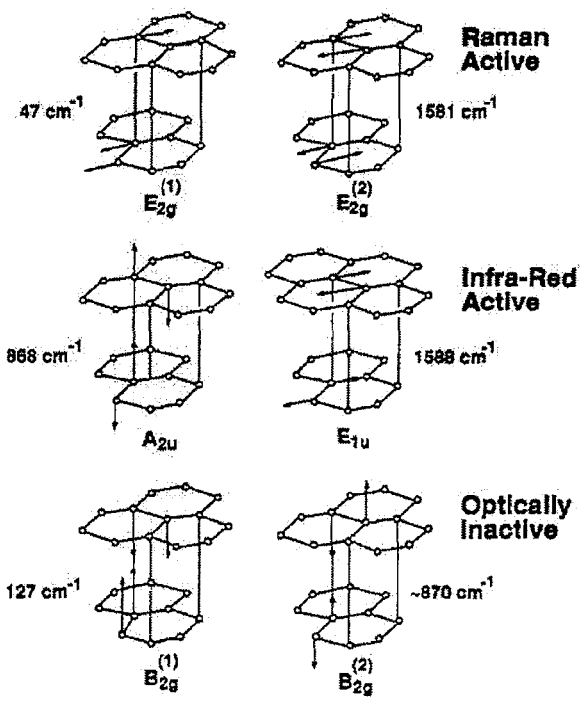


Fig. 3.12: Illustration of vibrational modes for single-crystal graphite. The diagram is adapted from Ref. [287]; the $B_{2g}^{(2)}$ is predicted but not yet observed experimentally

3.4.2 X-ray Diffraction (XRD) analysis of carbon fibres

(The XRD-spectra were recorded by Mr Richard Sweeney, Department of Materials, Imperial College London)

X-ray diffraction (XRD) is a versatile, non-destructive technique that allows the crystallographic structure of materials to be determined [288]. A crystal lattice is a regular three-dimensional distribution of atoms in space. These are arranged so that they form a series of parallel planes separated from one another by a distance *d*, which varies according to the nature of the material. In a crystal, planes exist in a number of different

orientations. X-rays are diffracted by crystals because the spacing between atoms is similar to the wavelength of X-rays. Bragg's Law (Eq. 3.15) explains the diffraction of X-rays as reflection on the lattice planes in a crystal (Fig. 3.14) [289,290].

$$n\lambda = 2d\sin\theta \tag{3.15}$$

When a monochromatic X-ray beam with wavelength λ is projected onto a crystalline material at an angle θ, diffraction occurs and is specific to the distance travelled by the rays reflected from crystal planes by a complete integer n of the light wavelength (Fig. 3.13).

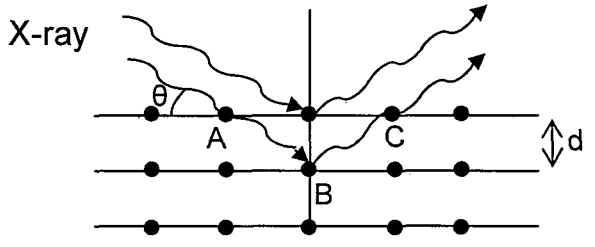


Fig. 3.13: Schematic illustration of a X-ray incident beam diffracting from crystal planes, obeying Bragg's Law [291]

A small aligned fibre batch was clamped flat onto a single crystal silicon wafer and aligned perpendicular to the incident X-ray beam. XRD analysis was undertaken using an automated powder diffractometer (Philips PW1700, Amsterdam, The Netherlands, in the Department of Materials, Imperial College London) operated at 40 kV and 40 mA with a secondary graphite crystal monochromator and Cu-K_α source, scanning between 5-80° in 0.04° steps. The crystallite size (L_c) which reflects the structural order, was determined using the Scherrer equation [292,293]:

$$L_c = \frac{K\lambda}{\beta cos\theta} \tag{3.16}$$

where β is the full width at half maximum of the carbon diffraction peak, K= 0.91 is a constant, λ is the X-ray wavelength and θ is the carbon peak position.

3.4.3 Electrical conductivity of carbon fibres

Carbon fibres are electrically conductive because of the delocalisation of π-bond electrons above and below the 6 member-carbon ring. These electrons are free to move and so are able to conduct electricity through the interlayer sheets of the graphite structure. However, fluorination was reported to lower the conductivity of carbon fibres significantly [294,295] and therefore the impact of atmospheric plasma fluorination on the conductivity of carbon fibres was studied.

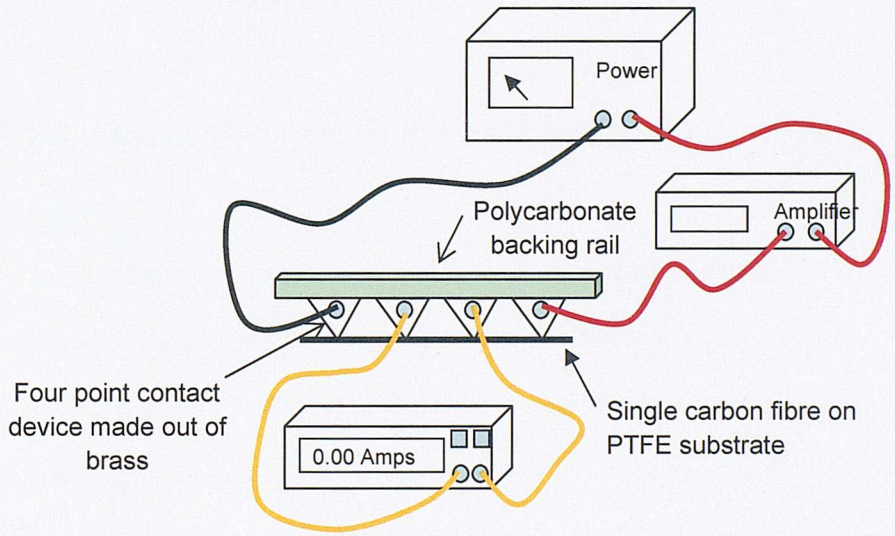


Fig. 3.14: Schematic illustration of the four point method (note: the schematic is not to scale)

The four-point method (Fig. 3.14) was used to determine the electrical conductivity of single carbon fibres, which eliminates problems of contact resistance of carbon fibres [296]. A single carbon fibre with a minimum length of 6 cm was carefully isolated from the 12K fibre bundle using clean tweezers and placed onto a Teflon sheet. The four point contact device was then carefully placed onto the single carbon fibre in order to

try not to break it and a constant amplified DC voltage (Krohn-Hite Model 7500 amplifier, Brockton, USA) was passed through the carbon fibre. The current across the two-point sector was then recorded using a digital multimeter (Keithley 195A, Ohio, USA). The electrical resistance (R) of carbon fibres was calculated using Ohm's law. The resistivity (ρ) of a single filament was calculated using the fibre length (l= 2 cm) and the previously measured fibre diameter ($d_f \approx$ 7 μm) (see section 3.3.1.1) using the following equation:

$$\rho = \frac{R\pi d^2}{4l} = \frac{U\pi d^2}{I4l} = \frac{1}{\kappa} \tag{3.17}$$

where κ is the specific conductivity, U is the applied voltage and I is the measured current.

3.4.4 Single fibre tensile strength measurements

From a practical point of view, the mechanical performance of unidirectional fibre reinforced composite is dominated by the properties of the fibre since the carbon fibres bear the load in a composite. When a single fibre in an unimpregnated bundle of fibres breaks, the broken fibre sheds its stress so the load is equally shared among the remaining fibres in the bundle. This is commonly referred to as Equal Load Sharing (ELS) [297]. However, when a single fibre breaks in a fibre reinforced composite, load sharing among the rest of the fibres is restrained by the matrix. In this case stress is redirected back into the broken fibre by plain shear interaction with the matrix at the interface. The matrix localises and redistributes the load, this overload is then carried by the fibres nearest to the broken fibre. This phenomenon is known as Local Load Sharing (LLS) [298]. In high loading structural applications the composite may exceed its

loading limit, which creates a knock on effect from fractured fibres and eventually results in the failure of the composite. Therefore, the impact of fibre modifications on tensile properties of the treated carbon fibres must be characterised.

The effect of fluorination on the tensile strength of carbon fibres was determined using a tensile stress tester (TST 350 Tensile Stress Testing System, Linkam Scientific Instruments, Surrey, UK) in the Department of Chemistry, Imperial College London, equipped with a 20 N load cell following the ISO standard 11566 [299]. A single carbon fibre was glued onto a paper frame using cyanoacrylate adhesive (Industrial Grade Superglue, Everbuild Building Products Ltd, Leeds, UK) (Fig. 3.15). Different gauge lengths, i.e. free fibre length of 20, 25, 30, 40 and 50 mm were tested (only a gauge length of 25 mm was chosen for qualitative ranking of the fibres used in the initial batch AP fluorination). The single fibre was loaded at a rate of 0.01 mm s^{-1} until the fibre failed while the loading force versus displacement were logged using a computer. The corresponding force and displacement at break are used to determine the tensile strength σ_f (Eq. 3.18) of a single carbon fibre, F is the measured tensile force (N) at break and A_f is the fibre cross-sectional area (mm^2), determined using the modified Wilhelmy method (section 3.3.1.1), L_0 is the original length of the fibre and ΔL is the change in length of the fibre when subjected to an applied force.

$$\sigma_f = \frac{F}{A_f} \tag{3.18}$$

All measurements were repeated on at least 25 different samples of the modified fibres to obtain a statistical average. The errors presented are standard errors.

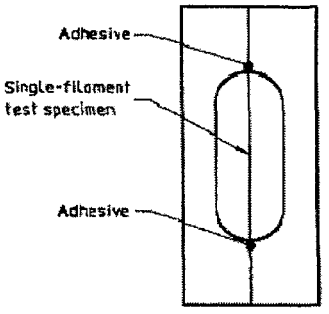


Fig. 3.15: Schematic illustration of single fibre tensile test specimen

The statistical distribution of the fibre strengths is commonly analysed using the two-parameter Weibull cumulative distribution [300] and was carried out for the continuous AP fluorinated carbon fibres using Eq. (3.19):

$$P_{f(L)} = 1 - \exp[-L(\frac{\sigma}{\sigma_0})^w] \tag{3.19}$$

where $P_{f(L)}$ is the probability of failure of a fibre of length L at a stress less than or equal to σ, σ_0 is the Weibull scale parameter or characteristic stress and w is the shape parameter or Weibull modulus which describes the variability of the failure strength. Weibull statistics assume that a single carbon fibre of L length has independent links of arbitrary unit length, each link or segment has equal probability of failing or withstanding a given stress level. Rearranging the two-parameter Weibull cumulative distribution (Eq. 3.20) leads to:

$$lnln\left(\frac{1}{1-P_f}\right) = w ln\sigma - w ln\sigma_0 + lnL \tag{3.20}$$

The equation allows for the determination of the Weibull scale and shape parameters by plotting $\ln\ln(1 / 1\text{-}P_f)$ as a function of $\ln \sigma$. The gradient is w and the intercept is σ_0. Once the Weibull parameters have been established from tests on shorter fibres, the tensile strength as well as the probability of the fibres to fail at a given length can be predicted using the following equation:

$$\sigma_{0(2)} = \sigma_{0(1)}\left(\frac{L_1}{L_2}\right)^{1/w} \tag{3.21}$$

where $\sigma_{0(2)}$ and $\sigma_{0(1)}$ are the lengths for L_2 and L_1, respectively.

3.4.5 PVDF crystallinity in the presence of atmospheric plasma fluorinated carbon fibres

Whether or not a transcrystalline phase develops around the (atmospheric plasma fluorinated) carbon fibres upon cooling of the PVDF melt to room temperature was investigated using a similar setup to that used to determine the direct wetting behaviour of single fibres (Section 3.3.7). In this case two fibres were fixed closely together under tension on a stainless steel washer using an epoxy adhesive. The fixed carbon fibres were dipped into a pool of PVDF powder and the excess polymer was shaken off. To examine the effect of crystallisation on carbon fibres, the impregnated fibres were heated to 200 °C (processing temperature) at 99 °C/min and held for 15 min before cooling to 180 °C (slightly above the melting temperature) at 10 °C/min and held for a further 5 min. The crystallisation behaviour of the PVDF droplets between the two fibres was observed under an optical microscope. During this time two images/s were captured while cooling the melt at 10 °C/min down to 120 °C (below the crystallisation temperature). At this temperature the sample was held for another 5 min.

Differential scanning calorimetry (DSC) (TA Instruments Q2000 DSC, Intertek ASG Laboratory, Manchester, UK), which is a thermal analysis technique that measures heat flow to and from a specimen as a function of time and temperature (Fig. 3.16) was used to determine the melting/ recrystallisation behaviour of PVDF droplets on carbon fibres as well as carbon fibre reinforced PVDF composites. There are four crystalline phases of PVDF: form I (alpha, α phase), form II (beta, β phase) and two forms of III (γ phase). A typical double melting peak was observed on the on the DSC curve of the as received PVDF polymer (Fig. 3.16). This was first observed by Kawai [301] and corresponds to the α (168 °C) and β phase (170 °C) of the PVDF chain configuration (Fig. 3.17).This is due to inversion of monomer units, which is influenced by the way PVDF is polymerised [302].

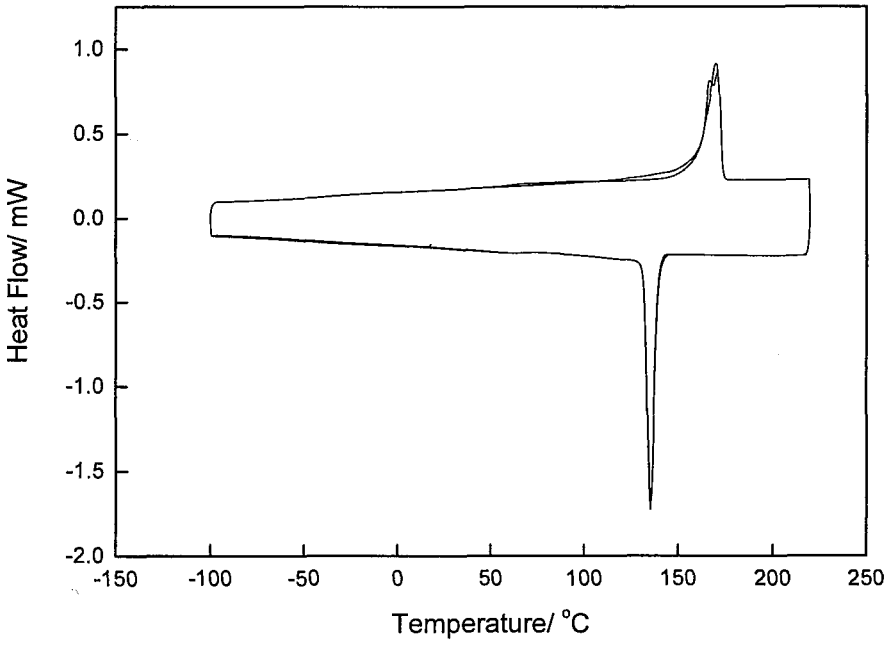


Fig. 3.16: A representative DSC curve of as received PVDF powder

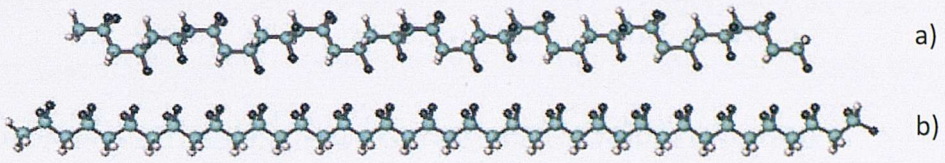


Fig. 3.17: View of a) alpha-PVDF chain and b) beta-PVDF chain. The diagram is adapted from Ref. [303]

The dynamic DSC scans were performed in a nitrogen atmosphere at a heating rate of 10 °C/min over the range from -100 to 220 °C. An appropriate amount of sample (typically 5 mg) was sealed in a tezro-aluminium pan and placed in the heating chamber together with an empty pan used as the reference. The melting temperature (T_m) and heat of melting (ΔH_m) were determined from the heat flow curves. The degree of crystallinity (X_c) was calculated as follows:

$$X_c = \frac{\Delta H_m}{H_f^0} 100\% \tag{3.22}$$

where H_f^0 is the heat of fusion of 100 % crystalline PVDF (104.5 J/g) [304].

3.5 Fabrication of carbon fibre reinforced PVDF Composites

3.5.1 Inline modification and manufacturing

Unidirectional (UD) unsized carbon fibre reinforced PVDF tape with a fibre volume content of 60 % was manufactured using a home built modular laboratory scale composite production line (CPL) built by the author and his co-workers in the research

group* (Fig. 3.18) based on the powder impregnation technique used for thermoplastic composites manufacturing [305,306,307,308,309,310]. This technique is commonly used to produce continuous fibre reinforced thermoplastic polymers such as PP, PA6, PPS, PEI and PEEK and can be applied in a range resin contents. The product is a highly flexible thin composite tape with a dimension of 12.5 mm width and 0.1 mm thick and can be used for fabric, braid and laminated panels. A real life example made from continuous fibre reinforced thermoplastic materials would be the bumper of a BMW M3†.

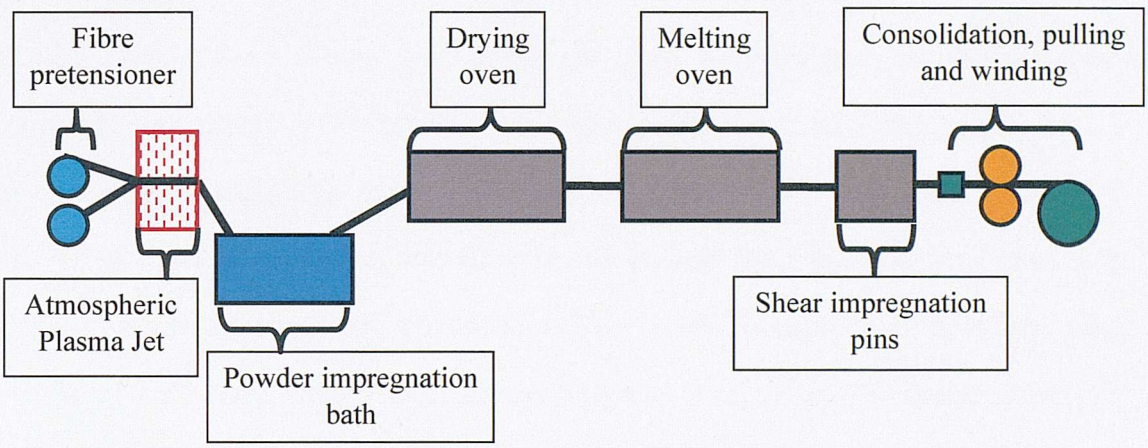


Fig. 3.18: Schematic illustration of the laboratory scale line for the production of UD fibre reinforced thermoplastic polymers

* A video of the home build modular laboratory scale composite production line in operation can be found on the author's group website: Research: Polymer and Composites Engineering. Link in: http://www3.imperial.ac.uk/polymersandcompositesengineering/researchareas/highperformancecomposites/kingsley Accessed on 18.03.08.

† Hexcel Thermoplastic TowFlex Featured in BMW M3 Bumper: Link in: http://composite.about.com/library/PR/2001/blhexcel21.htm. Accessed on 08.09.08

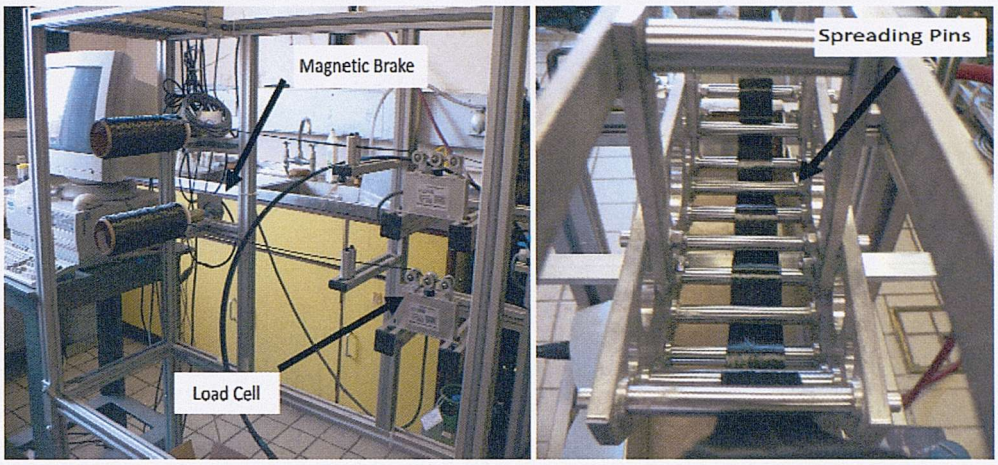


Fig. 3.19: A representative example of photographic images of fibre pretension unit (left) and spreading pins to be immersed into the impreganation bath

A 12K carbon fibre roving was taken off from a modulated tension controlled pretension unit (DTH-6100 Ogura Clutch, Japan) (Fig. 3.19, left) and passed through the continuous atmospheric plasma treatment system (section 3.2.2) over a series of set pins to promote spreading of the fibre in the powder impregnation bath (Fig. 3.19, right). The impregnation bath contained a 9 wt-% PVDF suspension stabilised using 2 wt-% of surfactant with respect to the polymer in 2.5 L of deionised water. The polymer powder impregnated fibre tow was then passed through an infra-red heated drying oven operated at 100 °C in order to dry off the water before entering an infra-red heated (Carbon Infrared Emitter CIR®, Heraeus Noblelight GmbH, Germany) home built melting oven operating at 220 °C in order to melt the polymer which causes the melt impregnation of the fibres (Fig. 3.20, left).

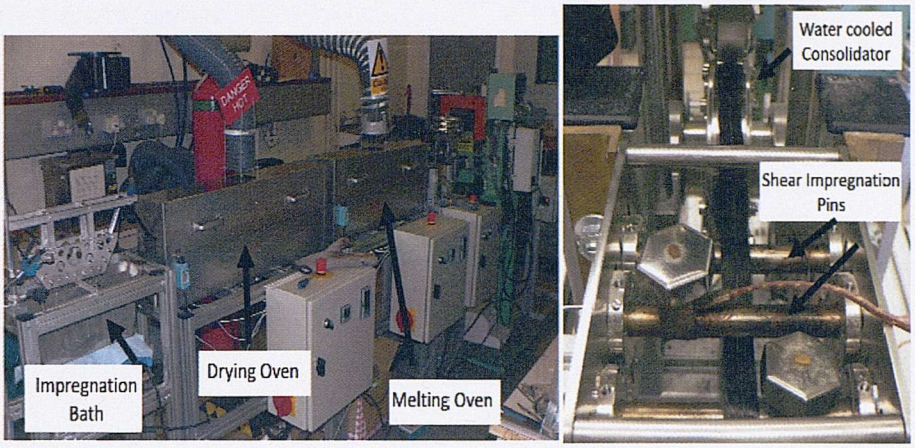


Fig. 3.20: A representative example of photographic images of IR ovens (left), cartridge heaters and consolidator (right)

The polymer melt impregnated fibre tow was then passed over a set of three heated shear impregnation pins (220 °C) (Fig. 3.20, right) to further spread the molten polymer along the fibre tow before being consolidated by water cooled rollers (Fig. 3.18) and into a continuous unidirectional carbon fibre reinforced composite tape with dimensions of 12 mm width and 0.1 mm thickness. Finally the tape was wound up onto a spool of a diameter of 15 cm. Three different manufacturing speeds (0.33 m/min, 0.75 m/min and 1.0 m/min) were chosen to consider with the speeds found to produce APF carbon fibres with varying fluorine content. The processing speed was controlled using a belt-drive pulling unit (Model 110-3, RDN manufacturing Co. lllonis, USA), which also determines the residual time (1.8 min, 0.8 min and 0.6 min) of the carbon fibres within the glass chamber for APF.

3.5.2 Quality control of the produced carbon fibre/ PVDF composite tape

Various methods were used to ensure the quality of the manufactured composite tape. Samples of the polymer impregnated fibre tow were taken at different stages during the drying (Fig. 3.21a) and melting process (Fig. 3.21b) from the CPL. The samples were

investigated using an optical microscope (BH2, Olympus, Tokyo, Japan). This allows the optical inspection of the polymer-impregnated fibre tow to ensure the temperature in the drying and the melting ovens are adequate with respect to the processing speed.

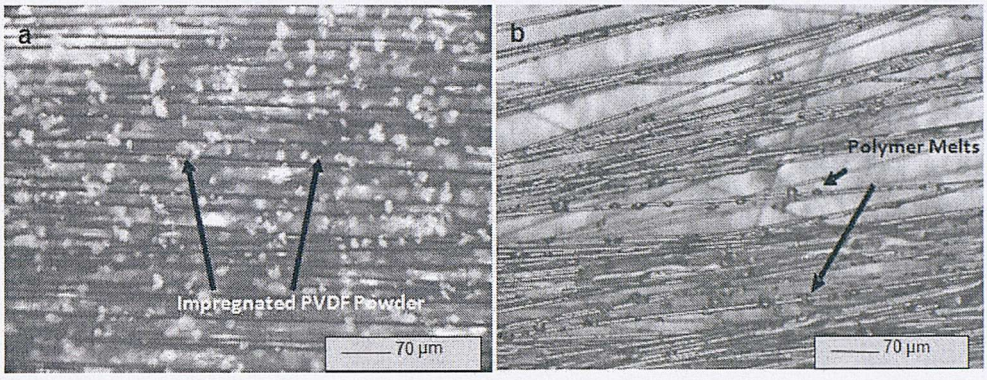


Fig. 3.21: Representative microscopic images of powder impregnated carbon fibre rovings during a) drying and b) melting

In the meantime, the width and the thickness of the composite tape produced, as determined by the spreading of the fibres, was closely monitored using a calliper (Series 500, Mitutoyo, Hampshire, UK; accuracy= 0.02 mm).

Trial runs were performed and recorded to determine the correct concentration of PVDF required in the impregnation bath to produce composite tapes with a volume fraction of 60 %. During these trial runs, different PVDF powder concentrations (2 wt-%, 4 wt-%, 9 wt-% and 10 wt-%) were chosen and tapes manufactured. A fixed operating speed of 1 m/min was set on the CPL whilst the atmospheric plasma system was turned off (compressed air flow was maintained instead) during this exercise. Unidirectional carbon fibre reinforced PVDF tape samples were collected, cut into 1 m long specimens (Fig. 3.22) and weighed using an analytical balance (HR-120-EC, A&D Instruments, Oxford, UK).

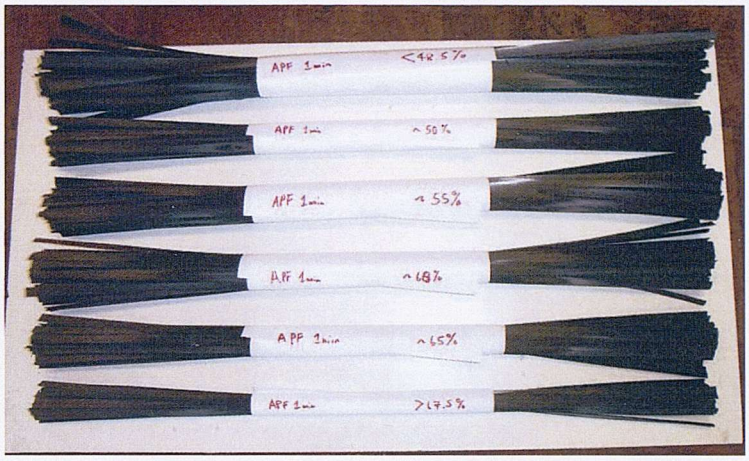


Fig. 3.22: A photographic image of 1m long carbon fibre reinforced PVDF tape specimens

The fibre volume content, FVC, of the carbon fibre/ PVDF tapes were calculated using the following equation:

$$FVC = \frac{\rho_m W_f}{\rho_f W_m + \rho_m W_f} \tag{3.23}$$

where ρ and W are the density and the weight and f and m correspond to the fibre and the matrix, respectively. (W_f of 1m AS4 carbon fibres* = 0.858 g, ρ_f = 1.79 gcm^{-3}, ρ_m = 1.80 gcm^{-3}). Carbon fibre reinforced PVDF tapes were then sorted into FVC range of < 48.5 %, 50 %, 55 %, 60 %, 65 % and > 67.5 %. Only tapes with a FVC of 60 and 65 % were used to prepare composite test specimens (see section 3.6.2.1 for details).

The fibre volume content of the manufactured composite tape changes as a function of processing time because the PVDF powder from the impregnation bath is consumed during the manufacturing process. This causes the fibre volume content of the produced

* HexTow AS4 carbon fibres product data sheet. Link in: http://www.hexcel.com/NR/rdonlyres/5659C134-6C31-463F-B86B-4B62DA0930EB/0/HexTow_AS4.pdf. Accessed on Dec 2007

composite tape to increase. Therefore, for a consistent carbon fibre/ PVDF composite with a fibre volume fraction of 60 % to be produced, the concentration of PVDF powder in the impregnation bath must be maintained as constant as possible. The polymer concentration in the impregnation bath was maintained by adding 50 ml batches of concentrated polymer suspension containing 30 wt-% of PVDF to the impregnation bath approximately every 10, 15 or 20 min depending on the manufacturing speed. These time intervals were established by monitoring the fibre volume fraction by measuring the weight of 1m of the produced carbon fibre/ PVDF composite tape every 10 min.

3.6 Mechanical properties of carbon fibre/ PVDF composites

3.6.1 Micromechanical characterisation of model composites: Single fibre pull-out test- Apparent interfacial shear strength as a measure of practical adhesion

(The experimental work of the following section was conducted by the author himself at the BAM Federal Institute for Materials Research and Testing, Berlin, Germany, under supervision of Dr Gerhard Kalinka)

The quality of adhesion at the fibre/matrix interface is often assessed by performing a mechanical test such as single fibre pull-out tests and this has received attention for some years [311,312,313,314]. This is because the single fibre pull-out test provides a direct measure of interfacial adhesion and can be used with both brittle and ductile matrices [311]. Single fibre pull-out tests were performed in order to determine the effect of atmospheric plasma fluorination on the apparent interfacial shear strength (τ_{IFSS}) which was used as a measure of the practical adhesion between the treated fibre and the PVDF.

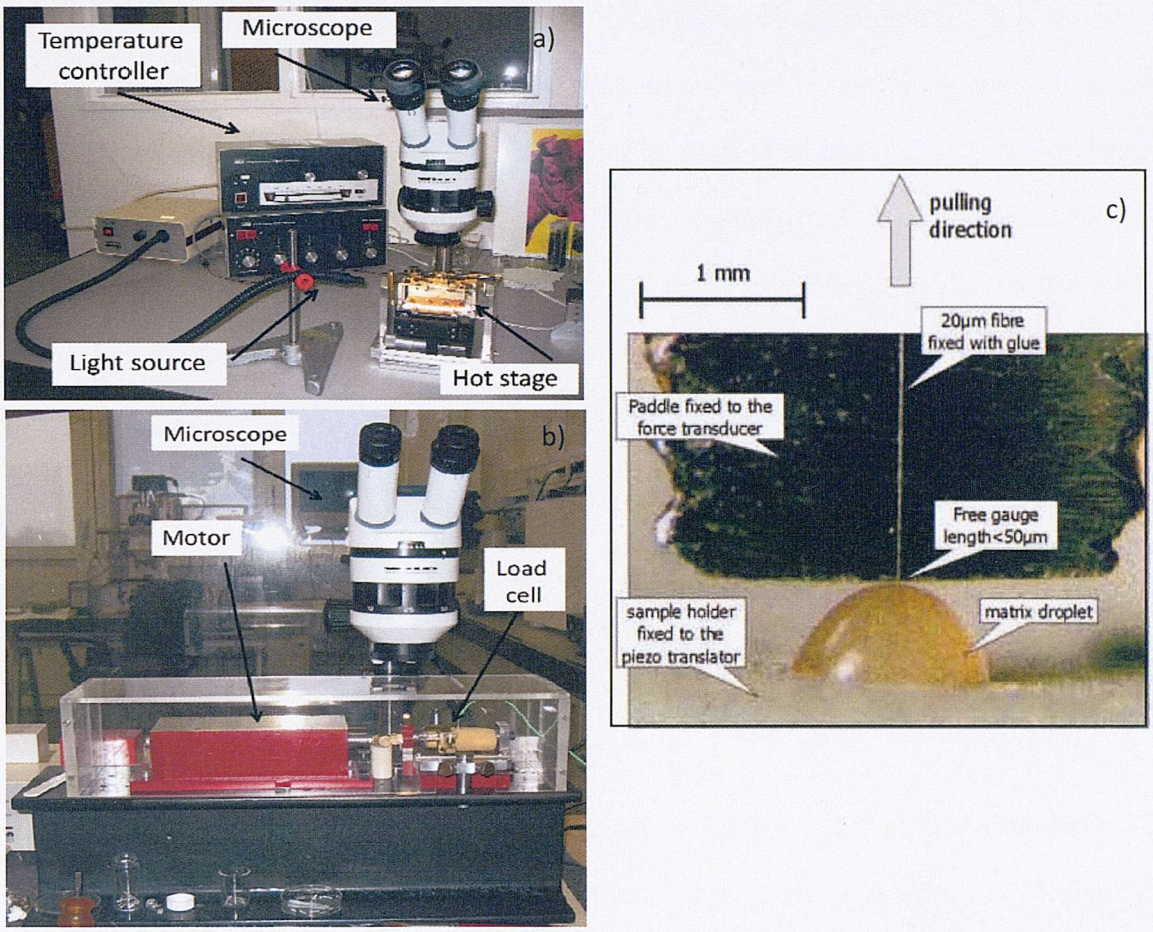


Fig. 3.23: A representative of photographic images of (a) the fibre embedding device, (b) pull-out device and (c) Side view of single fibre pull-out setup*

A single fibre was partially embedded to a pre-determined length between 50-150 µm in a polymer melt droplet by using a homemade embedding apparatus (Fig. 3.23a) [315]. The solid PVDF was placed on an aluminium sample carrier, heated and held at a temperature of 205 °C whilst the fibre was penetrated into the melt. Afterwards the sample was cooled to room temperature using an air stream. The fibre pull-out test was performed using a piezo-motor fixed on a very stiff frame in order to avoid energy storage in the free fibre length between the matrix surface and the clamping device (Fig. 3.23b).

*BAM Federal Institute for Materials Research and Testing, Berlin, Germany
http://www.bam.de/en/kompetenzen/fachabteilungen/abteilung_5/fg56/fg56_ag1a.htm accessed 18.03.08.

The fibre was loaded at a speed of 0.2 μm /s and pulled out of the matrix while the force was recorded throughout the experiment by a load cell and logged using a computer. A typical load-displacement curve is shown in Fig. 4.19. The maximum pull-out force, F_{max}, was correlated to the debonding event along the interface between the embedded fibre length from the matrix. The shape of the curve itself reflects the failure event occurring at the interface [316]. The apparent interfacial shear strength τ_{IFSS} can be calculated from the F_{max} required to trigger the debonding of the embedded carbon fibre from the matrix using the following equation:

$$\tau_{IFSS} = \frac{F_{max}}{\pi d_f L} \tag{3.24}$$

where d_f is the diameter of the fibre (determined using the modified Wilhelmy method, section 3.3.3.1) and L is the embedded fibre length. The apparent shear strength between fluorinated carbon fibres and fluoropolymer matrices was determined from at least 6 measurements in order to obtain a statistically significant average. The values presented were averaged and errors are presented as standard deviation.

3.6.2 Macromechanical characterisation of carbon fibre/ PVDF composites

3.6.2.1 Preparation of composite test specimen

Unidirectional carbon fibre reinforced PVDF composite laminates test specimens were prepared by cutting the produced composite tape into 20 cm long strands. In total 34 layers of the cut composite tapes were stacked and tightly wrapped using a release film

(Upilex 25S, UBE Industries Ltd., Japan) before placing them into a steel mould (cavity dimensions: 200 mm × 12 mm × 5 mm) (Fig. 3.24).

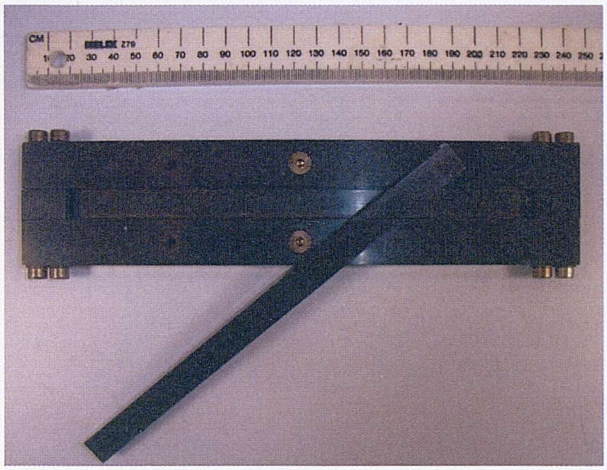


Fig. 3.24: A photographic image of the steel mould used for hot pressing

The mould containing the stacked carbon fibre tapes was then placed in to a hot press (George E. Moore and Son, Birmingham, UK) at 190 °C and pre-heated for 10 min. After which the pressure was increased slowly to a pressure of 1 tonne and held for 2 min before transferring the mould to another hot press (P319, Moore, Birmingham, UK) operated at 80 °C and where it was held for 10 min at a pressure of 0.5 tonne. The mould was then allowed to cool to ambient temperature before the specimen was removed from the mould. Test specimens were cut to the required dimensions for mechanical testing using a diamond blade cutter (Diadisc 4200, Mutronic GmbH & Co, Rieden am Forggensee, Germany). The quality of the edges was improved by grinding using P60 grid sandpaper. All specimens were annealed in a vacuum oven (8465F, Weiss Gallenkamp, Loughborough, UK) overnight at a temperature of 80 °C was chosen.

(The work for the remaining of this section was conducted by Mr Matthew Laffan, Department of Aeronautical Engineering, Imperial College London)

Transverse sections of moulded specimens were embedded into a polyester resin. The resin was cured at room temperature with the addition of an initiator for 24 hr before being polished using abrasion discs following the guidelines for soft material (Buehler Ltd, Illinois, USA). Samples were carefully polished due to the fact that carbon dust can easily scratch the resin surface and fill possible voids in the material. Processed specimens were then examined under an optical microscope.

3.6.2.2 Flexural testing of carbon fibre/ PVDF composites

Flexural properties are important in engineering practice to determine the flexural modulus and flexural loading whilst the material is in use. Laminated composite bars with dimensions of 95 mm × 10 mm × 2 mm were prepared for the three-point bending test. Each composite specimen was loaded into a three-point bending rig at 32:1 span-to-thickness ratio, equipped with a 10 kN load cell (Model 4502, Instron, Buckinghamshire, UK) and secured with the support span set to 64 mm. The crosshead rate was set to 1 mm/min and each specimen was tested until failure following the ASTM D790-03 standard [317].

The loading force versus displacement was logged throughout the experiment using a computer and the flexural modulus E_f was then calculated using:

$$E_f = \frac{L^3 m}{4bd^3} \tag{3.25}$$

where L is the specimen length, m is the gradient of the initial part of the force-displacement curve, b is the specimen width and d is the specimen thickness. The specimen flexural strength σ_f was calculated using the following equation:

$$\sigma_f = \frac{3P_{MAX}L}{2bd^2}\left[1+6\left(\frac{D}{L}\right)^2 - 4\left(\frac{d}{L}\right)\left(\frac{D}{L}\right)\right] \tag{3.26}$$

where D is the central deflection of the specimen at failure load P_{MAX}. The flexural strength and modulus of unidirectional carbon fibre reinforced PVDF were determined from at least 8 measurements in order to obtain a statistically significant average. The values presented are averaged values and errors are standard deviations.

3.6.2.3 Apparent short beam shear testing of carbon fibre/ PVDF composites

The short beam shear strength method which is based on classical beam theory is the simplest and the most commonly used test. This is used to characterise interlaminar shear behaviour of composite laminates and in this case APF carbon fibre reinforced PVDF. Short beam shear testing is very similar to flexural testing described in the previous section. This test allows maximum shear stresses to be introduced throughout the thickness of the test specimen whilst reducing the tensile and compressive flexural stresses to a minimum by reducing the length of the test specimens i.e. lowering the span-to-thickness ratio.

Unidirectional carbon fibre reinforced PVDF laminates of 20 mm × 10 mm × 2.2 mm were prepared and secured again into the same test rig used for flexural test with a span-to-thickness ratio of 32:1, equipped with a 10 kN load cell (Model 4502, Instron, Buckinghamshire, UK). Specimens were then loaded at 1 mm/min until failure following the ASTM standard D2344 [318]. The short beam strength F^{SBS} was calculated using equation:

$$F^{SBS} = 0.75\frac{P_{MAX}}{bd} \tag{3.27}$$

where P_{MAX} is the force at composite failure load, b is the specimen width and d is the specimen thickness. All measurements were repeated on at least 8 different samples to obtain a statistical average. The errors presented are standard deviations.

Chapter 4

Results and Discussion

The main aim of this research was to develop an atmospheric plasma system that allows carbon fibres to be fluorinated feasibly and homogeneously. It was anticipated that the surface and maybe even the bulk properties of carbon fibres will be altered as a result of atmospheric plasma modification. Therefore, the surface and bulk properties of batch modified T700 and continuously modified AS4 carbon fibres were compared. In addition, micro- and macromechanical properties of carbon fibre reinforced PVDF composites made using a home built single fibre embedding machine or the composite line with implemented atmospheric plasma fluorination (APF) are also presented.

4.1 Surface characterisation of carbon fibres

4.1.1 Influence of atmospheric plasma modification on wetting behaviour, surface area and morphology of carbon fibres

4.1.1.1 Atmospheric plasma batch modified T700 carbon fibres

Desized T700 carbon fibres were treated in 3 different atmospheric plasma environments (N_2, N_2 + SF_6 and N_2 + $CHClF_2$) for a period of 4 min and characterised using contact angle measurements (Table 4.1). When carbon fibres were treated in N_2 plasma, they became significantly more hydrophilic as shown by the decrease of the advancing water contact angle from 81° to 55°. When adding the maximum possible amount of SF_6 (1:70 ratio, as determined by trials in order to sustain a stable plasma jet)

to the N_2 plasma jet whilst treating the carbon fibres, the water contact angle did not increase. However, when adding $CHClF_2$ to the N_2 plasma jet, the wettability of the treated fibres decreased drastically the water contact angle increased from 81° to 103° which highlighted the increased hydrophobicity of the fibres. The increased water contact angle can only be due to the presence of fluorine containing surface groups even more so since the oxygen content of the fibre surfaces increased after the plasma fluorination (see later discussion of the XPS results). The feed gas contains only a small amount of $CHClF_2$ ($CHClF_2$ to N_2 ratio is 1:70) with respect to overall feed gas mixture (Table 4.1), which was also the highest $CHClF_2$ content at which a stable atmospheric plasma jet could be operated.

Table 4.1: Dynamic contact angles of 4 min atmospheric plasma fluorinated (APF) desized T700 carbon fibres against water (W), diiodomethane (DIM) and formamide (FA)

Sample	d_f / μm	θ_a(W) / °	θ_r(W) / °	Δθ (W)	θ_a(DIM) / °	θ_r(DIM) / °	θ_a(FA) / °	θ_r(FA) / °
original	6.3±0.6	80.9± 2.7	43.6± 4.8	37.3	60.1±3.2	56.7±2.9	38.0±2.4	28.0± 1.6
N_2	6.6±0.4	55.2± 2.7	41.9± 2.4	13.3	46.4±3.6	33.4±2.6	33.4±3.5	32.8±3.2
N_2+SF_6	6.0±0.3	61.2± 3.2	47.6± 3.3	13.6	40.3±5.5	23.8±3.5	21.8±3.6	20.2±1.2
N_2 + $CHClF_2$	6.7±0.3	102.7± 2.1	36.8± 6.2	65.9	55.8±3.3	23.8±3.5	57.2±2.5	32.7±2.3
N_2 + $CHClF_2$ (After 1 month)		95.8± 2.3	42.9± 4.7	52.9	41.0±6.0	29.9±8.1	28.9±4.9	20.0±1.1

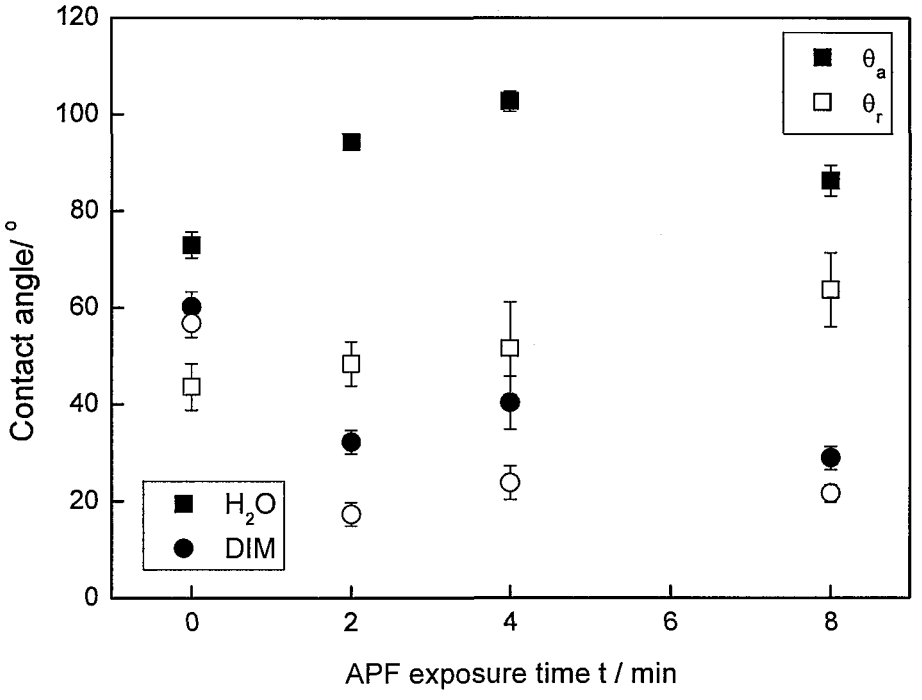


Fig. 4.1: Advancing θ_a and receding θ_r contact angles of desized T700 carbon fibres APF in a 70:1 N_2:$CHClF_2$ plasma jet

The carbon fibres were treated for various times in the N_2 + $CHClF_2$ plasma jet. Initially the advancing water contact angles increased with increasing treatment time of the carbon fibres in the N_2 + $CHClF_2$ gas mixture (Fig. 4.1). The contact angle was highest for a treatment time of 4 min, after which it decreased again with the increasing exposure time to the plasma jet. The measured contact angles between the plasma fluorinated carbon fibres and diiodomethane had significantly decreased already after a treatment time of 2 min and stayed almost constant with increasing treatment time. The lower contact angles measured against the non-polar test liquid indicate that the dispersive interactions at the fibre surface should improve after APF.

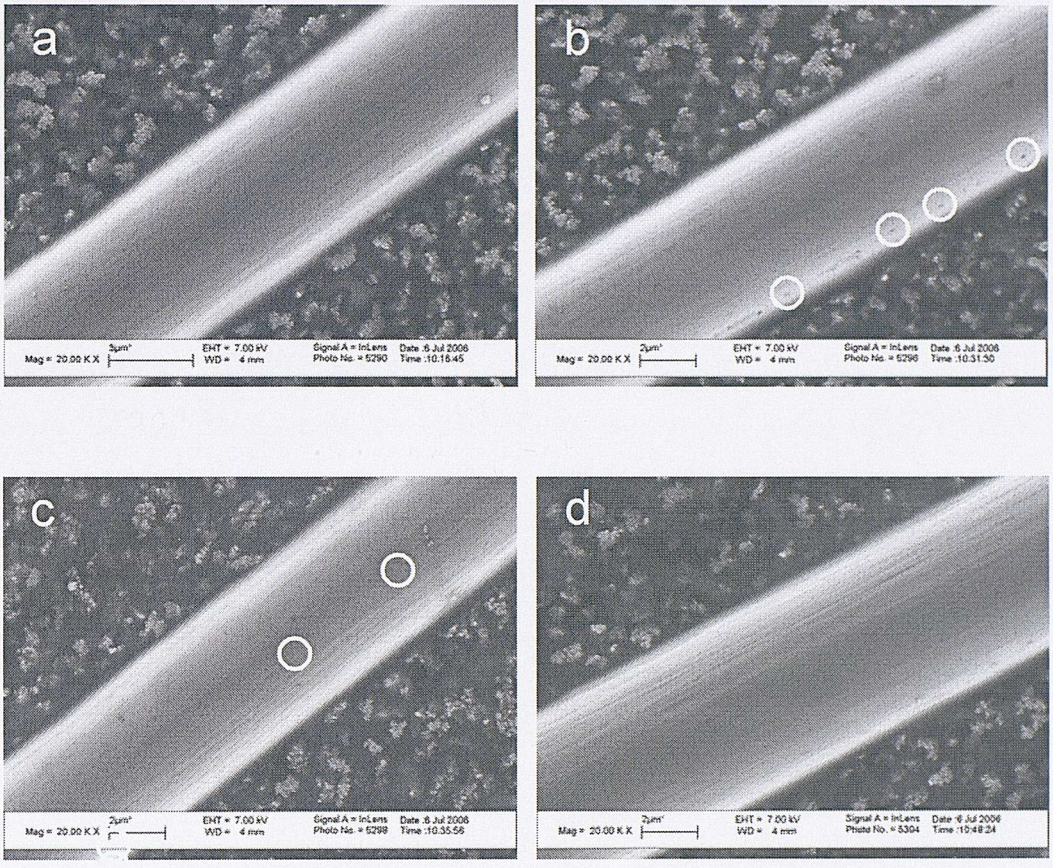


Fig. 4.2: Representative SEM images of desized T700 carbon fibres APF in a N_2 + $CHClF_2$ plasma jet for a) 0 min, b) 2 min, c) 4 min and d) 8 min

The water contact angle hysteresis, defined as the difference between θ_a and θ_r, for the atmospheric plasma fluorinated carbon fibres increased initially with the increasing treatment time up to 4 min after which it decreased again. In the case of the diiodomethane contact angles, an increase in the contact angle hysteresis after exposure to the plasma jet was observed as well. The contact angle hysteresis is due to chemical heterogeneities and/or due to an increasing surface roughness [319,320].

During the surface treatment of carbon fibres in the plasma jet, deposition of sputtered carbon on the glass enclosure was observed. The sputtering caused significant surface damage of the carbon fibres as can be seen in the SEM images (Fig. 4.2a-d). The SEM image of desized but industrially oxidised PAN based T700 carbon fibres (Fig. 4.2a) with a smooth surface. Already after 2 min exposure to the plasma jet the formation of

micro pinholes at the fibre surfaces was observed (Fig. 4.2b), which can enhance interlocking to epoxy matrix [321]. As the duration of the atmospheric plasma fluorination increased, more surface defect sites become visible (Fig. 4.2c). However, extending the treatment time to 8 min seemed to smoothen the surfaces again. No pinholes are visible on the carbon fibres exposed to APF for 8 min (Fig. 4.2d). Even though significant sputtering of the carbon fibres took place, no changes in the overall diameter of the fibres could be detected, as determined using modified Wilhelmy measurements (Table 4.2).

Table 4.2: Fibre diameters (d_f) and surface free energies γ_s(EoS) calculated using the Equation-of-State approach of desized T700 carbon fibres APF for various times in a $N_2 + CHClF_2$ plasma jet

APF Duration / min	d_f / μm	γ_s(EoS) / mN/m
0	6.3±0.6	44.0±3.9
2	6.7±0.1	35.2±12.2
4	6.7±0.3	31.0±8.7
8	6.4±0.2	38.3±7.5

From the contact angles measured between the modified fibres, water, formamide and diiodomethane the surface free energy γ_s for atmospheric plasma treated carbon fibres was calculated using acid-base approach (section 2.4.1) (Tables 4.2 and 4.3). However, this method does not provide valid results when contact angles exceed 90°, which is the case for $N_2 + CHClF_2$ atmospheric plasma treated carbon fibres. Therefore, the surface free energies for $N_2 + CHClF_2$ atmospheric plasma treated carbon fibres were determined using the alternative Equation-of-State method (section 2.4.1).

Table 4.3: Surface free energies calculated using both the Equation-of-State (γ_s(EoS)) and acid-base approach (γ_s (AB) of 4 min AP treated desized T700 carbon fibres

APT	γ_s (EoS) / mN/m	γ_s (AB) / mN/m	γ_s^{AB} / mN/m	γ_s^{LW} / mN/m	γ_s^+ / mN/m	γ_s^- / mN/m
original	44.0±3.9	48.7±2.1	4.7±2.1	44.0±2.1	1.4±0.6	4.1±1.8
N_2	46.1±7.2	48.7±5.5	12.4±3.6	36.3±2.0	2.1±0.6	18.6±3.6
N_2+SF_6	47.9±6.0	52.1±3.2	10.4±3.2	41.7±3.2	3.1±0.7	8.6±2.9
N_2 + $CHClF_2$	31.0±8.7	-	-	-	-	-

Apart from the carbon fibres which were fluorinated in the N_2 + $CHClF_2$ atmospheric plasma jet for which the contact angle exceeded 90°, the surface energy γ_s of the carbon fibres treated in nitrogen plasma jet remained virtually constant as compared to desized but industrially oxidised carbon fibres. As expected the Lifshitz/ van der Waals component (γ_s^{LW}) of the surface energy decreased significantly because of the damage to the graphitic surface structure of the carbon fibres due to the sputtering caused by the bombardment of the fibres by highly energised gas species. However, the decrease in γ_s^{LW} was balanced by the dramatically increased acid/ base component (γ_s^{AB}) due to the incorporation of the more polar functional groups. Treating the carbon fibres in a N_2 + SF_6 plasma jet did not seem to be so damaging to the fibre surfaces as γ_s^{LW} decreased only slightly. Combined with the increase in γ_s^{AB} this led to a slight increase of the overall fibre surface energy γ_s. γ_s^{AB} consists of the acid γ_s^+ and base γ_s^- parameters of the surface energy. In all cases the fibres are much more Lewis basic after the APF.

The surface free energies of carbon fibres that were successfully fluorinated in the N_2 + $CHClF_2$ atmospheric plasma jet could only be calculated using the Equation-of-State approach (section 2.4.1). As can be seen from the results summarised in Table 4.3, γ_s decreased significantly, from 44 to 31 mN/m, due to the incorporation of fluorine moieties into the fibre surfaces.

In order to confirm the fact that the atmospheric plasma fluorination results in a long lasting surface modification, contact angles of the carbon fibres treated in $N_2 + CHClF_2$ atmospheric plasma were re-measured a month after they were initially treated. The water contact angle values reduced slightly but the values were roughly within the standard deviation (Table 4.1), i.e. APF of carbon fibre was stable over time.

It is well known that mechanical interlocking (chemical anchoring) can be a major contribution to the measured practical adhesion [322,120]. In order to quantify the effect of APF on the surface roughness, the surface area A_s of the carbon fibres was determined using BET N_2 adsorption (Fig. 4.3). The BET surface area A_s of the plasma treated carbon fibres increased slightly but steadily from 0.22 m^2/g for the T0 fibres to 0.44 m^2/g after 8 min exposure to APF. During the surface treatment of carbon fibres in the plasma jet the deposition of sputtered carbon on the glass enclosure was observed. This significant sputtering caused the formation of pits on the treated fibre surfaces which led to the increase in the BET surface area. Although an increase of 100% in surface area of treated carbon fibres was observed, it was in the range of typical type II electrochemically oxidised PAN based carbon fibres (< 1 m^2/g) and therefore should not have any significant effect on the practical adhesion. The small changes in surface area observed after the APF treatment of the carbon fibres were not expected to favour any anchoring between the fibres and the matrix polymer [323, 324].

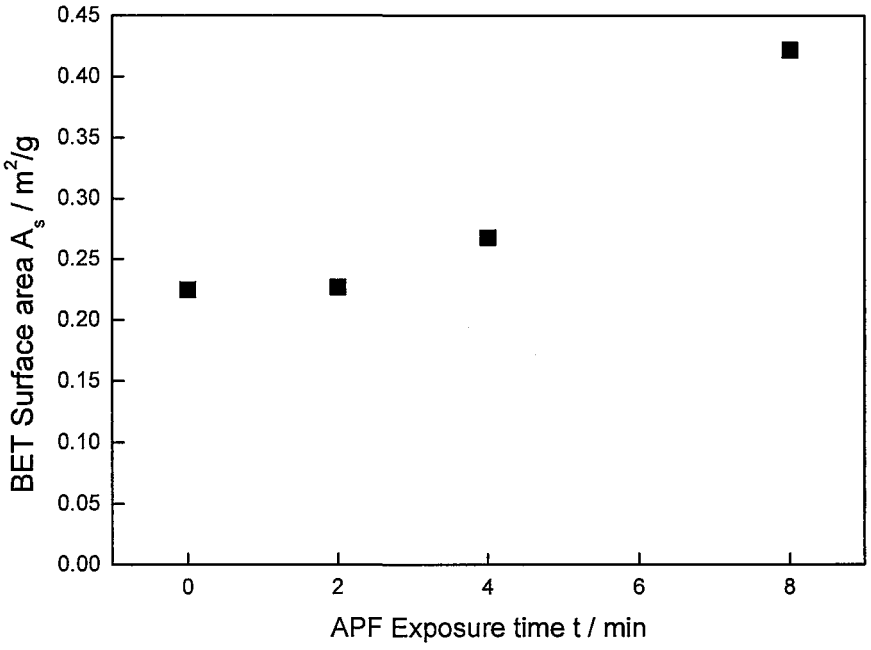


Fig. 4.3: Effect of atmospheric plasma fluorination on T700 fibre (BET) surface area

4.1.1.2 Continuously atmospheric plasma fluorinated AS4 carbon fibres

As mentioned earlier, the homogeneity of the atmospheric plasma treatment along AS4 fibres is of interest. Please see section 3.2.2 for the reasons for fibre selection. An advancing water contact angle of 77° was obtained for the standard industrially oxidised but unsized AS4 fibres. APF resulted in an increase in the water contact angle depending on the setup used (Table 4.4), which implied that the fibre surfaces became significantly more hydrophobic.

Table 4.4: Dynamic contact angles of APF AS4 carbon fibres against water (W), diiodomethane (DIM) and formamide (FA)

Fibres treatment	Speed/ m min^{-1}	Retention time/ min	θ_a(W) / °	θ_r(W) / °	$\Delta\theta$ (W)	θ_a(DIM) /°	θ_r(DIM) /°	θ_a(FA) / °	θ_r(FA) / °
Original	0	0	77.2 ± 4.4	56.8 ± 5.7	20.4	59.7 ± 2.9	58.8 ± 0.7	46.3 ± 2.6	35.9 ± 0.5
Batch	0	4	90.9 ± 8.3	45.9 ± 4.5	45	47.6 ± 2.0	47.3 ± 2.7	45.6 ± 1.4	38.5 ± 2.7
Continuous single sided	0.15	1.3	92.4 ± 6.0	51.5 ± 8.2	40.9	46.2 ± 1.8	45.6 ± 1.2	53.5 ± 5.3	34.8 ± 1.8
Continuous double sided	0.75	0.8	78.3 ± 4.2	63.7 ± 5.2	14.6	47.2 ± 1.6	47.0 ± 0.1	67.7 ± 4.4	48.2 ± 2.2
	0.33	1.8	78.5 ± 8.7	58.9 ± 5.9	19.6	50.3 ± 4.0	48.1 ± 1.0	55.3 ± 3.1	40.7 ± 3.0
	0.15	4	88.4 ± 3.3	55.1 ± 6.2	33.3	47.8 ± 1.1	45.6 ± 0.9	50.3 ± 3.1	34.9 ± 3.1

For the 4 min batch fluorinated AS4 fibres, the advancing water contact angle θ_a increased to 91°. All continuously APF treated carbon fibres have a θ_a of ~ 90°. The water contact hysteresis $\Delta\theta$, defined as the difference between θ_a and θ_r, indicates chemical surface heterogeneity and/or a change of the surface roughness [201,202]. The fibres with the highest $\Delta\theta$ were the batch and continuous single sided APF treated carbon fibres (Table 4.4), which suggested that these two processing conditions caused significant surface inhomogeneities. A much smaller $\Delta\theta$ (as little as 15°) was observed for the double sided APF treated fibres. However, as the residence time of the fibres in the plasma increased to 4 min, the $\Delta\theta$ increased to 33° indicating an increase in chemical surface inhomogeneity or roughness of the treated fibres.

Table 4.5: Fibre diameters (d_f), BET surface area and surface free energies (γ_s(EOS)) of APF AS4 carbon fibre

Fibres treatment	Residence time in APF/ min	d_f / μm	A_s / m^2/g	γ_s(EOS) mN/m
Original	0	7.0 ± 0.1	0.31	37.5 ± 6.1
Batch	4	7.2 ± 0.1	0.40	36.6 ± 7.7
Continuous single sided	1.3	6.8 ± 0.1	0.47	35.2 ± 6.5
Continuous double sided	0.8	7.0 ± 0.1	0.31	36.3 ± 5.7
	1.8	6.8 ± 0.1	0.38	37.2 ± 1.6
	4	6.9 ± 0.1	0.38	35.3 ± 2.7

Although fluorine moieties were incorporated into the fibre surfaces (see XPS section 4.1.3.2) as a result of APF, γ_s(EOS) remained constant at ~35 mN/m (Table 4.5). This is expected as APF is a mild fluorination technique and unlike direct fluorination for which a decrease in γ_s(EOS) down to ~20 mN/m is reported, with carbon fibre surfaces becoming Teflon-like [177,220].

The SEM micrographs of the APF treated carbon fibres (Fig. 4.4) show that AS4 fibres had a smooth surface appearance, similar to T700 fibres (Fig. 4.2). However in this case, after continuous APF there was no apparent pin hole surface damage on the fibres (like that seen on batch APF T700 fibres, Fig. 4.2) was observed at the magnifications used.

During continuous APF, weakly bound amorphous carbon material was sputtered off the fibres but nevertheless the fibre diameter remained constant (Table 4.5). An increase in the fibre surface area and the removal of weakly attached surface layers could enhance the measured practical adhesion between modified fibres and the matrix in carbon fibre composites [325]. As a consequence the influence of continuous APF on

the surface area of the APF AS4 carbon fibres was investigated. The original unsized but industrially oxidized AS4 carbon fibres have a BET surface area of 0.31 $m^2 g^{-1}$ prior to the exposure to APF. As a result of batch and continuous single sided APF treatment, the BET surface area of the fibres increased to 0.40 and 0.47 $m^2 g^{-1}$, respectively (Table 4.5).

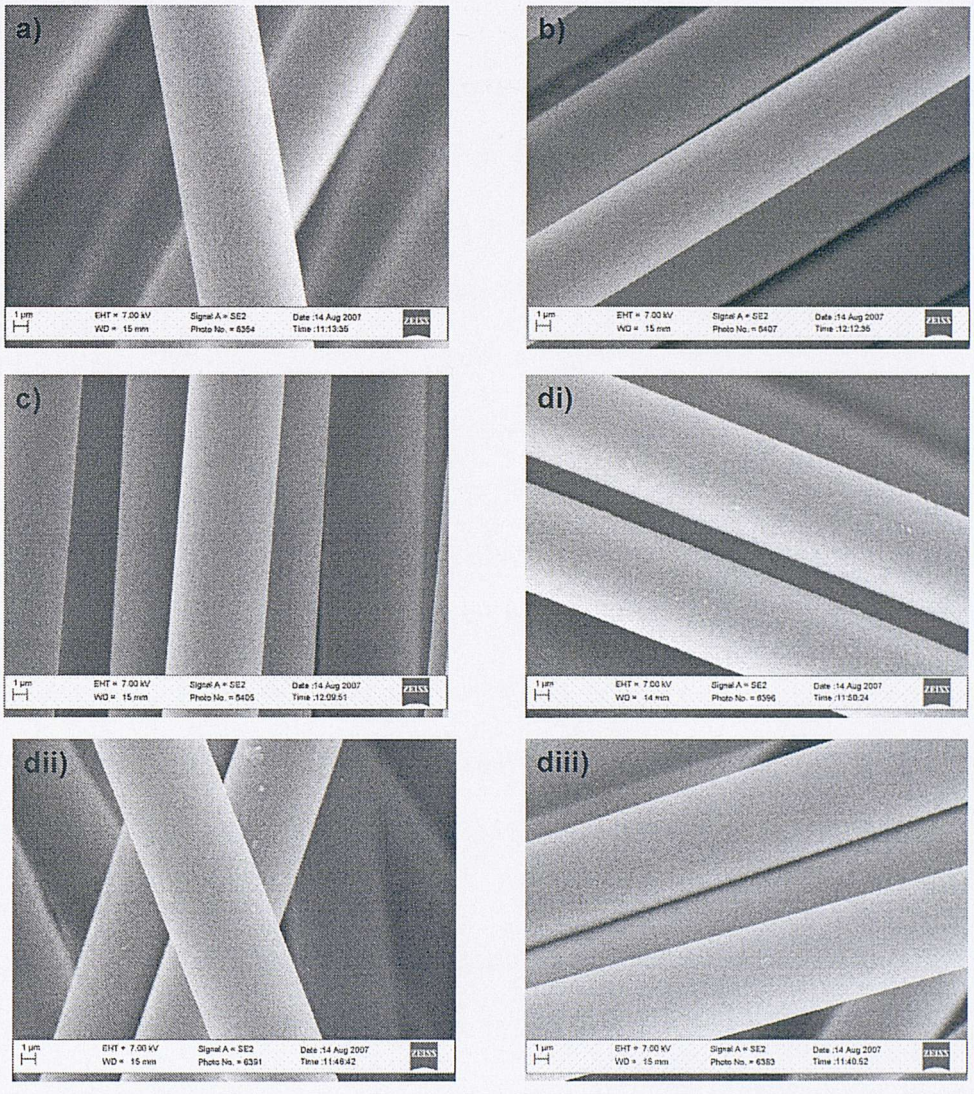


Fig. 4.4: Representative SEM images of atmospheric plasma fluorinated AS4 carbon fibres a) original, b) batch, c) continuous straight, d) continuous double sided i) 0.75m/min, ii) 0.33m/min, iii) 0.15m/min

The BET surface area of the continuous double sided APF AS4 fibres increased steadily with increasing fluorination time up to 0.38 $m^2 g^{-1}$. The slight increase in surface area

indicated some, although small, degree of roughening of the carbon fibres during APF. Although mechanical interlocking can be a major contribution to practical adhesion, an increase of at least 5-10 m^2/g is said to be required to have any impact on the adhesion [323,324].

4.1.2 Influence of AP batch treated T700 fibres on ζ-potential

The pH-dependent ζ-potential (Fig. 4.5a) of desized but industrially oxidised T700 carbon fibres shows the typical behaviour of solids containing Brønsted acid groups as indicated by the low isoelectric point (iep), where $\zeta = 0$, and the ζ-potential plateau area in the alkaline region. At high pH all acidic functional groups were dissociated. When reducing the pH the dissociation of acidic groups was repressed until the iep was reached and all acid groups were fully protonated so that the surface carried no charge. Lowering the pH beyond the iep leads to proton (H_3O^+) adsorption and the surface charge reverses. Atmospheric nitrogen plasma treated carbon fibres displayed a less acidic character compared to the original T700 fibres, as can be seen from the shift of the iep from pH 3.7 to pH 4.1. The position of iep was determined by the concentration and relative strength (pK_a) of all dissociating surface groups present and was therefore a measure of the degree of acidity/ basicity of a solid.

After exposure to atmospheric plasma fluorination $\zeta = f(pH)$ changes, the surfaces of the fibres were more acidic as compared to the original T700 carbon fibres. The iep for all atmospheric plasma fluorinated fibres shifted from pH 3.7 to an extrapolated pH 2.8 which indicated a homogenisation of the chemical nature of the fibre surfaces. In the next section (4.1.3.1), it can be seen that after exposure to the plasma jet more carboxylic acid groups were present on the fibre surfaces, even though the overall number of oxygen functional groups was drastically reduced. The reason for the

presence of oxygen containing groups is the fact that fluorine is electronegative and draws electrons from a carbon atom, i.e. polarising the carbon, which makes it susceptible to further oxidation, as can be seen in the significant amount of O on the fibre surface (this will be discussed later in the XPS section 4.1.3.1). Furthermore, it can be seen that the $\zeta_{plateau}$ value increased with increasing treatment time (Fig. 4.5b).

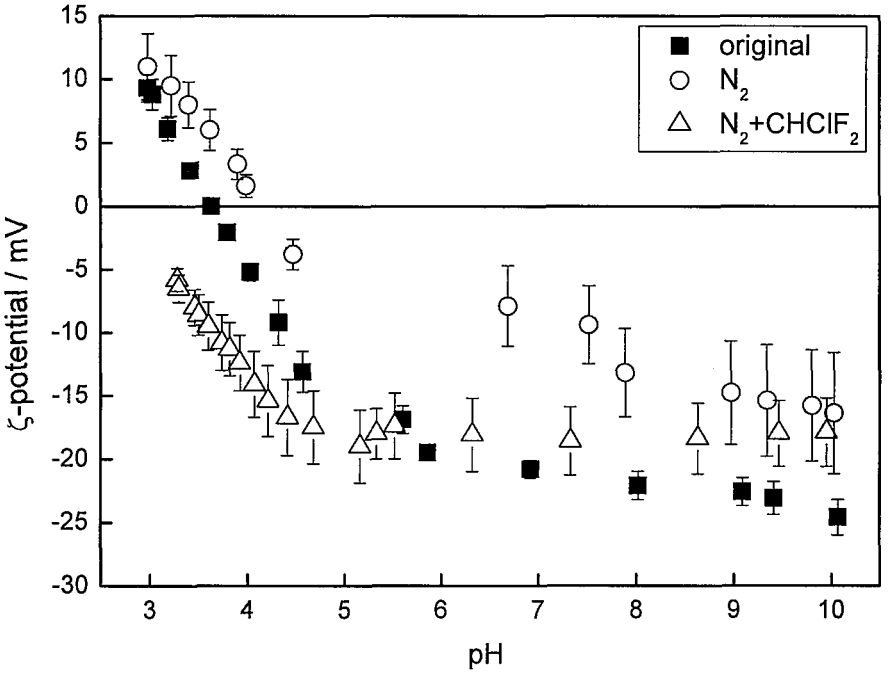


Fig. 4.5a: ζ-potential as function of pH of desized T700 carbon fibres and of carbon fibres AP treated in a nitrogen and N_2 + $CHClF_2$ plasma jet for 4 min

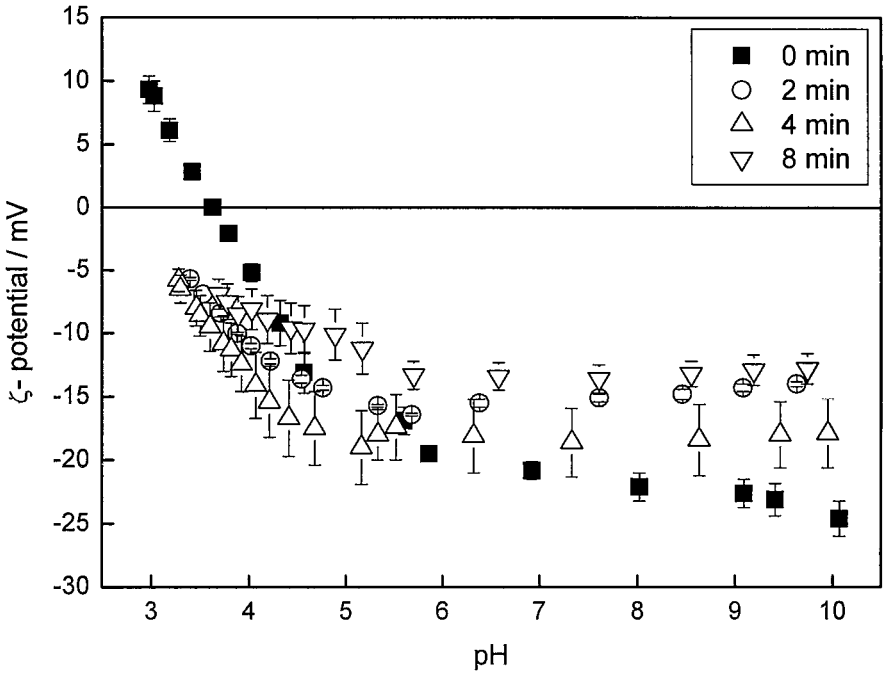


Fig. 4.5b: ζ-potential as function of pH of desized T700 carbon fibres and of carbon fibres AP treated for various times in a N_2 + $CHClF_2$ plasma jet

4.1.3 XPS surface analysis of atmospheric plasma fluorinated carbon fibres subjected to configurations

(The work presented in the follow section is the work done jointly* performed with Dr. Adam F Lee, Department of Chemistry, University of York; as an adaption to form an integral part of a relevant contribution to the main theme of the thesis)

4.1.3.1 Atmospheric plasma batch fluorinated T700 carbon fibres

The influence of the treatment time of carbon fibres in N_2 + $CHClF_2$ atmospheric plasma on the fibre surface composition was investigated by XPS. The elemental composition of the fibres is presented in Table 4.6:

* Published in Carbon 2007; 45: 775-784 and Composites Part A 2007; 39:364-373.

Table 4.6: Surface composition (in at.-%) of AP batch fluorinated T700 carbon fibres in a N_2 + $CHClF_2$ plasma jet determined by XPS

APF Duration / min	C / at.-%	O / at.-%	N / at.-%	F / at.-%	Si / at.-%	O:C ratio
0	75.4	18.0	1.2	-	5.4	0.24
1	82.4	12.5	1.6	1.1	0.6	0.15
4	80.8	13.6	2.0	1.6	1.3	0.17
8	84.5	9.5	1.8	1.5	0.8	0.11

The original industrially oxidised but desized T700SC fibre contained a relatively high heteroatom content, predominantly oxygen (which may be residuals of sizing), along with significant surface silicon impurities from handling, but is entirely fluorine-free. The T700 fibres were already pre-oxidised by the manufacturer. Plasma treatment in a N_2 + $CHClF_2$ jet resulted in significant changes in the overall surface composition, resulting in both heteroatom removal, presumably via simple surface sputtering and this revealed of the underlying carbon shelvedge, and the introduction of surface fluorine functionalities. The fluorine content rapidly increased from 0 to 1.1 at.-% after 1 min plasma exposure. After 4 min, the level of surface fluorine present reached 1.6 at.-% and after 8 min the fluorine content was around 1.5 at.-%. This method allowed for a very mild fluorination of carbon fibres as compared to direct fluorination; only 30% of the lowest surface fluorine content was achieved with APF compared to the reported surface fluorine content of direct fluorinated carbon fibres [177,220]. A measure of the changes in surface polarity/hydrophobicity can also be garnered by examining the evolution of the O:C ratio across the series. This showed a sharp decrease from 1:4 to 1:9 following the longest fluorination treatment, i.e. the oxygen content decreased from 18 to 12.5 at.-% after only 1 min exposure to APF. The oxygen content decreased further and after 8 min, half of the initial oxygen functional groups were removed from the carbon fibre surface. This was consistent with a sharp rise in the surface hydrophobicity. The nitrogen content detected in the T700 carbon fibres is most likely due to the fact that the industrially oxidised fibres were electrolytically treated in

ammonium salt electrolytes. Nitrogen levels remain low and indicate independency to plasma treatments.

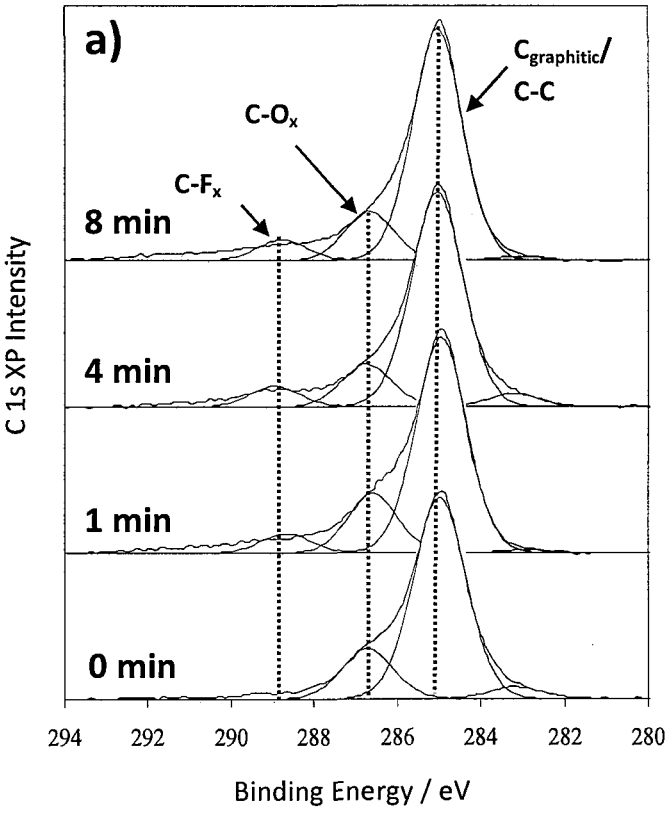


Fig. 4.6a: Carbon 1s XP spectra of T700 carbon fibres AP fluorinated in N_2 + $CHClF_2$ plasma jet

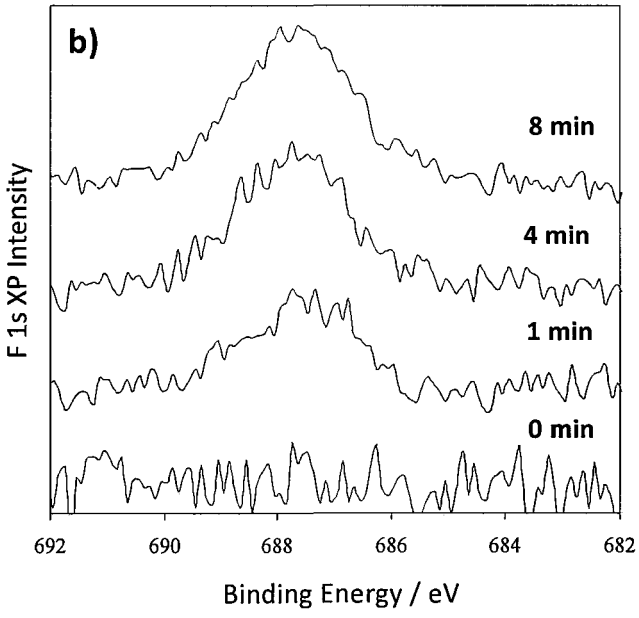


Fig. 4.6b: Fluorine 1s XP spectra of T700 carbon fibres AP fluorinated in N_2 + $CHClF_2$ plasma jet

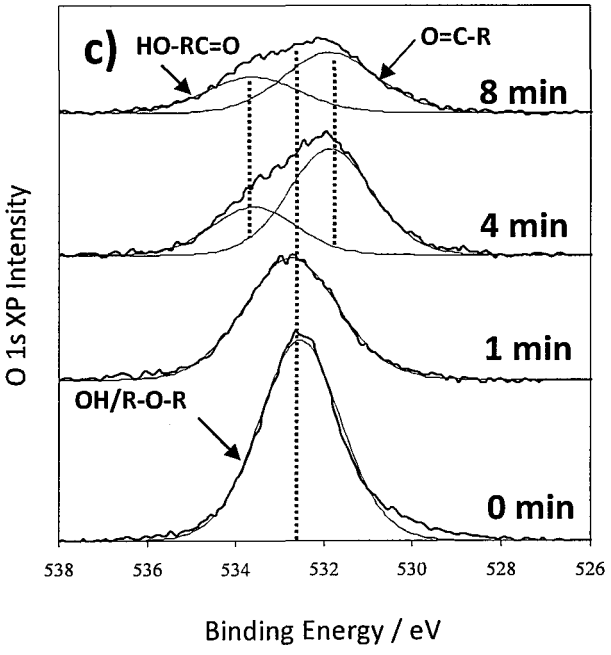


Fig. 4.6c: Oxygen 1s XP spectra of carbon fibres AP fluorinated in N_2 + $CHClF_2$ plasma jet

These gross compositional changes are reflected in the corresponding high resolution C 1s XP spectra shown in Fig. 4.6a, which confirmed the gradual growth of

graphitic/aliphatic carbon surface environments at 285 eV, relative to the C-O_x state at 286.7 eV, and the concomitant emergence of a pronounced high binding energy tail which contained at least one well-defined chemical state around 288.9 eV. These latter features are associated with F functionalisation. The corresponding F 1s XP spectra in Fig. 4.6b show the appearance of a single, broad F feature (indicative of a distribution of chemical environments) centred around 687.7 eV. This feature did not shift with increasing treatment time, indicating fluorine is incorporated into the carbon fibre surfaces in a common fashion irrespective of the accompanying evolution of surface moieties, e.g. loss of Si contaminants and hydroxyl groups. The oxygen spectra in Figure 4.6c were also consistent with the net loss of polar surface groups and associated surface chemical activation of the fibres in the plasma. Both the original T700 and 1 min exposed fibres exhibited a single broad O 1s feature at 532.6 eV, in the fingerprint regime for both hydroxyl and ether moieties. Prolonged plasma treatment resulted in peak splitting into new high and low binding energy states at 533.6 eV and 531.8 eV; these values lie in the general region for bridging oxygens in an acid HO-RC=O and those in carbonyl R-C=O environments, respectively [263]. Their simultaneous appearance and the loss of the 532.6 eV peak indicated plasma-induced carbonylation of surface hydroxyls. Note all fitted components had identical line shapes and peak widths to ensure the validity of the peak deconvolution. In conclusion XPS revealed that plasma surface modification results in both fibre surface cleaning, the loss of hydrophilic R-O_x groups, and the incorporation of hydrophobic C-F_x functionalities.

4.1.3.2 Continuously atmospheric plasma fluorinated AS4 carbon fibres

The influence of continuous APF treatment time and the configuration used to treat the AS4 fibres on the surface composition of the fibres was investigated by XPS (Table 4.7).

Table 4.7: Surface composition (in at.-%) of atmospheric plasma fluorinated AS4 carbon fibres determined by XPS

Fibres treatment	Residence time in APF/ min	C / at. -%	O / at. -%	N / at. -%	F / at.-%	Cl / at. -%	O:C
Original	0	90.6	7.0	2.4	-	-	0.08
Batch	4	77.4	12.9	1.8	4.7	3.2	0.17
Continuous single sided	1.3	83.8	9.7	3.1	1.3	0.9	0.11
Continuous double sided	0.8	79.3	12.1	2.7	2.9	1.5	0.15
	1.8	76.3	12.6	1.7	3.6	2.1	0.16
	4	76.6	14	2	4.9	2.6	0.18

As expected the original industrial oxidised AS4 carbon fibres are fluorine-free but again contain significant amounts of oxygen and traces of nitrogen. Atmospheric plasma fluorination results in a dramatic change in the overall surface composition for both batch and continuously APF treated fibres and as a result, fluorine was introduced and the amount of carbon in the fibre was reduced. The surface fluorine content of continuous APF treated carbon fibres was found to depend on the residual time of the AS4 fibres in the plasma environment. When the processing speed was constant (0.15 m/min), continuously double sided APF allows for a longer residence time of the fibre in the jet and resulted in almost a four fold increase in the surface fluorine content (4.9 at.-%) as compared to continuously single sided APF treated fibres (1.3 at.-%). An increase in the O:C ratio was also observed for all carbon fibres. This was attributed to the AP activated fibre surface reacting with atmospheric oxygen in the plasma plume to

generate surface ethers and carbonyl moieities. As a result of amorphous carbonaceous material being sputtered off, the small increase in surface oxygen content would be expected to provide extra H-bonding sites on the fibre surface and thus boost hydrophilicity, but this is more than compensated by the large increase in surface fluorine content (see section 4.1.1.2 for water contact angle data). In any event it should be noted that in comparison to deliberate surface oxidation of carbon fibres in an air plasma, which is known to increase the hydrophilicity of the surface, the present increase in surface oxygen content was very small [92]. The O 1s spectra show the oxygen content of the fibres were again identical for batch and continuous modes.

Switching from batch to continuous plasma modification treatment offers great processing advantages, however it is essential to ensure that both approaches result in the same surface functionalities. High resolution XP spectra were therefore recorded for AS4 fibres exposed to APF batch and continuous double-sided treatments with equal total residual times of 4 min. The resulting C, F, N and O 1s XP-spectra are shown in Fig. 4.7). It is evident from the XP spectra that both fluorination methodologies resulted in identical surface functionalisation. The C 1s spectra contains components due to both the C-C backbone (285 eV) and fluorine group (289 eV), while the N 1s spectra exhibited a single chemical environment at 399 eV, in excellent agreement with literature values [243]. The F 1s spectra for both treatments indicate the presence of a single, well-defined fluorocarbon environment at 686 eV.

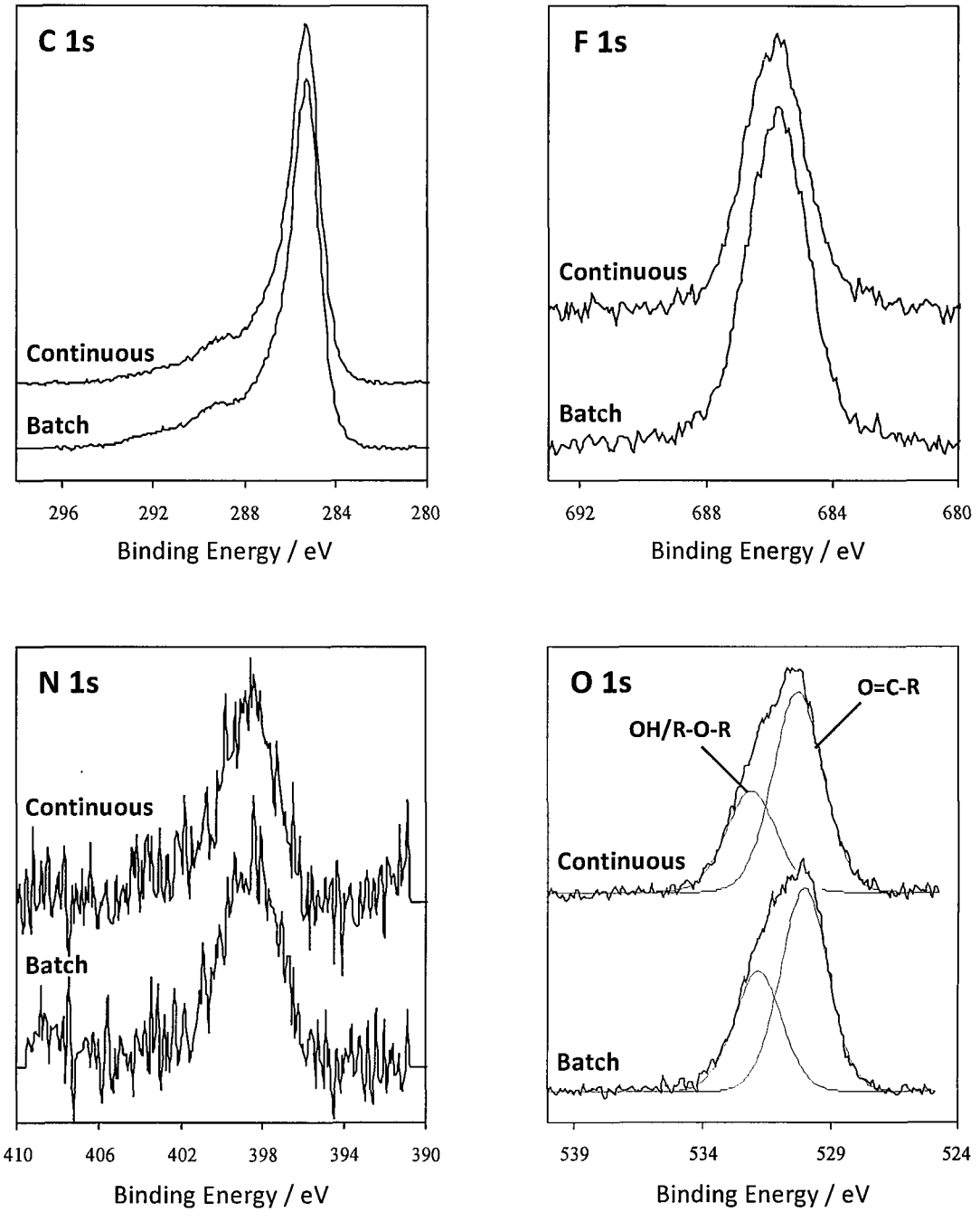


Fig. 4.7: High resolution C 1s, F 1s, N 1s and O 1s XP spectra of AS4 PAN based carbon fibres exposed to either batch or double-sided continuous APF treatments (4 min total exposure)

4.1.4 Influence of atmospheric plasma batch fluorination on wetting behaviour between T700 carbon fibres and PVDF melt

PVDF melt droplets form from a receding movement on powder impregnated carbon fibres and, therefore, it can be assumed that the measured contact angles are equal to the receding contact angles (θ_r). Receding contact angles are typically considered to be more representative for high energy parts of the wetted surface and less sensitive to minor changes on the fibre surfaces. The effect of the exposure time of T700 fibres to APF on the wetting behaviour between AP T700 fluorinated carbon fibres and PVDF is shown in Fig. 4.8.

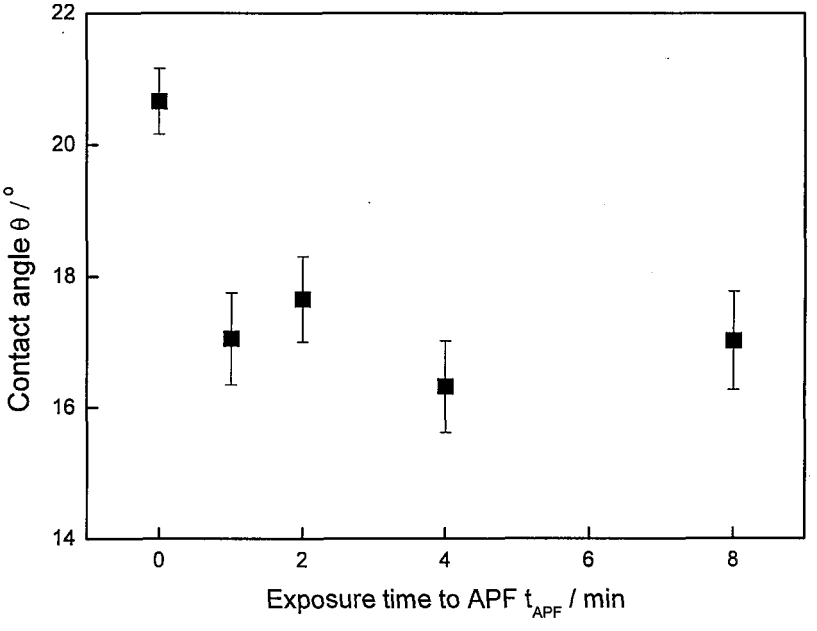


Fig. 4.8: Contact angles between atmospheric plasma fluorinated T700 carbon fibres and PVDF melt as function of exposure time to atmospheric plasma fluorination

The contact angles of PVDF on APF T700 carbon fibres were found to decrease from about 21° to 16° with increasing exposure to atmospheric plasma. This decrease in contact angles implied that APF treated carbon fibre surfaces were becoming slightly

more compatible to PVDF, which suggested that the interaction between atmospheric plasma fluorinated fibres and PVDF improved with increasing surface fluorine content. Comparing the directly measured PVDF melt contact angles with those obtained on directly fluorinated fibres [326], a PVDF melt contact angle of about 16° was observed for fibres with a surface fluorine content of 4 at.-%. Therefore, an improvement should be expected in the adhesion behaviour between PVDF and AP fluorinated fibres as was detected for the directly fluorinated fibres [173].

4.2 Bulk characterisation of carbon fibres

4.2.1 Raman spectroscopy

4.2.1.1 Atmospheric plasma batch fluorinated T700 carbon fibres

Raman spectroscopy (Fig. 4.9) of APF T700 carbon fibres showed the two most prominent Raman-active modes for carbon materials: the deformation mode (D) at 1580 cm^{-1} and the polycrystalline graphite mode (G) at 1355 cm^{-1}. Although no particular trend and shifts could be seen for the D and G peaks from the spectra (Fig. 4.9) but Fig. 4.10 shows that the trend for the calculated integral ratio of the deformation and crystalline mode increased initially upon exposure to 1 min plasma treatment and declined gradually. During the first minute of surface modification, the energised and ionised gas started to sputter the T700 carbon fibre surfaces which caused significant damage to the fibre surfaces (see also Fig. 4.2). This result was consistent with SEM observation, BET and XPS data highlighting that the surface was being damaged due to the sputtering action of the plasma species. As the treatment time increased, more ordered graphite structures were exposed and consequently the d-mode decreased. This

explanation is supported by the observation of sputtered residual carbon deposited on the cylindrical glass cell already observed after 2 min treatment time.

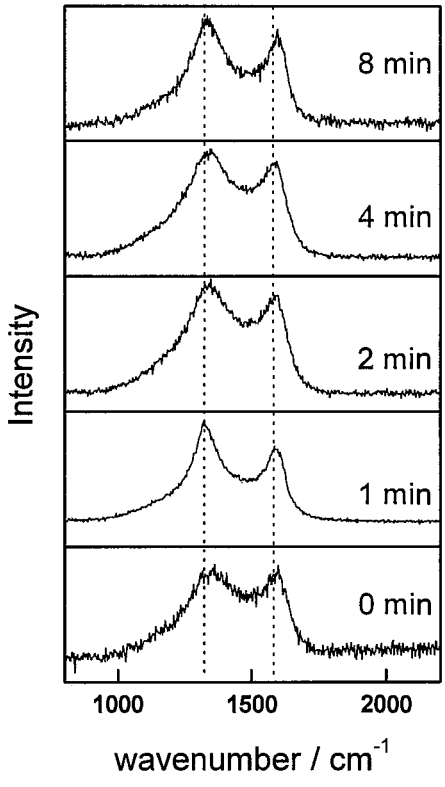


Fig. 4.9: Raman spectra of T700 carbon fibres AP fluorinated (APF) in a N_2 + $CHClF_2$ plasma jet

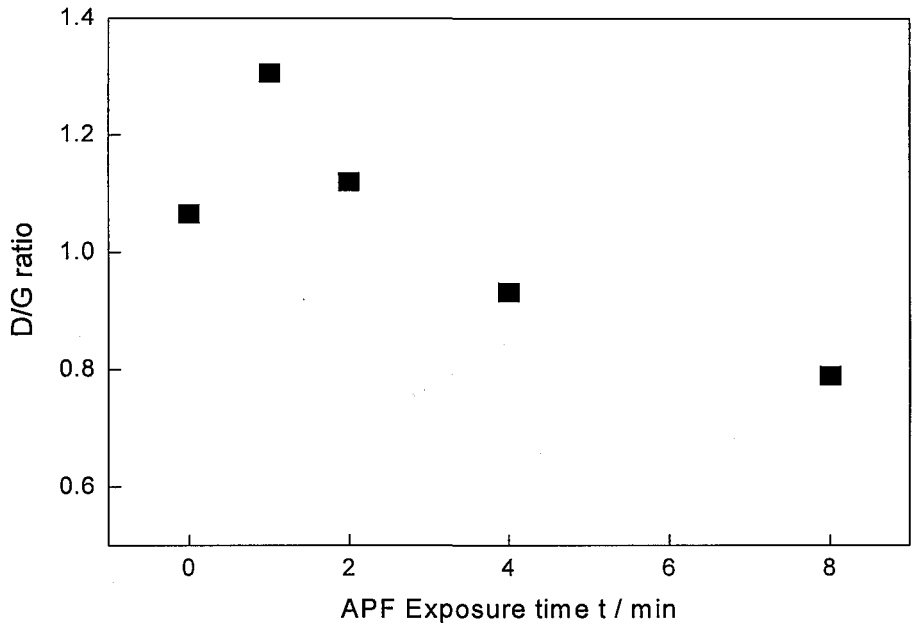


Fig. 4.10: Ratio of degenerate deformation mode and polycrystalline crystallite graphite mode of APF desized T700 carbon fibres in a N_2 + $CHClF_2$ plasma jet as function of treatment time

4.2.1.2 Continuous atmospheric plasma fluorinated AS4 carbon fibres

Once again two characteristic disorder finite-sized microcrystalline carbon (D-band) and graphitic structure of carbon (G-band) peaks were observed at around 1355 cm^{-1} and 1580 cm^{-1} for continuously atmospheric plasma fluorinated AS4 carbon fibres. No peaks shifting could be observed for batch APF treated AS4 fibres compared to the as-received fibres, which was also true for the continuously APF modified AS4 fibres. A decrease in the D/G ratio of the batch APF AS4 carbon fibres was observed, which corresponded to a lower level of disorder graphite in the bulk of the fibres, that could be due to the removal of amorphous carbon (Fig. 4.11).

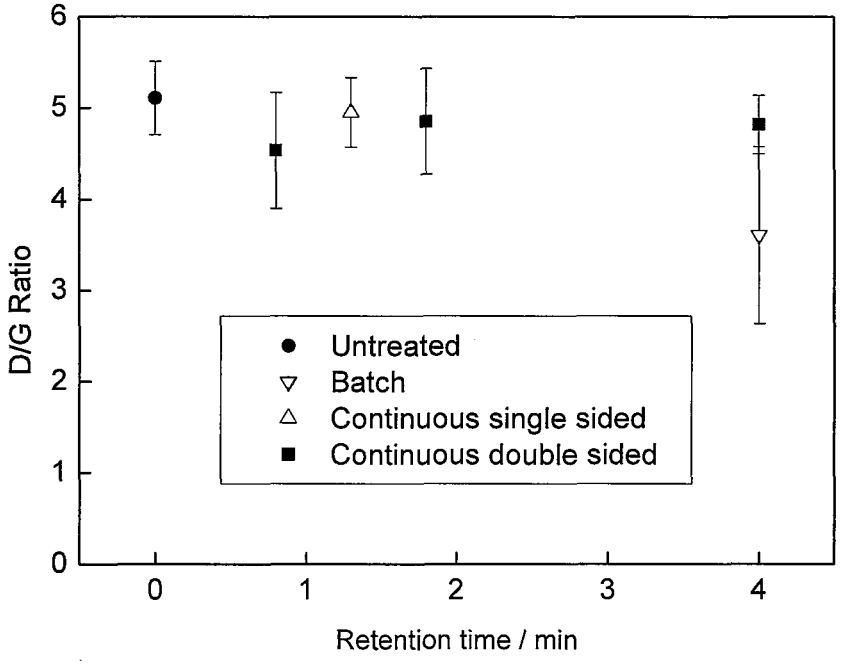


Fig. 4.11: Ratio of degenerate deformation mode (D-band) and crystallite mode (G-band) of original and continuous APF AS4 carbon fibres as function of residence time

4.2.2 X-ray diffraction (XRD) and conductivity analysis of atmospheric plasma batch fluorinated T700 carbon fibres

The XRD patterns of atmospheric plasma fluorinated T700 carbon fibres treated for increasing times are shown in Fig. 4.12:

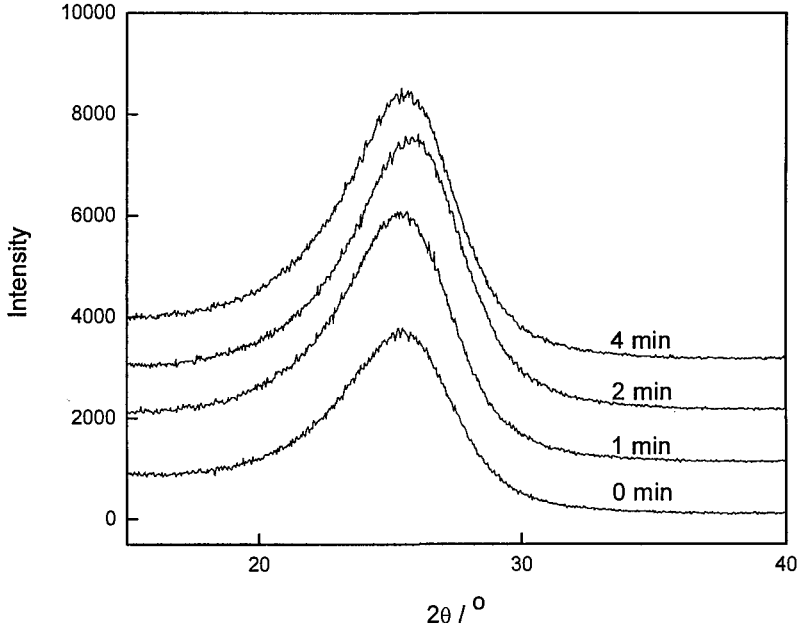


Fig. 4.12: X-ray diffraction patterns of carbon fibres AP fluorinated (APF) in a N_2 + $CHClF_2$ plasma jet

Table 4.8: 2θ values, half width at half maximum ($\Delta\theta_{1/2}$) and calculated interlayer distance (d) of APF T700 carbon fibres in a N_2 + $CHClF_2$ plasma jet

APF Duration / min	$\Delta\theta_{1/2}$ / °	2θ / °	d / Å
0	9.96	25.34	3.60
1	11.04	25.55	3.57
2	10.82	25.77	3.55
4	10.61	25.55	3.57

There are no changes in the intense diffraction pattern, i.e. the calculated interlayer distance, of the APF carbon fibres (002 plane), which suggested that the basal planes

had not slipped sideways relative to each other. This indicates that the bulk structure of the T700 fibre was not largely affected by atmospheric plasma fluorination (Table 4.8). In this case no significant peak broadening ($\Delta\theta_{1/2}$) was observed. This indicates also that only surface carbon layers were removed during atmospheric plasma fluorination which caused slight damage to the crystalline structure.

Conductivity measurements allow detection of possible changes in the π-electron system of the graphitic parts of the carbon fibres. Such changes in the π-electron system would indicate a major change in the bulk properties which could be caused by chemical reactions occurring inside the fibres. The data in Table 4.9 show that atmospheric plasma fluorination only marginally affected the electrical conductivity of the fibres. A slight increase of the mean of the conductivity could be observed after exposing the fibres for 8 min to atmospheric plasma fluorination. These results can be explained by a decreased contact resistance because the fibres are now more graphitic after sputtering in APF (section 4.2.1.1). These minor changes are also likely to have been due to the changes occurring at the fibre surface; from the original desized and mildly oxidised fibres over sputtered fibres leading to a more graphitic structure.

Table 4.9: Resistance (R), conductivity (κ) and resistivity (ρ) of APF T700 carbon fibres in a N_2 + $CHClF_2$ plasma jet

APF Duration / min	R / Ω	κ / S cm^{-1}	ρ / m Ω cm
0	9565 ± 600	660	1.51
2	8627 ± 400	665	1.50
4	8670 ± 600	652	1.53
8	8569 ± 400	727	1.37

4.2.3 Impact of atmospheric plasma fluorination on single fibre tensile properties of T700 carbon fibres

A drop in the fibre tensile strength could disqualify the APF treated fibres from being used in composites, if other physical properties remained unchanged. Therefore, the impact of APF on the tensile properties of the treated carbon fibres was characterised. Single fibre tensile tests were performed as a fast screening tool to assess potential damage of APF to T700 carbon fibres.

4.2.3.1 Atmospheric plasma batch fluorinated T700 carbon fibres

The tensile strength of single atmospheric plasma fluorinated T700 carbon fibres remained constant ($\sigma_f = 4500 \pm 500$ MPa) up to 8 min atmospheric plasma exposure (Fig. 4.13). The measured strength was in excellent agreement with the claims of the manufacturer ($\sigma_f = 4900 \pm 500$ MPa)*. This preliminary result showed that batch APF did not affect the mechanical properties of T700 carbon fibres.

* Source: http://www.torayca.com/properties/en/images/report_eng01_2.html accessed on 8.02.05

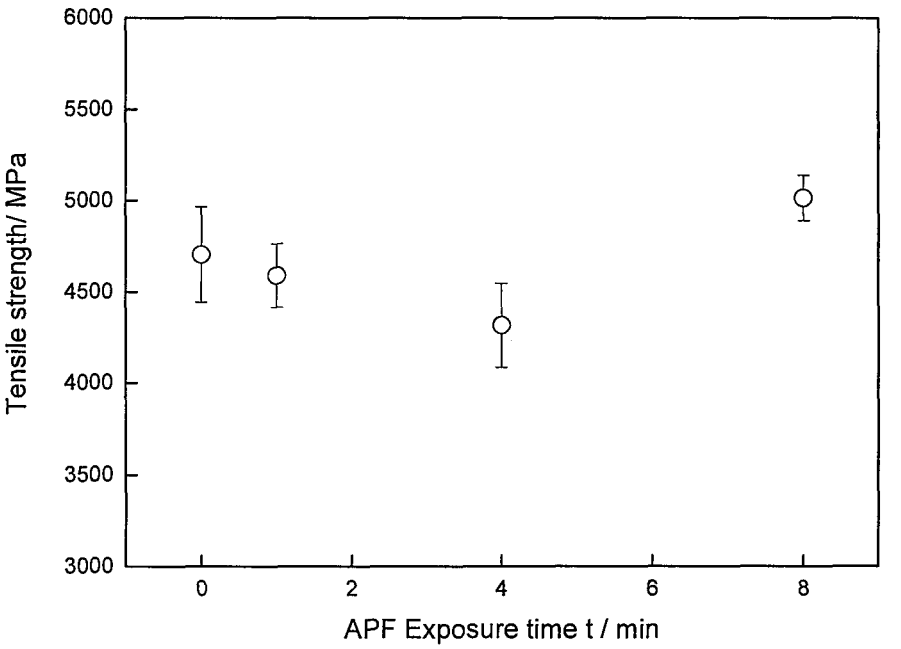


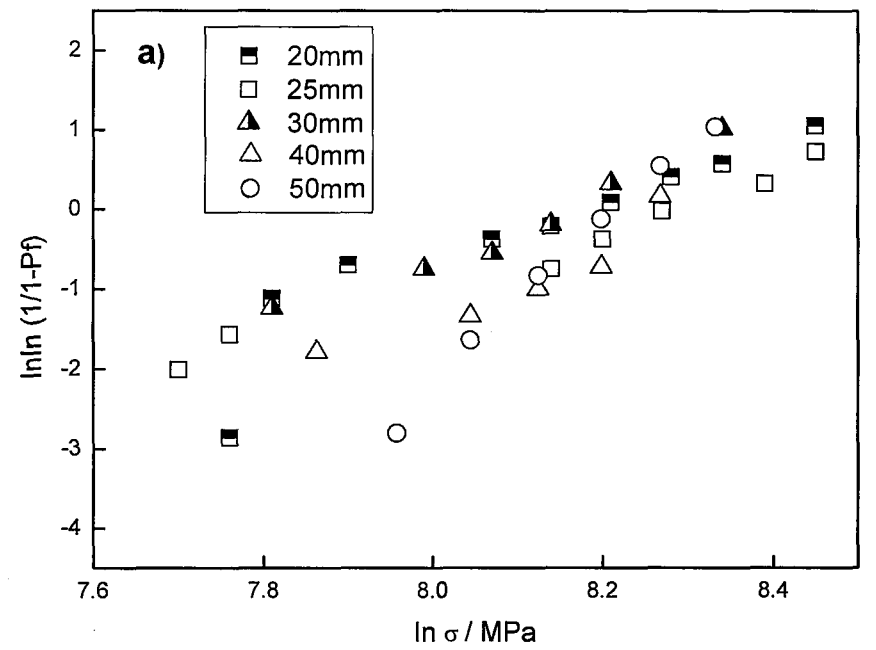
Fig. 4.13: Variation in tensile strength of APF T700 carbon fibres as a function of exposure time

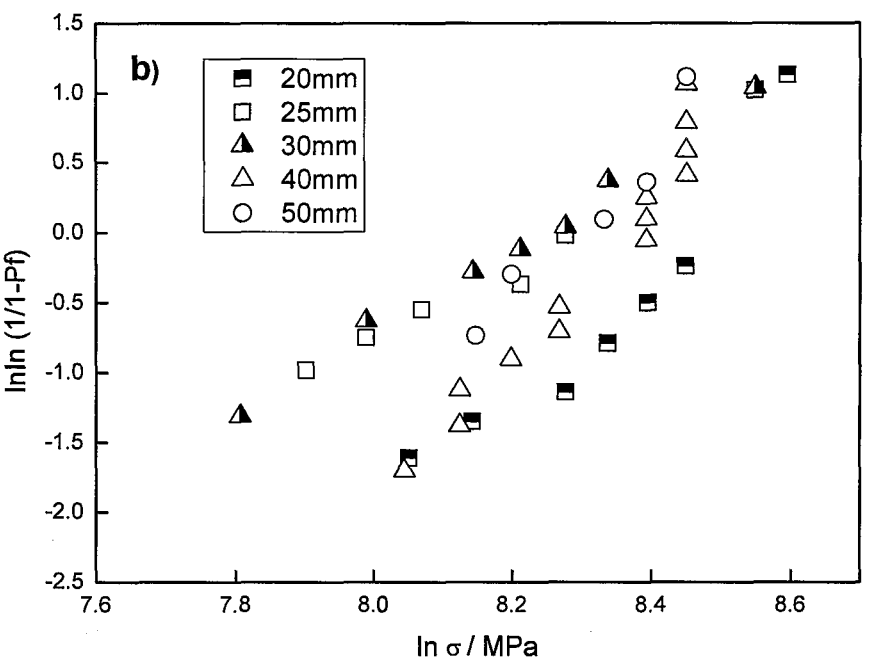
4.2.3.2 Continuous atmospheric plasma fluorinated AS4 carbon fibres

A marginal decrease in the tensile strength of all the investigated AS4 carbon fibres was observed as the fibre gauge length increased (Table 4.10). For the original carbon fibres the tensile strength at a gauge length of 20 mm was 3810 ± 200 MPa while the tensile strength dropped to 3520 ± 230 MPa at gauge length of 30 mm. On average as the gauge length increased by 10 mm, the fibre tensile strength decreased by approximately 300 MPa. In general a higher tensile strength was expected for the shorter fibres. Unfortunately, batch APF treated fibres of longer gauge lengths (40 and 50 mm) could not be tested due to the size limitation of the glass tee piece (Fig. 3.1) used for APF as well as the nature of APF batch configuration.

Table 4.10: Tensile strength, Weibull modulus and scale parameter at different gauge lengths of APF AS4 carbon fibres as a function of residence time

	Fibres treatment	Residence time/ min	Gauge length/ mm				
			20	25	30	40	50
Tensile strength/ MPa	Original	0	3810 ± 200	3550 ± 310	3520 ± 230	3660 ± 160	3650 ± 90
	Batch	4	3930 ± 100	3420 ± 220	3660 ± 200	-	-
	Continuous single sided	1.3	3930 ± 190	3470 ± 260	3600 ± 130	3680 ± 160	3360 ± 180
	Continuous double sided	0.8	3800 ± 290	3510 ± 220	3440 ± 180	3880 ± 170	3770 ± 140
		1.8	3720 ± 240	3820 ± 150	3490 ± 150	3680 ± 190	3600 ± 110
		4	4090 ± 220	3560 ± 190	3360 ± 170	3540 ± 140	3540 ± 150
Weibull modulus	Original	0	4.40	3.35	3.90	5.11	10.18
	Continuous double sided	0.8	4.26	3.77	3.75	5.52	7.03
		1.8	4.03	5.01	3.28	4.95	6.94
		4	2.88	2.78	2.91	6.17	4.90
Weibull Parameter	Original	0	8.19	8.10	8.30	8.27	8.22
	Continuous double sided	0.8	8.24	8.26	8.24	8.37	8.30
		1.8	8.28	8.27	8.60	8.27	8.26
		4	8.57	8.24	8.23	8.33	8.28


a)
20mm
25mm
30mm
40mm
50mm
lnln (1/1-Pf)
ln σ / MPa
2
1
0
-1
-2
-3
-4
7.6
7.8
8.0
8.2
8.4


b)
20mm
25mm
30mm
40mm
50mm
lnln (1/1-Pf)
ln σ / MPa
1.5
1.0
0.5
0.0
-0.5
-1.0
-1.5
-2.0
-2.5
7.6
7.8
8.0
8.2
8.4
8.6

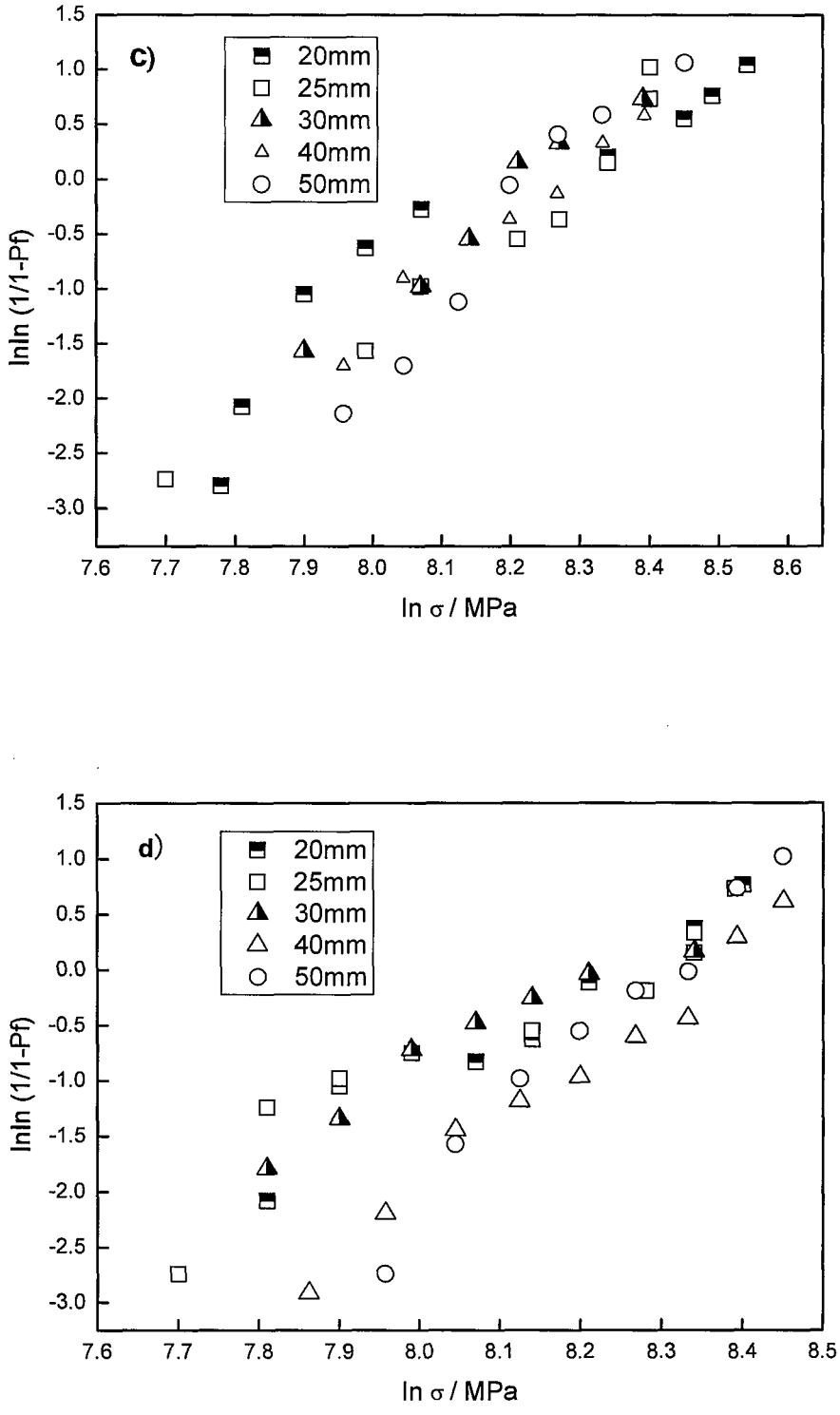


Fig. 4.14: Weibull plots of continuous double sided APF treated AS4 carbon fibres at a) original, b) 0.15 m/min, c) 0.33 m/min and d) 0.75 m/min. Examples of linear regression analysis can be found in Appendix D.

The mechanical data from continuous APF treated AS4 carbon fibres measured from single fibre tensile tests widely scattered. This scatter was mainly due to the flaws along the fibres and, therefore, the Weibull distribution was used to analyse the data. The Weibull modulus and parameters obtained from the experimental data of continuously double sided APF treated carbon fibres are shown in Table 4.10. Batch and continuously single sided APF treated fibres were not analysed due to their high degree of surface inhomogeneity and low surface fluorine content, as shown by $\Delta\theta$ and XPS (Table 4.4 and 4.7). Weibull plots (Fig. 4.14) of the investigated fibres at all gauge lengths showed good conformity, demonstrating a linear relationship with the probability of fibres failing increased as loading on the fibre increased. The Weibull modulus can be used to predict the approximate fibre tensile strength at any length of interest. The tensile strength of continuously APF treated fibres of 40 and 50 mm gauge lengths were predicted from samples of shorter gauge lengths (Table 4.11). A 20% difference between predicted and experimental tensile strength can be observed when the predictions are made from 20 and 25 mm gauge length fibres. However, the errors can be significantly reduced when predictions are made from longer fibres closer to the predicted length. The error in the predicted tensile strength of 40 mm gauge length fibres using 20 mm gauge length was found to be 12%, whereas when the strength of 40 mm gauge length fibres was predicted using carbon fibres tested at 50 mm gauge length, the error was reduced to 2%. This shows that higher accuracy can be obtained if the predicted and the actual gauge length are within $\pm$ 20% of each other i.e. using tensile strength from 40 mm gauge length to predict the tensile strength of fibres with 50mm gauge length and vice versa.

From a more detailed study on the tensile strength of the AS4 fibres, it could be seen that continuous APF marginally affect the tensile properties of the carbon fibres. Furthermore, the Weibull distribution showed reasonable agreement of the predicted tensile strength with the measured tensile strength of the APF treated carbon fibres.

Table 4.11: Predicted tensile strength of continuous double sided plasma fluorinated AS4 carbon fibres at a) 40mm and b) 50mm gauge length

Predicting gauge length	Residence time/ min	Gauge length/ mm used for σ/ mm prediction	Predicted σ/ MPa	% difference between measured and predicted
40	0	20	3250	12
		25	3080	16
		30	3270	11
		50	3730	2
	0.8	20	3230	17
		25	3100	20
		30	3180	18
		50	3920	1
	1.8	20	3130	15
		25	3480	5
		30	3200	13
		50	3720	1
	4	20	3220	9
		25	3000	15
		30	3040	14
		50	3700	4
50	0	20	3090	15
		25	2880	21
		30	3090	15
		40	3500	4
	0.8	20	3060	19
		25	2920	22
		30	3000	20
		40	3810	1
	1.8	20	2960	18
		25	3330	8
		30	3080	15
		40	3520	2
	4	20	2980	16
		25	2780	22
		30	2820	20
		40	3700	4

4.2.4 Effects on the PVDF matrix crystallinity in the presence of APF carbon fibres

PVDF is a semi-crystalline thermoplastic polymer and, therefore, not only the interaction between the fibre and the matrix interface but also the degree of crystallinity of the matrix play a major role in determining the mechanical performance of the composite. The phenomenon of transcrystallinity is often found in thermoplastic matrix composites where an orderly layer of transcrystallites is formed around the reinforcing fibres [327]. However, this very much depends on both the nucleation capacity of the fibre surface and the ability of the polymer to crystallise. Unfortunately, little is known about the effect of transcrystallinity on interfacial parameters [328] and particularly between carbon fibres and PVDF.

The transcrystalline layer is claimed to reduce processing related residual thermal stresses which result from differential shrinkage of the constituents upon cooling from the processing temperature. This is due to a large amount of crystallisation associated matrix shrinkage as well as the thermal strain and in turn lowers the performance of composite materials [329]. Optical micrographs (Fig. 4.15, 4.16) taken under cooling conditions similar to those used during composite preparation show that crystallisation of PVDF for both T0 and T1 fibres (1 min batch AP fluorinated T700 carbon fibres) initiates from the bulk of the PVDF melt and only occurs at a temperature around 140 °C. This suggested that APF T700 carbon fibres, as a substrate, has a low surface nucleation efficiency [330] as no transcrystalline region is formed, due to primary nucleation, around the carbon fibres during the composite preparation conditions. The presence of carbon fibres (both original and APF) caused the melting temperature and enthalpy, i.e. the degree of crystallisation, to drop by 4 °C from 170 °C to 166 °C and by approximately 50 % (Table 4.12). This is because the presence of carbon fibres,

which limits the volume of the crystallising PVDF melt because of the high volume portion occupied by the fibres [331]. Therefore, resulting in more amorphous regions, this leads to a lower degree of crystallinity and a reduced melting point.

Furthermore the crystallinity X_c, as determined by DSC analysis, of the PVDF matrix impregnated in desized T700 carbon fibre (both original and batch APF)/ PVDF composites (un-annealed) shows that APF had no significant effect on the degree of crystallinity (Table 4.12). Similar results were found for the crystallinity X_c of the PVDF matrix (X_c= 19 ± 2 %) impregnated in unidirectional AS4 carbon fibre (both original and continuously APF) reinforced composites (annealed).

Therefore, if there is any enhancement in mechanical properties (both micromechanics and macromechanics) in the composites manufactured, it is not due to a change in the crystallisation behaviour of the matrix.

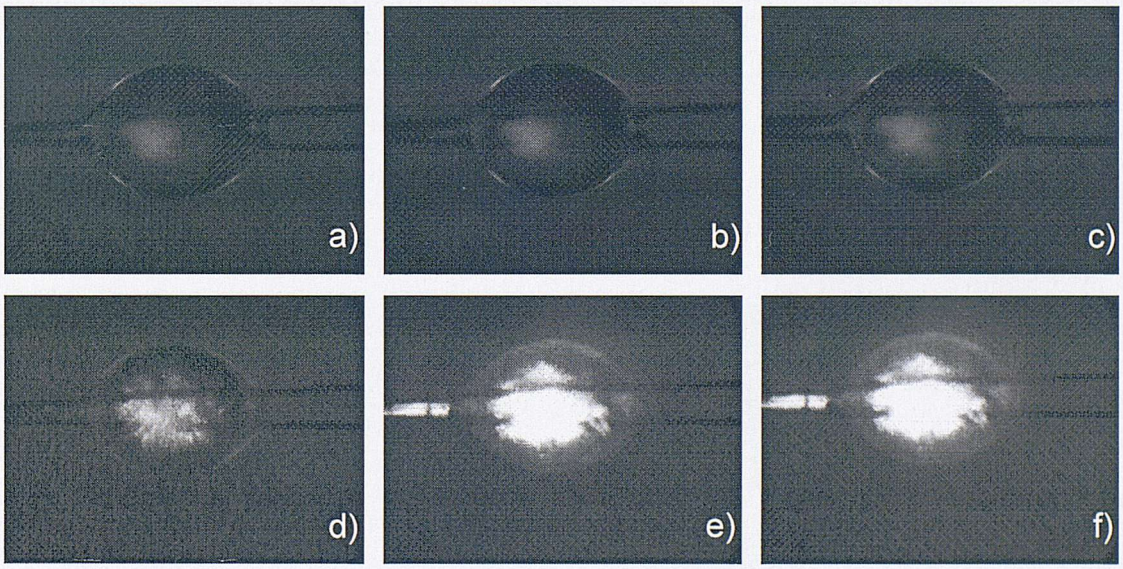


Fig. 4.15: Optical microscopic images of desized and original (T0) carbon fibres, images taken at a) 180 °C, b) 150 °C, c) 140 °C, d) 130 °C, e) 120 °C and f) 120 °C for 5 min

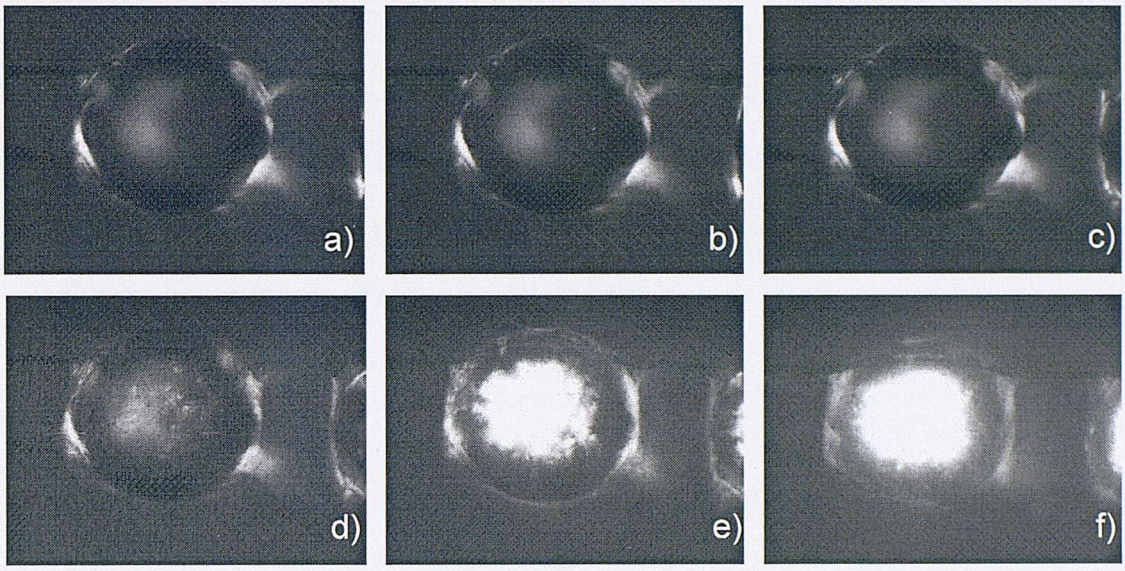


Fig. 4.16: Optical microscopic images of 1 min exposure (T1) to APF carbon fibres, images taken at a) 180 °C, b) 150 °C, c) 140 °C, d) 130 °C, e) 120 °C and f) 120 °C for 5 min

Table 4.12: Melting points (T_m), heat of melting (H_m) and degree of crystallinity (X_c) of pure PVDF powder, desized and original (T0) carbon fibres/ PVDF and 1 min exposure (T1) to APF carbon fibres/ PVDF

	T_m / °C		H_m/ Jg^{-1}	X_c / %
Pure PVDF powder	1st heating	170	29.5	28.2
	2nd heating	171	32.9	31.5
T0 carbon fibres / PVDF	1st heating	166	19.5	18.7
	2nd heating	167	20.7	19.8
T1 carbon fibres / PVDF	1st heating	167	17.4	16.6
	2nd heating	167	18.2	17.4

4.3 Quality control of carbon fibre reinforced PVDF composite via powder impregnation

As described in the experimental chapter, initially the PVDF powder concentration in the impregnation bath needs to be optimised to manufacture unidirectional carbon fibre reinforced PVDF composite tapes with a consistent fibre volume content of 60 %. Fig. 4.17 shows the fibre volume content of as produced carbon fibre reinforced PVDF composite tapes as a function of PVDF bath concentration. From the graph one can see

that the optimum concentration can be identified as 9 wt%. Given the regular addition of concentrated PVDF suspension to maintain a constant bath concentration of 9 wt%, the fibre volume content of as produced carbon fibre reinforced PVDF tape was found to vary slightly during the process duration (2 h) but overall the produced composite had FVC = 62 % with a standard deviation of 3 % (Fig. 4.18).

Fig. 4.19 shows optical micrographs of typical transverse sections of the manufactured PVDF composite laminates containing unidirectionally aligned APF carbon fibres. The fibre distribution within the composite was generally uniform, although the form of the original individual composite tapes moulded to form the laminates remain clearly evident, as shown by the presence of resin rich regions between the layers of composite tapes.

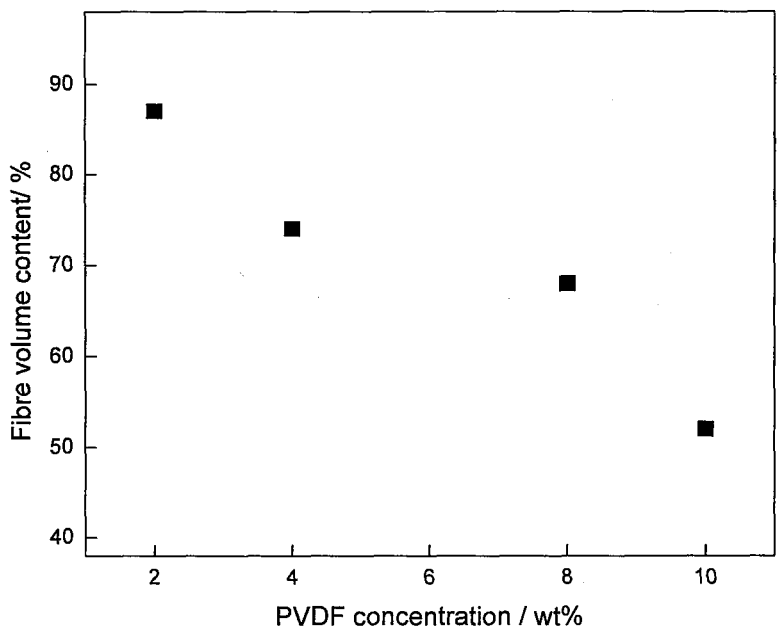


Fig. 4.17: Fibre volume content of as produced carbon fibre/PVDF tape as function of PVDF powder concentration in the impregnation bath

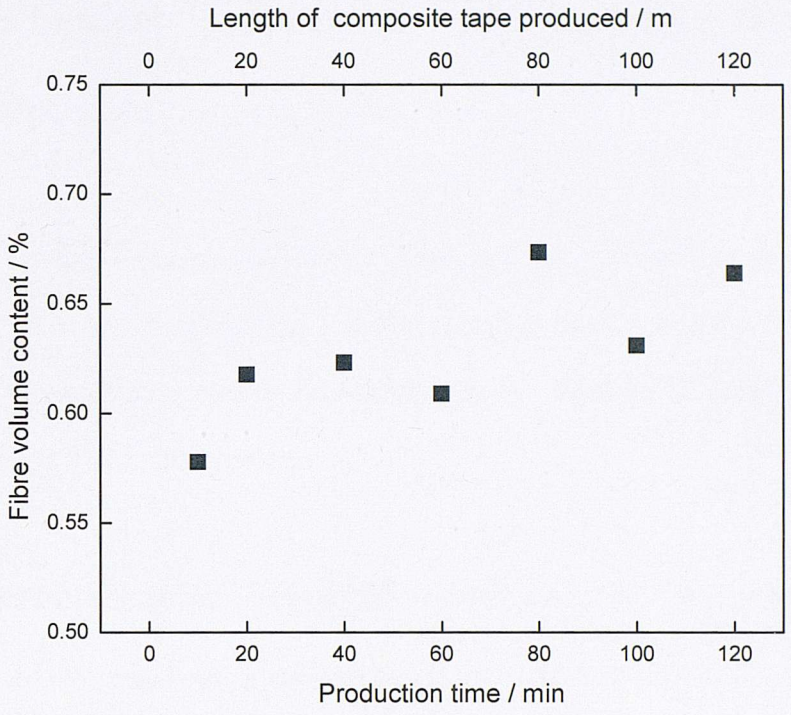


Fig. 4.18: Fibre volume content of as produced carbon fibre/PVDF composite tape as function of manufacturing time

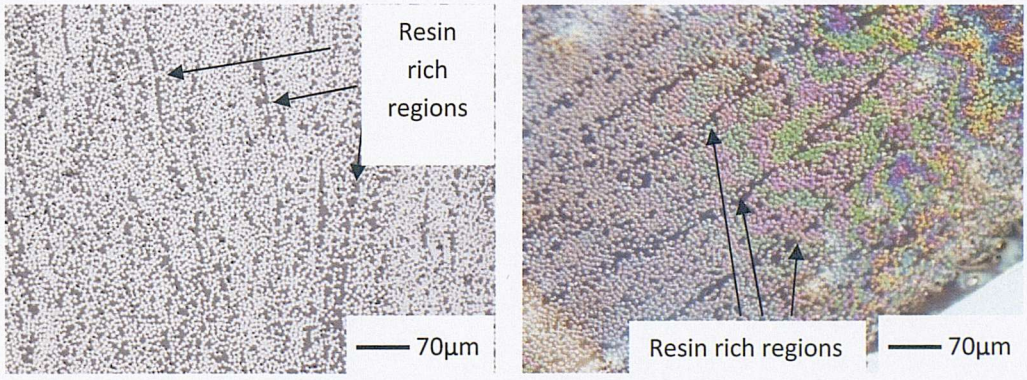


Fig. 4.19: Representative optical microscopic images of as produced laminated unidirectional carbon fibre reinforced PVDF composites after consolidation and compression moulding

4.4 Mechanical properties of carbon fibre/ PVDF composites

The bond strength between reinforcing fibres and the surrounding matrix was studied using direct micromechanical and indirect macromechanical test methods to examine the effect of atmospheric plasma fluorination on the mechanical performance of carbon fibre reinforced PVDF composites.

4.4.1 Micromechanics: Single fibre pull-out test: Apparent interfacial shear strength as a measure of practical adhesion

(The work presented in the following section* was performed by the author under the supervision of Dr. Gerhard Kalinka, BAM-Federal Institute for Materials Research and Testing, Division V.6. Germany; as an adaption to form an integral part of a relevant contribution to the main theme of the thesis)

The effect of atmospheric plasma batch fluorinated T700 carbon fibres on the apparent interfacial shear strength (IFSS) to PVDF was examined using the single fibre pull-out test. From a typical measurement, the force required to debond the interface between atmospheric plasma fluorinated fibres was determined (Fig. 4.20) and this in turn allows the adhesion behaviour at the fibre to matrix interface in a single fibre composite to be investigated. The apparent IFSS increased from 10.2 MPa for the oxidised but non-fluorinated T0 carbon fibres to 16 MPa for the carbon fibres exposed for 1 min to APF (Fig. 4.21). As the APF exposure time continued to increase from 2 to 8 min, the IFSS remained unaffected even though the fibre surface area increased from 0.22 to 0.44 m^2/g (Fig. 4.3, section 4.1.1.1). This suggests that the formation of surface defects and the increase in the surface roughness caused by the surface sputtering during the APF does not contribute to the improvement of the interfacial shear strength. The pits formed

* Published in J Coll Interf Sci 2007; 313: 476-484.

could even result in the formation of voids at the fibre/matrix interface if the surface is not fully wetted by PVDF.

The maximum improvement in apparent interfacial shear strength between carbon fibres and PVDF was achieved only after 1 min exposure to atmospheric plasma. The increase in practical adhesion follows the general trend (Fig. 4.8, section 4.1.4) predicted from the measured direct contact angles, i.e. the smaller the contact angle the higher the interfacial shear strength.

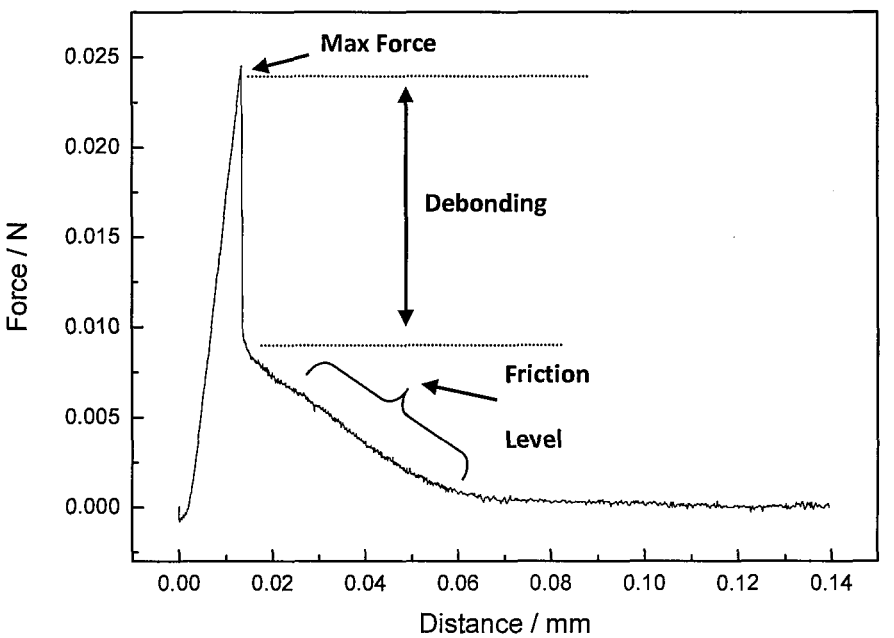


Fig. 4.20: A graph (exemplary shown) of pull-out force as function of displacement of a single fibre pull-out test. Further examples can be found in Appendix E.

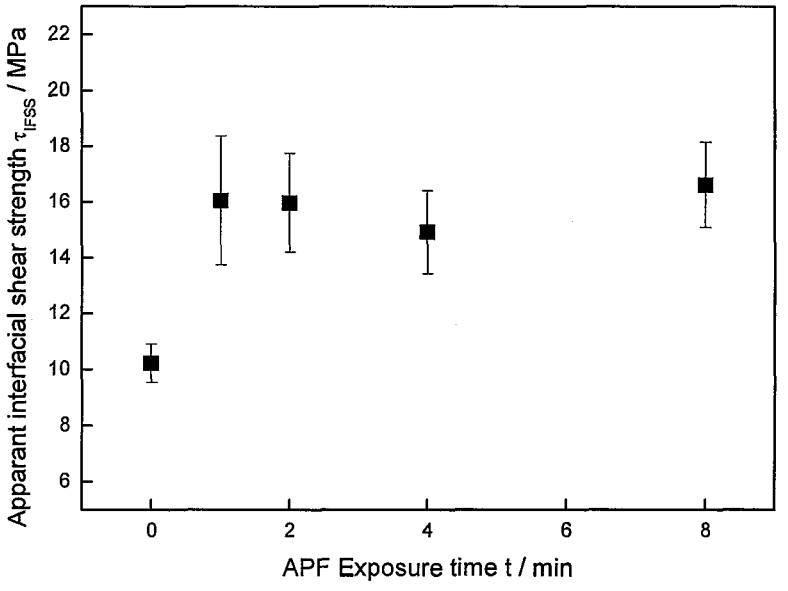


Fig. 4.21: Apparent interfacial shear strength between APF T700 carbon fibres and PVDF as function of exposure time to atmospheric plasma fluorination

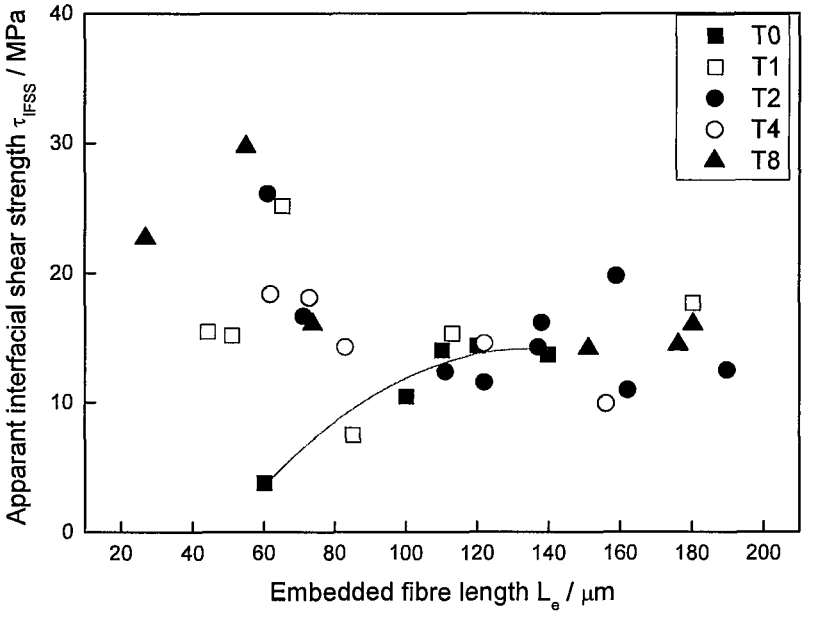


Fig. 4.22: Apparent interfacial shear strength between APF T700 fibres and PVDF as function of the embedded fibre length

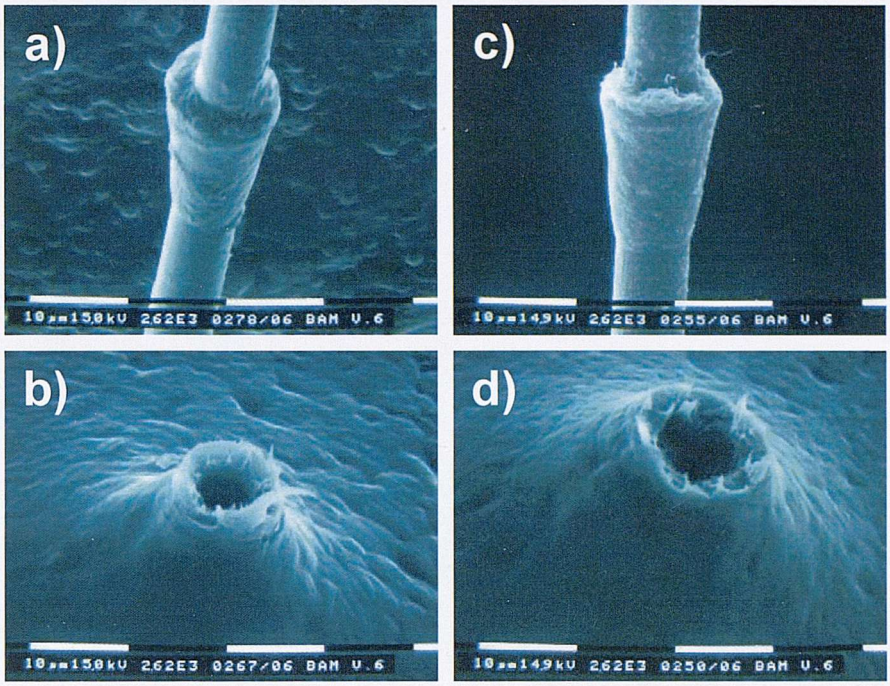


Fig. 4.23: Representative SEM images showing 2 min a), b) and 4 min c), d) APF T700 carbon fibres pull-out from PVDF droplets

The measured apparent IFSS as function of the embedded fibre length provides information about the fracture behaviour of the fibre/matrix interface [332].The IFSS between the original desized fibre T0 and PVDF is virtually independent of the embedded fibre length (Fig. 4.21). The IFSS does not decrease with increasing embedded fibre length. This indicates that the displacement of the fibre-matrix interface during the pull-out tests leads to a ductile type failure, which suggests that the fracture does not occur instantaneously and the boundary layer is predominantly amorphous. On the other hand for all atmospheric plasma fluorinated fibres, the interfacial shear strength decreased with increasing embedded length and this indicated a brittle fracture behaviour of the model composite and that the interface failed at once [333]. SEM images of fibres after the pull-out as well as the corresponding PVDF droplets were taken (Fig. 4.23) to investigate the change in the apparent fracture behaviour. The SEM micrographs show clearly that a wetting cone i.e. a meniscus, formed when the PVDF polymer melt comes into contact with the fibre. Three factors determine the size and shape of the meniscus; 1) the contact angle between fibre and matrix which is a function

of the surface energies of both materials, 2) the droplet flows under the influence of gravity and thus moves relative to the fibre and 3) the droplet shrinks onto the fibres during the cooling process. When pulling at the end of the embedded fibre, the weakest part of the system fails first. Usually, the highest stresses arise in the region, where the fibre is in contact with the matrix droplet. The failure may start with the fracture of the meniscus or the fibre/matrix interface inside the droplet near the meniscus. Therefore, the fracture type is related to the fibre roughness and wetting behaviour of the fibre by the polymer melt as well as the cooling of the embedded system. As can be seen in the SEM images, the energy required for a matrix crack separating the meniscus from the droplet is lower than that for complete interface separation. Therefore, after the single fibre detached from the matrix droplet, a small part of the meniscus remained on the surface of the pulled-out part of the fibre (Fig. 4.23a, 4.23c).

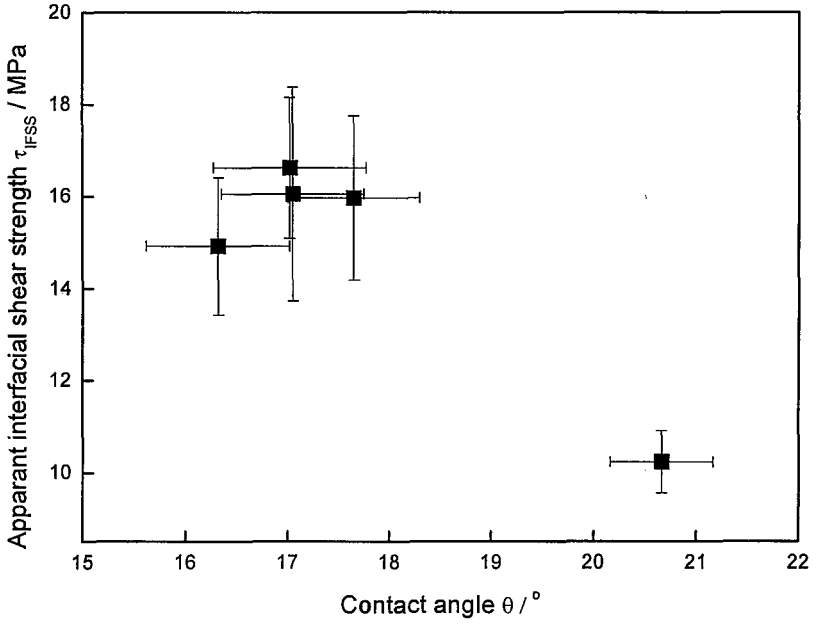


Fig. 4.24: Apparent interfacial shear strength as function of contact angles between APF T700 carbon fibres and PVDF melt

From a micromechanics point of view, the results from single fibre pull-out test compliment the wetting behaviour of single carbon fibres by PVDF melt (Fig. 4.3,

section 4.1.1.1). As the contact angle decreased, i.e. the PVDF polymer melt wetted the carbon fibres better, the apparent interfacial shear strength increased i.e. the stronger the adhesive bond at the interface (Fig. 4.24).

4.4.2 Macromechanical properties

In this section, indirect macromechnical test methods including flexural and apparent short beam shear testing were employed to study the effect of inline atmospheric plasma fluorination of AS4 carbon fibres on mechanical performance of unidirectional fibre reinforced PVDF.

4.4.2.1 Impact of APF on flexural properties of carbon fibre reinforced PVDF

A typical force-displacement curve obtained during flexural testing of unidirectional carbon fibre reinforced PVDF composite is shown in Fig. 4.25.

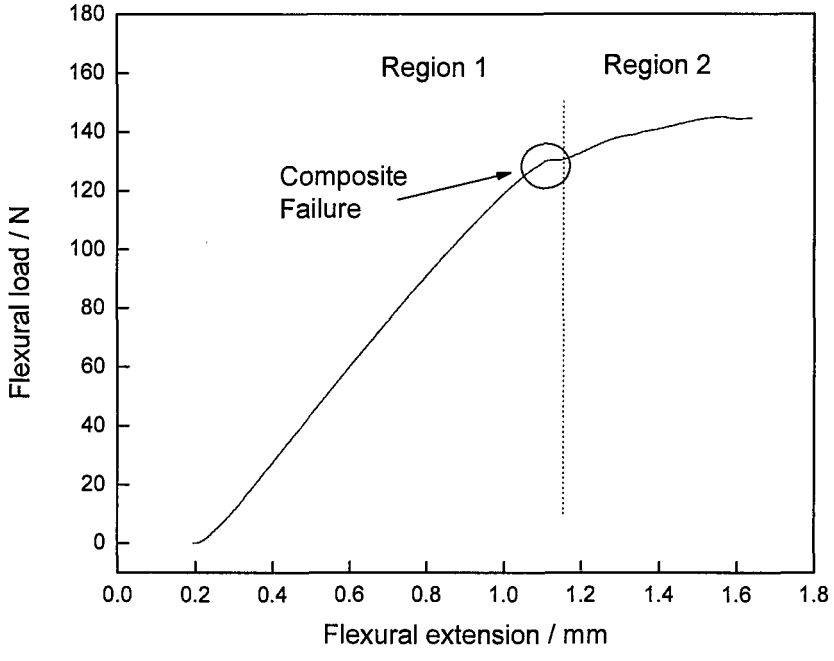


Fig. 4.25: Flexural load as function of flexural extension during flexural testing

Region 1 of the force-displacement curve shows a linear flexural load as a function of extension until compressive failure of the upper surface which was due to the roller (as highlighted). In accordance with the standard, this steady state load was used for the calculations of the flexural strength. When the specimen was subjected to a steady state load, the load is transferred from the matrix to the fibres via the interface and is in this case directly related to the shear stress causing interfacial failure. The force as function of displacement further increases in Region 2. In this region the composite undergoes plastic deformation while the crosshead is crushing the test piece inside the test jig. A flexural tensile strength of 225 ± 7 MPa was obtained for standard industrially oxidised but unsized AS4/ PVDF composites produced at a line speed of 1 m/min (Fig. 4.26). For the composites containing carbon fibres that were continuously APF with a degree of fluorination of 2.8 at.-% (produced at 1 m/ min), the flexural strength increased to 250 ± 12 MPa, which corresponded to a 10 % increase. As the fluorine content of the carbon fibres increased to 3 at.-% and 3.7 at.-%, the flexural strength of the composites (produced at 0.75 m/min and 0.33 m/min, respectively) was found to increase further by 60 % and 110 %, respectively.

The flexural modulus increased from 80 ± 2 GPa for the standard oxidized but unsized AS4/PVDF composites to 86 ± 3 GPa for composites that contained carbon fibres that were continuously APF with a degree of fluorination of 2.8 at.-% (Fig. 4.26). As the surface fluorine content of the reinforcing fibre increased further to 3 at.-%, the flexural modulus increased to 105 ± 3 GPa and even further to 110 ± 2 GPa for composites containing carbon fibres with 3.7 at.-% fluorine content.

Therefore, increasing the fluorine content of the fibres improved wettability of PVDF to carbon fibres (section 4.1.4) and improved the apparently interfacial shear strength between the fibres and the matrix (section 4.4.1). As a result, significant improvement

in the flexural properties of unidirectional carbon fibres reinforced PVDF composite laminates was apparent.

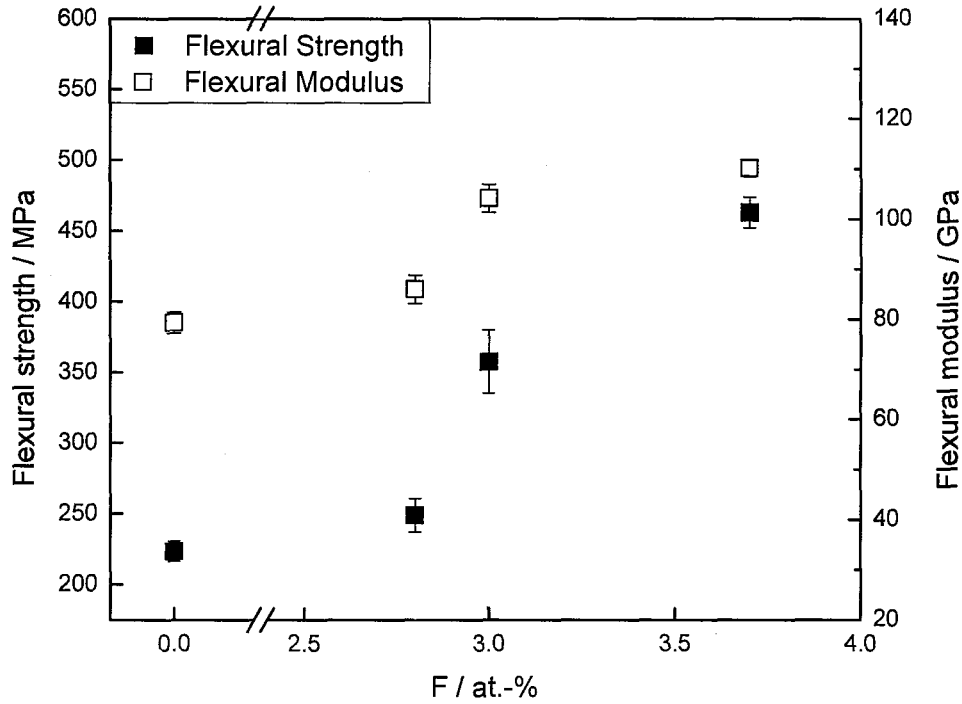


Fig. 4.26: Flexural strength and modulus of laminated carbon fibre/PVDF composites as function of fluorine content of the fibres fluorinated in atmospheric plasma

4.4.2.2 Impact of APF on apparent short beam shear strength of carbon fibre reinforced PVDF

The ASTM Standard D2344 [318] states that during conventional short beam shear testing of unidirectional fibre reinforced thermoplastics, the stress that is induced in the specimen is neither a pure shear stress nor a pure flexural stress but a mixture of both stresses and, therefore, the test is called apparent short beam shear test. The apparent short beam shear strength increases from 7 ± 0.2 MPa for the standard oxidized but unsized AS4/PVDF composites to 9.5 ± 0.5 MPa and to 11 MPa for composites containing carbon fibres with a degree of fluorination of 2.8 at.-% and 3 at.-% (Fig. 4.27).

As the surface fluorine content of the reinforcing carbon fibre continues to increase to 3.7 at.-%, the apparent short beam shear strength was found to increase further to 20.6 ± 0.2 MPa. Results obtained indicate that appropriate degree of inline carbon fibre modification improves the interface dominated mechanical properties of unidirectional carbon fibre reinforced PVDF.

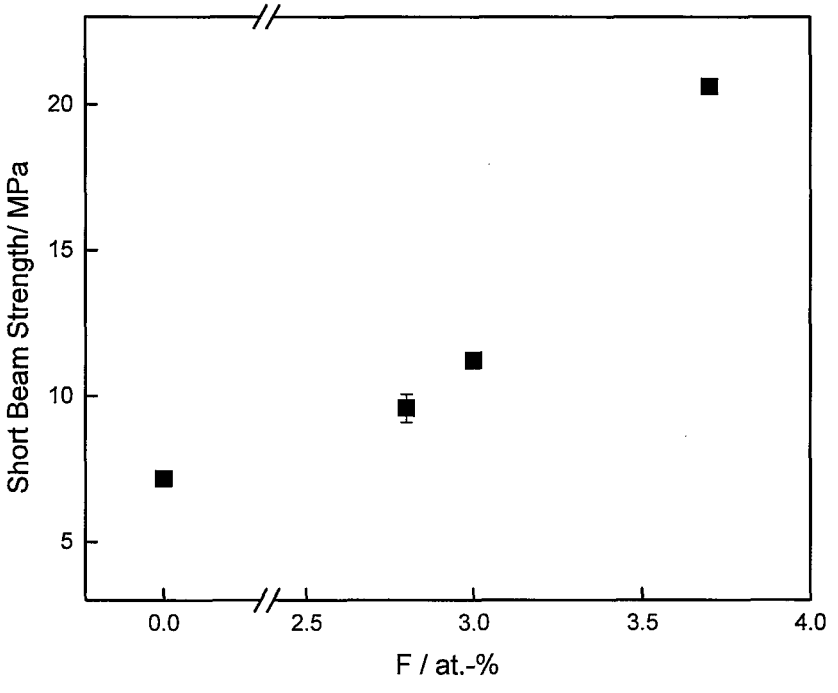


Fig. 4.27: Short beam shear strength of laminated carbon fibre/PVDF composites as function of surface fluorine content of the carbon fibres

Chapter 5

Conclusions

A procedure to fluorinate carbon fibres using an atmospheric pressure plasma system was developed. The carbon fibres were successfully fluorinated in a chlorodifluoromethane containing nitrogen atmospheric pressure plasma jet. Numerous analytical techniques were used to characterise the impact of atmospheric plasma fluorination (APF) on the surface and bulk properties of the modified carbon fibres. Micro- and macromechanical tests were conducted on single fibre model composites and unidirectional carbon fibre reinforced polyvinylidene fluoride (PVDF) laminates. The aim of these tests was to deduce the impact of APF of carbon fibres on interfacial properties of carbon fibre reinforced PVDF composites. From this study, the following conclusions were drawn:

1) XPS measurements were conducted to confirm the success of fluorination of carbon fibres using atmospheric plasma. Results show that up to 1.6 at.-%, 4.7 at.-% of fluorine functional groups were successfully introduced to the batch fluorinated T700 and AS4 carbon fibres, respectively. In addition, up to 4.9 at.-% of fluorine functional groups were also introduced to continuous double side treated AS4 carbon fibres. It should be noted that all APF of investigated fibres were conducted using a gas mixture of chlorodifluoromethane and nitrogen in a 1:70 ratio, with a treatment/ residence time.

2) Wettability measurement is a quick and easy analytical technique to assess whether fluorination has been successful, this is because fluorine functionalities

with a covalent bond character would result in an increase in the fibres surface hydrophobicity. Modified Wilhelmy water contact measurements show an increase in fibre surface hydrophobicity from 81° to 103° for the batch APF T700 fibres and from 77° to 88° for the continuous APF AS4 fibres. A decrease in surface free energy from 44.0 mN/m to 31.0 mN/m for the batch APF T700 fibres and from 37.5 mN/m to 35.3 mN/m for the continuous APF AS4 fibres was also observed. These were attributed to the fluorination of the fibre surface as a result of APF.

3) One of the main mechanisms of adhesion is mechanical interlocking at the fibre/ matrix interface and is governed by the surface roughness. Since APF of carbon fibres results in amorphous carbon being sputtered off the surface, the effect of APF on the surface area of treated fibres was investigated. An increase in fibre surface area from 0.22 m^2/g to 0.44 m^2/g was triggered as a result of batch APF on T700 carbon fibres. However, the overall diameter of investigated carbon fibres remained constant, as determined using the modified Wilhelmy method. The increase in surface roughening is, therefore, too small and not expected to favour any mechanical anchoring/ interlocking between the treated fibres and the matrix polymer bonding.

4) Electrostatic charges on the surface of carbon fibres play a major role in fibre/ matrix adhesion. These electrostatic charges can be determined by measuring the potential difference at zero electric current, i.e. ζ-potential, caused by the flow of the electrolyte under a pressure gradient across a plug of carbon fibres based on streaming potentials. ζ-potential measurements of batch APF T700 showed an increase in the acidic character of carbon fibres, which is in agreement to the XPS findings. The increase in acidity of the fibres was due to the loss of

hydrophilic R–O*x* groups and the increase of carboxylic acid groups on the fibre surfaces.

5) The exposure of the carbon fibres to the atmospheric plasma jet caused surface sputtering. However, XRD analysis, Raman spectroscopy and electrical conductivity measurements performed on the APF batch T700 fibres showed that atmospheric plasma treatment only modified the surface of the carbon fibres without affecting the bulk properties.

6) The fibres tensile strength measured using single fibre tensile tests show that APF of T700 and AS4 fibres do not affect the fibre strength. The measured values were in excellent agreement with the manufacturer data. This confirmed that APF had a minimal effect on the corresponding bulk mechanical properties of investigated carbon fibres.

7) Contact angles of PVDF melt droplets on batch APF T700 fibres were measured to assess the carbon fibre/ PVDF interaction. The θ decreased from 21° to 16° indicating an improved wettability of the fibres by PVDF melts. The interfacial shear strength between batch APF T700 fibre and PVDF, as determined by single fibre pull-out tests, increased by 65%. This shows that as the contact angle between the PVDF melts and the fibres decreased, the apparent interfacial shear strength increased.

8) DSC investigations showed that the incorporation of original T700 carbon fibres in PVDF caused an apparent decrease in the T_m and the X_c of the matrix. This was due to the presence of carbon fibres, which limited the volume of the crystallising PVDF melt because a high portion of the volume of the composite

was occupied by the fibres. However, the T_m and the X_c of PVDF matrix incorporated with batch APF T700 remained constant, as compared to incorporating original T700 carbon fibres in PVDF. These effects can be attributed to the fact that the surface of batch APF T700 carbon fibres did not act as nucleating sites for the crystallisation of PVDF. In addition, no transcrystalline region were detected from around both original and batch APF T700 carbon fibres during composite sample preparation.

9) A modular laboratory scale composite production line (CPL) was partly built by the author. This CPL is capable of manufacturing unidirectional carbon fibre reinforced thermoplastics with a processing temperature of up to 400 °C at up to 1 m/min. In addition, atmospheric plasma modification was integrated into the manufacturing process.

10) APF treated carbon fibre reinforced PVDF tapes, with a consistent fibre volume content of 62 ± 3 %, were manufactured via a powder impregnation process. These tapes were processed into composite laminate test pieces by compression moulding. The interface dominated properties of the APF carbon fibre/ PVDF composite laminates were studied. The short-beam shear test showed improvements of up to 200 % in apparent short beam shear strength for the composite laminates containing APF AS4 carbon fibres with a fluorine content of 3.7 at.-%, as determined by XPS. The flexural strength and modulus of the laminated carbon fibre/ PVDF composites containing APF AS4 carbon fibres also increased by 110 % and 40 %, respectively.

5.1 Possible future work

The selection of macromechanical testing methods used in this study for determining interface relevant properties of carbon fibre reinforced PVDF laminates was restricted because of material consumption, simplicity and time. Arguably this is an important area to address, however, the main aim of this research was to develop a continuous process with integrated surface modification technology to manufacture unidirectional carbon fibre reinforced PVDF composites. Therefore, this work could be extended by further investigating additional direct mechanical methods (see section 5.1.2) in order to determine the improvements achieved by using inline APF of carbon fibres during manufacturing of carbon fibre reinforced PVDF.

5.1.1 Impact of plasma fluorination on the environment

In this study, the success of the developed APF of carbon fibres involved the use of chlorodifluoromethane (Freon 22), a hydrochlorofluorocarbon (HCFC). Although Freon 22 has less effects on global warming and ozone depletion, as compared to chlorofluorocarbons (CFCs), the environmental impact should not be ignored [334,335]. Since the signing of the Montreal Protocol on Substances that Deplete the Ozone Layer in 1987 [336], the production and use of CFCs has been phased out. All CFCs have been replaced by HCFCs and hydrofluorocarbons (HFCs). The advantages of HCFCs and HFCs over CFCs are that they are less inert in the troposphere and have shorter lifetimes. However, both HCFCs and HFCs are more expensive to produce than CFC but the real benefits are reduced health costs and reduced global warming. Under new EC regulations introduced in year 2000 [337], Freon-22, being a HCFC, would not be allowed to be used in new equipment from 1st January 2001 (with some exemptions) and from 2010 – 2014, servicing HCFC systems are to be restricted to the use of

recovered/ reclaimed refrigerant only. No virgin HCFCs are to be supplied after the end of 2009. Considering such legislation, although HCFC systems can be considered as acceptable for the time being, in the long term a more suitable gas (potentially: 1,1,1,2-tetrafluoroethane (R-134a) or a mixture of difluoromethane and pentafluoroethane (R-410A) needs to be identified for atmospheric plasma fluorination of carbon fibres, if the process is to be developed commercially.

5.1.2 Post manufacturing development of composite parts

In continuing the research in the design and fabrication of novel high performance fibre reinforced PVDF with stable and durable fibre/ matrix interfaces, there are a number of technical issues which remain. As mentioned earlier, only a couple of interfacial dominated mechanical tests were conducted to characterise the unidirectional carbon fibre reinforced PVDF composites manufactured. Given that initial results from short beam shear and flexural testings show an improvement in carbon fibre/ PVDF composite performance, other direct interface testing methods should be performed.

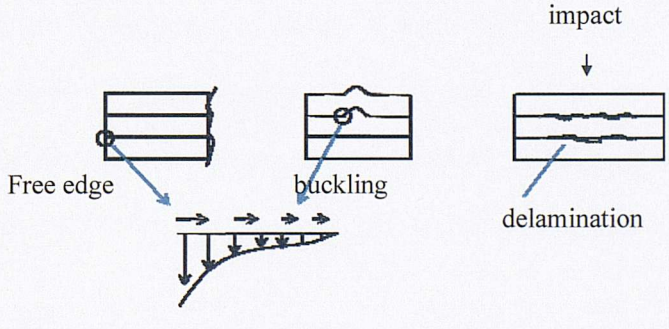


Fig. 5.1: Examples of possible sources of delamination initiation caused by through-thickness stresses. Redrawn from Hodgkinson [338]

Evidence from theliterature [338,339] suggest that double cantilever beam (DCB), End-Notched Flexure (ENF) and Edge Crack Torsion (ECT) tests are particular useful tests for studying delamination (Fig. 5.1), which is a major concern for the out-of-plane

properties of laminated composites. Composite laminates of high strength fibres are notoriously susceptible to through-thickness failure via interface delamination. The DCB test reveals the delamination resistance i.e. the interlaminar fracture toughness or critical energy release rate (G_{Ic}) of laminated composites under mode I loading (Fig. 5.2a). Initiation of interlaminar crack propagation via Mode I failure in composite laminates is dominated by the resin toughness and is less sensitive to fibre/ matrix strength. However, if the fibre/ matrix interface is weak, this would lead to a large R-curve effect due to the fact that fibre bridging develops and promotes fibre/ matrix failure. The ENF test characterises the mode II (Fig. 5.2b) dominated interlaminar fracture toughness (G_{IIc}) of high performance carbon fibre composites at the fibre/ matrix interface. Generally a low G_{IIc} is observed on materials with a weak fibre/ matrix interface regardless of how tough the matrix is. On the other hand if the fibre/ matrix interface is moderate or good, then the matrix toughness becomes more important. In general for a given thermoset composite the G_{IIc} is roughly half of the G_{Ic}, whereas for a thermoplastic composite the G_{Ic} is roughly equal to the G_{IIc}. The ECT test reveals the strain energy release when a crack propagate through an interface between the laminates under mode III loading (Fig. 5.2c). ECT is not a recognised test and has a lot of problems such as it does not generate a pure delamination failure because of ply splitting, etc. Anyhow, information obtained from DCB, ENF and ECT allows the assessment of the adhesive strength at the interface of the laminates in the APF carbon fibre reinforced PVDF composites manufactured and allows fibre/ matrix to be tailored.

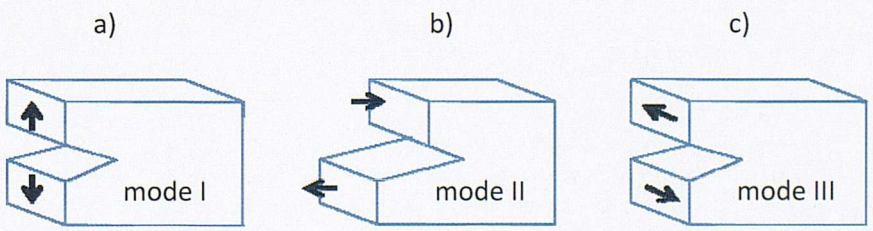


Fig. 5.2: Schematic of the basic modes of crack loading, a) mode I (opening), b) mode II (shear) and c) mode III (tearing). Redrawn from Hodgkinson [338]

There has been considerable research into the development of suitable test methods for the measurements of interlaminar toughness. All strategies require measurement of the load and applied displacement at which a delamination of known length grows. The commonest test standards DCB mode I test on unidirectional laminates are Japanese Industry Standards, JIS and the American Society of Testing and Materials, ASTM. For further details regarding these two methods see Ref. [340,341]. Three-point ENF, standardised by JIS [340], is commonly used for measuring the interlaminar toughness in mode II. There are concerns over the variability of measured mode II toughness data and the dependence on delamination insert thickness and the presence of any precracking at mid-plane. Further discussion regarding the difficulties surrounding the measurement of G_{IIc} in terms of nature of failure processes and the involvement of the variety fracture modes can be found in Ref. [342,343]. The development for measuring the interlaminar toughness in mode III is not as far advanced as for modes I and II. Although proposals have been made [344], it is difficult to achieve a pure mode III fracture and, therefore, none so far has been found to be fully satisfactory. After all delaminations in real composite structures often grow in a combination of mode I, II and III, so there is considerable interest in establishing mixed mode growth criteria [345,346].

References

[1] A Sas-Jaworsky, *US Patent*, **5 988 702** (1999).

[2] R Matthews, *US Patent*, **3 116 760** (1964).

[3] A Besche, R Hecker, K Schwarze, *US Patent*, **4 662 405** (1986).

[4] F J Policelli, *US Patent*, **4 530 379** (1985).

[5] P A Quigley, S C Nolet, J G Williams, *US Patent*, **6 357 485**, (2002).

[6] M Baviere, *Basic concepts in Enhanced Oil Recovery Processes*, Elsevier, 1991.

[7] D W Green, G P Willhite, *Enhanced Oil Recovery*, Society of Petroleum Engineers. Richardson, Texas, 1998.

[8] L W Lake, *Enhanced Oil Recovery*, Prentice Hall: Englewood Cliffs, 1989.

[9] A Carcoana, *Applied Enhanced Oil Recovery*, Prentice Hall: Englewood Cliffs, 1991.

[10] A Jackson, in *3rd Materials Engineering Research Laboratory Limited (MERL) Oilfield Engineering with Polymers Conference,* London, 2001.

[11] D Janoff, in *3rd Materials Engineering Research Laboratory Limited (MERL) Oilfield Engineering with Polymers Conference*, London, 2001.

[12] S A Silverman, W Butler, T Ashby, K Snider, *Materials Performance*, **36**, 54 (1997).

[13] G J Williams, in *2000 Offshore Technology Conference*, Houston Texas, 2000.

[14] C Ruggiere, J A Ferrari Jr, *J. Offshore Mech. Arct. Eng.*, **126**, 191 (2004).

[15] B Yong, B Qiang, *Subsea Pipeline and Risers*, Elsevier, 2005.

[16] J Remery, A Coutarel, *Pipeline heat loss in rigid, flexible, and pipe-in-pipe deepwater transport*, Offshore, Jan 2001.

[17] S R Balkanyi, J G Broze, J O Esparza, G J Hatton, A P Mehta, C K Tsai, M Wicks, G J Zabaras, *US Patent*, **20 060 175 063** (2005).

[18] T Bayart, D Szyszka, C Geertsen, in *5th PetroMin Deepwater and Subsea Technology Conference & Exhibition*, Kuala Lumpur, 2007.

[19] L Slagsvold, O A Grytå, in *Composite materials for offshore operations – 3*, eds: S S Wang, J G Williams, K H Lo, University of Houston-CEAC, 2001.

[20] M George, in *7th Middle East Corrosion Conference*, Bahrain, 1988.

[21] A U Malik, I Andijani, S Ahmed, F Al-Muaili, *Desalination*, **150**, 247 (2002).

[22] J G McKechnie, D T Hayes, in *Long Distance Subsea Tiebacks Conference*, Amsterdam, 2001.

[23] X H Yang, W L Zhu, Z Lin, J J Huo, *Progress in Organic Coatings,* **54**, 73 (2005).

[24] Y Charron, C Mabile, *Pipeline Gas J.*, **36**, 231 (2004).

[25] R Zamorano, *Pipeline Gas J.*, **10**, 30 (2002).

[26] J Tiratsoo, *Pipeline Pigging and Integrity Technology*, Gulf Publishing Company, 2003.

[27] G Hiltscher, W Mühlthaley, J Smits, *Industrial Pigging Technology: Fundamentals, Components, Applications*, Wiley, 2003.

[28] H Lührsen, *Reinforced Thermoplastic Pipes* (RTP), 3R International, **40** (2001).

[29] R J Diefendorf, in *Engineered Materials Handbook, Vol 1, Composites*, eds: C A Dostal, M S Woods, H J Frissel, ASM International, Ohio, 1987.

[30] T Edison, *US Patent*, **0 223 898** (1880).

[31] P Israel, *Edison: A life of invention*, Wiley, 2000.

[32] S Otani, *Carbon*, **3**, 31 (1965).

[33] G Dorey, *Phys. Technol.*, **11**, 56 (1980).

[34] S C Bennett, D J Johnson, W Johnson, *J.Mater. Sci.*, **18**, 3337 (1983).

[35] W Paton, in *Carbon fibres 3rd International.Conference,* London, 1985.

[36] S Otani, *Mol. Cryst. Liq. Cryst.*, **63**, 249 (1981).

[37] D R Lovell, in *Carbon fibres 3rd International Conference,* London, 1985.

[38] D J Johnson, *J. Phys.*, **29,** 286 (1987).

[39] F R Jones, *Handbook of Polymer-Fibre Composites*, Longman Scientific & Technical, 1994.

[40] J B Donnet, O P Bahl, *Encyclopedia of Physical Science and Technology*, **2**, 517 (1987).

[41] P Bajaj, R B Chavan, B Manjeet, *J. Macromol. Sci. Chem.*, **3**, 335 (1986).

[42] T Muller, *I.F.J.*, **46** (1988).

[43] Mitsubushi Rayon Co, Ltd. Tokyo, Japan, **62**, 27 (1987).

[44] Toray Industries, Inc. Tokyo, Japan, **59**, 128 (1984).

[45] Han Exlan Co, Ltd. Tokyo, Japan, **58**, 704 (1984).

[46] Asahi Chemical Industries Co, Ltd. Tokyo, Japan, **61**, 709 (1986).

[47] W N Reynolds, R Moreton, *Phil. Tran. R. Soc. Ln.*, **294,** 451 (1980).

[48] X Zeng, J Hu, J Zhao, Y Zhang, D Pan, *J. Appl. Polym. Sci.*, **106**, 2267 (2007).

[49] M R Padhya, A V Karandikar, *J. Appl. Polym. Sci.*, **33**, 1675 (1987).

[50] Mitsubushi Rayon Co, Ltd. Tokyo, Japan, **59**, 914 (1984).

[51] T Nakajima, K Kajiwara, J E Mclntyre, *Advanced Fiber Spinning Technology*, Woodhead Publishing, 1994.

[52] R Moreton, W Watt, *Carbon*, **12**, 543 (1974).

[53] N Grassie, R McGuchan, *Eur. Polym. J.*, **7**, 1503 (1971).

[54] A K Gupa, D K Paliwal, P Bajaj, *J.M.S. Rev. Macromol. Chem. Phys.*, **1**, 1 (1991).

[55] J B Donnet, R C Bansal, *Carbon fibres 2nd ed.*, Marcel Dekker, 1990.

[56] Toray Industries Inc., *European Patent*, **4 526 770** (1987).

[57] A A Berlin, A M Dubinskaya, Y S Moshkovskii, *Vysokomo Soedin*, **2**, 1938 (1964).

[58] W Fester, *Textil. Rundschau*, **20**, 1 (1965).

[59] W J Burlant, J L Parsons, *J. Polym. Sci.*, **22**, 249 (1956).

[60] N Grassie, J N Hay, *J. Polym. Sci.*, **56**, 189 (1962).

[61] H N Friedlander, L H Peebles, J Brandrup, J R Kirby, *Marcromol*, **1**, 79 (1968).

[62] W Johnson, W Watt, *Polym. Prepr.*, **2**, 9 (1968).

[63] J W Johnson, L N Philips, W Watt, *British Patent*, **1 110 791** (1968).

[64] S K Rosembaum, *J. Appl. Polym. Sci.*, **9**, 2071 (1965).

[65] G K Layden, *J. Appl. Polym. Sci.*, **15**, 1709 (1971).

[66] S B Warner, L H Peebles, D R Uhlmann, *J. Mater. Sci.*, **14**, 565 (1979).

[67] E Fitzer, D J Muller, *Macromol. Chem.*, **144**, 117 (1971).

[68] E Fitzer, M Heym, *Chem. Ind.*, **16**, 663 (1976).

[69] O P Bahl, L M Manocha. *Angew. Makromol. Chem.*, **48**, 145 (1975).

[70] E Fitzer, W Frohs, M Heins, *Carbon*, **24**, 387 (1986).

[71] P B Racke, H Schurmus, J Verhoest, *Inorganic Fibres and Composites*, Pergamon, New York, 1984.

[72] O P Bahl, R B Mathur, K D Kundra, *Fiber Sci. Technol.*, **13**, 155 (1980).

[73] V Roskovic, S. Marinkovic, *Carbon*, **16**, 351 (1978).

[74] E Fitzer, D J Muller, *Carbon*, **13**, 63 (1975).

[75] O P Bahl, L M Manocha, *Carbon*, **12**, 17 (1974).

[76] J Mittal, *Studies on the processing of PAN fibres to develop high performance carbon fibres.* PhD Thesis, Indian Institute of Technology, Delhi, 1994.

[77] W Watt, L N Phillips, W Johnson, *The Engineer*, **221**, 815 (1966).

[78] J W Johnson, in *Appl. Polym. Symp,* ed: J Preston, Amer. Chem. Soc., **9**, 229 (1969).

[79] P J Goodhew, A J Clarke, J E Bailey, *Mater. Sci. Eng.*, **17**, 3 (1975).

[80] W Watt, *Nature*, **236**, 10 (1972).

[81] A Shindo, in *Carbon Fibres- Their Composites and Applications*, The Plastic Institute, London, 1971.

[82] Toray Industries Inc. Tokyo, Japan **59**, 531 (1984).

[83] J W Johnson, *Appl. Polym. Symp.*, **9**, 229 (1969).

[84] R Moreton, W Watt, W Johnson, *Nature*, **213**, 690 (1967).

[85] G A Cooper, R M Mayor, *J. Mater. Sci.*, **213**, 690 (1971).

[86] D H Kaelble, P J Dynes, L W Crane, L Maus, *J. Adhesion*, **7**, 25 (1975).

[87] J V Larsen, T G Smith, P W Erickson, *Carbon Fibre Surface Treatment*, NOLTR, 1971.

[88] R J Daukeys, *J. Adhesion*, **5**, 211 (1973).

[89] A Deurbergue, A Oberlin, *Carbon*, **30**, 981 (1992).

[90] J P Rieux, P J Lehurreau, *French Patent*, **72 13 950** (1972).

[91] C Jones, E Sammann, *Carbon*, **28**, 509 (1990).

[92] A Bismarck, M E Kumru, B Song, J Springer, E Moos, J Karger-Kocsis, *Composites A*, **30**, 1351 (1999).

[93] A Bismarck, A F Lee, A S Sarac, E Schulz, K Wilson, *Comp. Sci. Tech.*, **65**, 1564 (2005).

[94] A Z Sarac, A Bismarck, M Kumru, J Springer, *Synthetic Metals*, **123**, 411 (2001).

[95] P Ehrburger, J J Herque, J B Donnet, in *American Chemical Society (ACS) Symposium Series No. 21*, eds: M L Beviney, T M O'Grady, Amer Chem Soc, Washington DC, 1975.

[96] P Ehrburger, J J Herque, J B Donnet, in *4th Intern. Conf. Carbon Graphite*. Soc Chem Ind., London, 1976.

[97] J P Hoare, *The electrochemistry of oxygen*, Interscience 1998.

[98] J Mahy, L W Jenneskens, O Grabandy, A Venema, G D B van Houwelingen, *Surf. Interface Anal.*, **21**, 1 (1994).

[99] F Nakao, Y Takenaka, H Asai, *Composites*, **23**, 365 (1992).

[100] C Kozlowski, P M A Sherwood, *Carbon*, **25**, 751 (1987).

[101] J Harvey, C Kozlowski, P M A Sherwood, *J. Mater. Sci.*, **22**, 1585 (1987).

[102] F R Jones, *Key. Eng. Mater.*, **116**, 41 (1996).

[103] W W Wright, *Polymers and Poly. Comp.*, **3**, 231 (1990).

[104] P Morgan, *Carbon fibers and their composites*, Taylor & Francis, CRC Press 2005.

[105] L T Drzal, M J Rich, M F Koenig, P M Lloyd, *J. Adhesion*, **16**, 133 (1983).

[106] R V Subramanian, V Sundaram, A K Patel, in *33rd Annual Technical Conference*, Ongena, 1978.

[107] R V Subramanian, *Adv. Polym. Sci.*, **33,** 33 (1979).

[108] B Z Zhang, H Das, L R Hwang, T C Chang, in *Interfaces in Polymer, Ceramic and Metal Matrix Composites*, ed: H. Ishida, Elsevier, 1988.

[109] I K Ismail, M D Vangsness, *Carbon*, **28**, 509 (1990).

[110] L T Drzal, M J Madhukar, *J. Mater. Sci.*, 28, 569 (1993).

[111] S Yumitori, D Wang, F R Jones, *Composites*, **25**, 698 (1994).

[112] P J Herrera-Franco, L T Drzal, *Composites*, **23**, 2 (1992).

[113] C I Weitzsacker, M Bellamy, P M A Sherwood, *J. Vac. Sci. Technol. A*, **12**, 2392 (1994).

[114] C E Carraher Jr, *Seymour/ Carraher's Polymer Chemistry 6th Ed*, Taylar & Francis, 2003.

[115] J G Drobny, *Macromol. Symp.*, **170**, 149 (2001).

[116] Fluoropolymers (study 2206). New US Industry forecast 2011 & 2016. Industry market research for business leaders, strategists, decision-makers. June 2007.

[117] R E Shalin, *Polymer matrix composites*, Chapman & Hall, 1995.

[118] A Ravve, *Principles of Polymer Chemistry 2nd Ed,* Springer, 2000.

[119] L Mascia, *Thermoplastic Materials Engineering 2nd Ed*, Elsevier Applied Science, 1989.

[120] A J Kinloch, *Adhesion and Adhesives Science and Technology*, Chapman and Hall, 1987.

[121] T M Dargaville, G A George, D J T Hill, A K Whittaker, *Prog. Polym. Sci.*, **28**, 1355 (2003).

[122] R L Clough, K T Gillen, in *Irradiation effects on polymers*, eds: D W Clegg, A A Collyer, Elsevier Applied Science, 1991.

[123] A Ravve, *Principles of Polymer Chemistry*, Springer, 2001.

[124] R A Craven, A J Ackermann, P L Tremont, *High purity water technology for silicon-wafer cleaning*, Microcontamination, Aug 1986.

[125] H J Krause, *Modern plastics industrial piping systems*, Engineering Digest, Nov 1987.

[126] J Scheirs, *Modern Fluoropolymers: High Performance Polymers for Diverse Applications*, Wiley, 1997.

[127] A Hauptschein, A H Feinberg, *US Patent*, **3 188 356** (1965).

[128] F Kaess, H Michaud, *US Patent*, **3 600 450** (1971).

[129] N Schultz, P Martens, H J Vahlensieck, *German Patent*, **2 659 712** (1976).

[130] F C Trager, J D Mansell, W E Wimer, *US Patent*, **4 818 513** (1989).

[131] Y Elsheikh, *US Patent*, **4 827 055** (1989).

[132] S Ebnesajjad, *Fluoroplastics: Melt Processible Fluoropolymers: User's Guide and Databook*, William Andrew Inc., 2002.

[133] J E Dohany, *US Patent*, **3 781 265** (1973).

[134] J E Dohany, *Kirk-Othmer Encyclopedia of Chemical Technology*, Wiley, 2000.

[135] J P Stallings, *US Patent*, **3 780 007** (1973).

[136] J Dumoulin, *US Patent*, **4 524 194** (1985).

[137] *British Patent*, **1 057 088** (1967).

[138] M Ichimura, Y Shi, *US Patent*, **3 616 371** (1967).

[139] J E Dohany. *US Patent*, **4 360 652** (1982).

[140] R Hanselka, R Williams, M Bukay, *Ultrapure water*, July 1987.

[141] A W Adamson, A P Gast, *The Physical Chemistry of Surfaces*, Wiley, 1997.

[142] T Young, *Phil. Trans.*, **95**, 82 (1805).

[143] L Safinia, *Surface modification and characterisation of polymer constructs for tissue engineering applications,* 2006 PhD Thesis, Department of Chemical Engineering, Imperial College London.

[144] R Aliev, *Polym. Bull.*, **47**, 99 (2001).

[145] E B Shand, *J. Am. Ceram. Soc.*, **47**, 102 (1964).

[146] E Bormashenko, Y Bormashenko, G Whyman, R Pogreb, A Musin, R Jager, Z Barkay, *Langmuir*, **24**, 4020 (2008).

[147] M O Robbins, J F Joanny, *Europhys. Lett.*, **3**, 729 (1987).

[148] B T Åström, *Manufacturing of polymer composites 1st Ed*, Chapman & Hall, 1997.

[149] E P Scala, *J. Metals*, **48**, 45 (1996).

[150] D A Riegner, *Composites in the automotive industry*, ASTM Standardization News, 1983.

[151] D G Fesko, P K Mallick, S Newman, in *Composite Materials in Automotive Composites Industry*, eds: S V Kulkarni, C H Zweben, R B Pipers, American Society of Mechanical Engineering, New York, 1978.

[152] N R Adsit, *Composites for space applications*, ASTM Standardization News, 1983.

[153] E G Wolff, *Metal Prog*, **115**, 54 (1979).

[154] L T Drzal, *Tough Composite Materials: Recent Develoments,* Noyes Publication, New Jersey, 1985.

[155] D D L Chung, *Carbon fiber composites*, Butterworth-Heinemann Massachusetts, 1994.

[156] E Mäder, K Grundke, H J Jacobasch, G Wachinger, *Composites*, **25**, 739 (1994).

[157] A Oken, in *12th National Society for the Advancement of Materials and Processing Engineering (SAMPE) Technical Conference*, Seattle, *1980.*

[158] A Offringa, P Zimmermann, in *Advanced Materials and Structures from Research to Application*, eds: J Rrandt, H Hornfeld, M Neitzel, Society for the Advancement of Materials and Processing Engineering (SAMPE) European Chapter, 1992.

[159] P K Mallick, *Fiber-reinforced composites,* Marcel Dekker, 1993.

[160] A R Bunsell, J Renard, *Fundamentals of Fibre Reinforced Composite Materials,* IOP Publishing, 2005.

[161] G Gonzáles, J L Lorca, *Comp. Sci. Tech.*, **67**, 2795 (2007).

[162] A Aatmeeyata, S K Gupta, *Polym. Plast. Technol. Eng.*, **37**, 201 (1998).

[163] M Vedula, M J Koczak, *J. Thermoplast. Comp. Mat.*, **2**, 154 (1989).

[164] G Schinner, J Brandt, H Richer, *J. Thermoplast. Comp. Mat.*, **9**, 237 (1996).

[165] M Connor, S Toll, J A E Manson, A G Gibson, *J. Thermoplast. Comp. Mat.*, **8**, 138 (1995).

[166] I Y Chang, J K Lees, *J. Thermoplast. Comp. Mat.*, **1**, 277 (1998).

[167] H Meng, Y Lin, W M Yui, *Plast. Rubber Comp. Process Appl.*, **23**, (1995).

[168] A Goto, M Matsuda, H Hamada, Z Maekawa, T Matsuo, T Hokudou, *Transactions of the Japan Society of Mechanical Engineers*, **61**, 50 (1995).

[169] M Neitzel, in *4th Japan International Society for the Advancement of Materials and Processing Engineering (SAMPE) Symposium*, Tokyo, 1995.

[170] G O Shonaike, T Matuo, in *4th Japan International Society for the Advancement of Materials and Processing Engineering (SAMPE) Symposium*, Tokyo, 1995.

[171] G Sala, D Cutolo, *Composites*, **27**, 387 (1996).

[172] A Fujita, Z Maekawa, H Hamada, M Matsuda, T Matsuo, *J. Reinf. Plast. Comp.*, **12**, 156 (1993).

[173] A Bismarck, E Schulz, *J. Mater. Sci.*, **38**, 4965 (2003).

[174] S J Park, M K Seo, Y S Lee, *Carbon*, **41**, 723 (2003).

[175] M Zayat, D Davidov, H Selig, *Carbon*, **32**, 485 (1994).

[176] Y Chong, H J Ohara, *J. Fluorine Chem.*, **57**, 169 (1992).

[177] A Bismarck, A Schulz, R Tahhan, H Zell, T M Klapötke, W Michaeli, J Springer, *J. Fluorine Chem.*, **84**, 127 (1997).

[178] N O V Plank, R Cheung, *Microelec. Eng.*, **73**, 578 (2004).

[179] V Gupta, R B Mathur, O P Bahl, A Tressaud, S Flandrois, *Synthetic Metals*, **73,** 69 (1995).

[180] A Tressaud, E Durand, C Labrugére, *J. Fluorine Chem.*, **125**, 1639 (2004).

[181] H Loh, R E Cohen, R F Baddour, *J. Mater. Sci.*, **22**, 2937 (1987).

[182] H Kasai, M Kogoma, T Moriwaki, S Okazaki, *J. Phys. D: Appl. Phys.*, **19**, 225 (1986).

[183] H Höcker, *Pure Appl. Chem.*, **3**, 423 (2002).

[184] E Selli, G Mazzone, C Oliva, F Martini, C Riccardi, R Barni, B Marcandalli, M R Massafra, *J. Mater. Chem.*, **11**, 1985 (2001).

[185] Y Khairallah, F Khonsari-Arefi, J Amouroux, *Thin Solid Films*, **241**, 295 (1994).

[186] T Yasuda, M Gazicki, H Yasuda, *J. Appl. Polymer Sci. Appl. Polymer Symp.*, **38**, 201 (1984).

[187] H Yasuda, C E Lamaze, K Sakaoku, *J. Appl. Polymer Sci.*, **17**, 137 (1973).

[188] G C S Collins, A C Lowe, D Nicholas, *Eur. Polymer J.*, **9**, 1173 (1973).

[189] M Anand, R E Cohen, R F. Baddour, *Polymer*, **22**, 361 (1981).

[190] A P Kettle, F R Jones, M R Alexander, R D Short, M Stollenwerk,

J Zabold, W Michaeli, W Wu, E Jacobs, I Verpoest, *Composite A*, **29**, 241 (1998).

[191] P Q Rose, O S Kolluri, R D Cormia, in *34th Society for the Advancement of Materials and Processing Engineering (SAMPE) Symp*, Nevada, 1989.

[192] N Dilsiz, *J. Adhes. Sci. Technol.*, **14**, 975 (2000).

[193] N Chand, E Schulz, G Hinrichsen, *J. Mater. Sci.*, **15**, 1374 (1996).

[194] Y Kusano, T L Andersen, B F Sørensen, P K Michelsen, in *28th Risø International Symposium on Materials Science: Interface Design of Polymer Matrix Composites – Mechanics, Chemistry*, Modelling and Manufacturing, Denmark, 2007.

[195] J B Donnet, M Brendle, T L Dhami, O P Bahl, *Carbon*, **24**, 757 (1986).

[196] J B Donnet, T L Dhami, S Dong, M Brendle, *J. Phys. D: Appl. Phys.*, **20,** 269 (1987).

[197] E D Edie, R J Cano, R A Ross, in *20th Biennial Conference on Carbon*, Santa Barbara, 1991.

[198] J C M Peng, S Rebouillat, in *Carfon fibers*, eds: J B Donnet, T K Wang, J C Peng, Marcel Dekker, 1998

[199] R F Hicks, H W Herrmann, *Atmospheric-Pressure Plasma Cleaning of Contaminated Surfaces*, Technical report, US Department of Energy, 2003.

[200] M J Shenton, M C Lowell-Hoare, G C Stevens, *J. Phys. D: Appl. Phys.*, **34,** 2761 (2001).

[201] S Kanazawa, M Kogoma, T Moriwaki, S Okazaki, *J. Phys. D: Appl. Phys.*, **21**, 838 (1988).

[202] E M Liston, L Martinu, M R Wertheimer, in *Polymer surface modification of polymers: relevance to adhesion*, eds: M Strobel, C S Lyons, K L Mittal, VSP BV, 1994.

[203] O S Kolluri, S L Kaplan, P W Rose, in *Society of Petroleum Engineer (SPE)/ Asia Pacific Committee (APC) Regional Technical Conference*, Los Angeles, 1998.

[204] Y Z Wei, Z Q Zhang, U Li, Z H Guo, B L Zheng, in *The 3rd International Conference on Composite Interfaces (ICCI)*, ed: H Ishida, Elsevier, 1990.

[205] R D Heap, R H. Norman, *Flexural testing of plastics*, The Plastics Institute, London, 1969.

[206] R Park, J Jang, *Comp. Sci. Tech.*, **58**, 1621 (1998).

[207] R E Chambers, F J McGarry, *ASTM Bull*, **38** (1959).

[208] N R Sottos, J M Hodgkinson, F L Matthews, in *6th International Conference on Composite materials (ICCM)- 2nd European Conference on Composite Materials (ECCM)*, London 1987.

[209] B D Agarwal, L. J. Broutman, *Analysis and Performance of Fibre Composites*, Wiley, 1990.

[210] W C Cui, M R Wisnom, M Jones, *J. Strain Anal.*, **27**, 235 (1992).

[211] N J Pagano, J C Halpin, *J. Compos. Mater.*, **2**,18 (1968).

[212] N J Pagano, *J. Compos. Mater.*, **3**, 398 (1969).

[213] N J Pagano, *J. Compos. Mater.*, **4**, 20 (1970).

[214] J M Whitney, A W Leissa, *J. Appl. Mech.*, **28**, 261 (1969).

[215] J M Whitney, *J. Compos. Mater.*, **3**, 534 (1969).

[216] D F Adams, E Q Lewis, *SAMPE Journal*, **31**, 32 (1994).

[217] G E Collins, *J. Textile Inst.*, **38**, T73 (1944).

[218] A W Neumann, *Chem.-Ing-Techn*, **42**, 969 (1970).

[219] A Bismarck, M E Kumru, J Springer, *J. Colloid Interface Sci.*, **210**, 60 (1999).

[220] K K C Ho, G Beamson, G Shia, N V Polyakova, A Bismarck, *J. Fluorine Chem.*, **128**, 1359 (2007).

[221] J Y Y Heng, D F Pearse, F Thielmann, T Lampke, A Bismarck. *Composite interfaces*, **17**, 581 (2007).

[222] A Dupré, *Théorie mécanique de la chaleur*, Gaitjoer Villars, Paris, 1869.

[223] F M Fowkes, *J. Phys. Chem.*, **66**, 382 (1962).

[224] F M Fowkes, *Ind. Eng. Chem.*, **56**, 40 (1964).

[225] F M Fowkes, M A Mostafa, *Ind. Eng. Chem. Prod. Res. Dev.*, **17**, 3 (1978).

[226] F M Fowkes, in *Physicochemical Aspects of Polymer Surfaces*, ed: K L Mittal, Vol. 2, Plenum Press, 1983.

[227] F M Fowkes, *J. Adhesion Sci. Technol.*, **4**, 669 (1990).

[228] D Y Kwok, D Li, W Neumann, *Langmuir*, **10**, 1323 (1994).

[229] J K Spelt, D Li, in *Applied Surface Thermodynamics,* eds: A W Neumann, J K Spelt, Marcel Dekker, 1996.

[230] C J van Oss, M K Chaudhury, R J Good, *Adv. Colloid Interface Sci.*, **28**, 35 (1987).

[231] R J Good, C J van Oss, in *Modern Approaches to Wettability Theory and Applications*, eds: M E Schrader, G Loeb, Plenum Press, 1991.

[232] C J van Oss, R J Good, M K Chaudhury, *J. Coll. Interf. Sci.*, **111**, 378 (1986).

[233] C J van Oss, M K Chaudhury, R J Good, *J. Coll. Interf. Sci.*, **128**, 313 (1988).

[234] C J van Oss, R F Giese, R J Good, *Langmuir*, **6**, 1711 (1990).

[235] C J van Oss, M K Chaudhury, H J Busscher, *Dispersion Sci. Technol.*, **11**, 77 (1990).

[236] D H Kaelble, *Physical chemistry of adhesives*, Wiley, 1971.

[237] S Wu, *Polymer Interface and Adhesion*, Marcel Dekker, 1982.

[238] H J Jacobasch, F Simon, C Werner, C Bellmann, *Technisches Messen*, **63**, 439 (1996).

[239] H J Jacobasch, F Simon, C Werner, C Bellmann, *Technisches Messen*, **63**, 447 (1996).

[240] R J Hunter, *Zeta potential in colloids science*, Academic Press, 1981.

[241] M Smoluchowski, *Handbook of electricity and magnetism Vol 2*, Barth, Leipzig, **366** (1921).

[242] C Werner, H Körber, R Zimmerman, S Dukhin, H J Jacobasch, *J. Colloid Interf. Sci.*, **208**, 329 (1998).

[243] C D Wagner, L E Davis, M V Zeller, J A Tayler, R M Raymond, L H Gale, *Surf. Interface Anal.*, **3**, 211 (1981).

[244] A T Hubbard, *Encyclopedia of Surface and Colloid Science*, CRC Press, 2002.

[245] D A Haydon, *The Royal Society of London. Series A, Mathematical and Physical Sciences*, **258**, 319 (1960).

[246] I Aranberri-Askargorta, T Lampke, A Bismarck, *J.Colloid Interf. Sci.*, **263**, 580 (1999).

[247] D W A Sharp, *Dictionary of Chemistry 2nd Ed*, Penguin References, 1990.

[248] E Uchida, Y Ikada, in *Encyclopedia of Surface and Colloid Science*, ed: A Hubbard, Marcel Dekker, 2002.

[249] H J Jacobasch, K Grundke, P Uhlmann, F Simon, E Mäder, *Compos. Interfaces*, **4**, 293 (1996).

[250] C Campagne, E Devaux, A Perwuelz, C Cazé, *Polymer*, **43**, 6669 (2002).

[251] A Bismarck, D Richter, C Wuertz, J Springer, *Colloids Surfaces A*, **159**, 341 (1999).

[252] H T Chiu, J H Wang, *Polym. Composites*, **19**, 347 (1998).

[253] G E Hammer, L T Drzal, *Appl. Surf. Sci.*, **4**, 340 (1980).

[254] A Tressaud, F Moguet, S Flandrois, M Chambon, C Guimon, G Nanse, E Papirer, V Gupta, O P Bahl, *J. Phys. Chem. Solids*, **57**, 745 (1996).

[255] M P Seah, D Briggs, *Practical Surface Analysis: Auger and Photoelectron Spectroscopy*, Wiley, 1990.

[256] J C Rivière, *Surface Analytical Techniques*, Oxford University Press, 1990.

[257] J M Walls, *Methods of Surface Analysis*, Cambridge University Press, 1989.

[258] T L Barr, *Modern ESCA: The Principles and Practice of X-ray Photoelectron Spectroscopy*, CRC Press, 1989.

[259] G Attard, C Barnes, *Surfaces*, Oxford Chemistry Primer 59, Oxford University Press, 1998.

[260] E M McCash, *Surface Chemistry*, Oxford University Press, 2001.

[261] C J Powell, *Suf. Sci.*, **299**, 34 (1994).

[262] D Briggs, J T Grant, *Surface Analysis by Auger and X-Ray Photoelectron Spectroscopy*, IM Publications, 2003.

[263] D Briggs, G Beamson, *High Resolution XPS of Organic Polymers: The Scienta ESCA300 Database*, Wiley, 1992.

[264] A P Pijpers, K Berresheim, M Wilmers, *Fresenius J. Anal. Chem.*, **346**, 104 (1993).

[265] W Egelhoff Jr, *Surf. Sci. Rev.*, **6**, 257 (1987).

[266] C S Fadley, in *Electron Spectroscopy: Theory, Techniques and Application*, eds: C R Brundle, A D Baker, Academic, 1978.

[267] N H Turner, in *Physical Methods of Chemistry Series, 2nd Ed*, eds: B W Rossiter, R C Batzold, Wiley, 1993.

[268] J F Watts, J Wolstenholme, *An introduction to surface analysis by XPS and AES*. Wiley, 2003.

[269] C D Wagner, A V Naumkin, A Kraut-Vass, J W Allison, C J Powell, J R Rumble Jr, *NIST Standard Reference Database 20, Version 3.4*, Link in: http://srdata.nist.gov/xps/ accessed on 14.07.06.

[270] P R Thornton, *Scanning electron microscopy: applications to materials and device science*, Chapman & Hall, 1968.

[271] S L Flegler, *Scanning and transmission electron microscopy: an introduction*, Oxford University Press, 1995.

[272] O C Wells, *Scanning electron microscopy*, McGraw-Hill, 1974.

[273] M K Ismail, *Carbon*, **25**, 653 (1987).

[274] N Setoyama, G Li, K Kaneko, F Okino, R Ishikawa, M Kanda, H Touhara, *Adsorption*, **2**, 293 (1996).

[275] Y S Lee, *J. Fluorine Chem.*, **128**, 392 (2007).

[276] S J Gregg, K S W Sing, *Adsorption, surface area and porosity*, Academic Press, 1982.

[277] ISO, ISO9227, *Determination of the specific surface are of solids by gas adsportion using the BET method*, International Organization for Standardisation, 1995.

[278] M Connor, P H Harding, J A E Månson, J C Berg, *J. Adhesion Sci. Technol.*, **9**, 983 (1995).

[279] B J Carroll, *Langmuir*, **2**, 248 (1998).

[280] R A Bucher, J A Hinkley, *J. Thermoplastic Composite Mater.*, **5**, 3 (1992).

[281] J Mayer, S Giorgetta, B Koch, E Wintermantel, J Patscheider, G Spescha, *Composites*, **25**, 763 (1994).

[282] B Song, A Bismarck, R Tahhan, J Springer, *J. Coll. Interf. Sci.*, **197**, 68 (1998).

[283] P Atkins, J De Paula, *Physical Chemistry 6th Ed*, Oxford University Press, 1998.

[284] F Tuinstra, J L Koenig, *J. Chem. Phys.*, **53**, 1126 (1970).

[285] H K Tse, *J. Appl. Polym. Sci.*, **59**, 577 (1996).

[286] O S Fleming, *Application of advanced vibrational spectroscopy to polymers processed with supercritical CO_2*, 2006 PhD Thesis, Department of Chemical Engineering, Imperial College London.

[287] R J Nemanich, G Lucovsky, S A Solin, *Mater. Sci. Eng.*, **31**, 157 (1977).

[288] L E Alexander, *X-ray diffraction methods in polymer science*, Wiley, 1969.

[289] J D Stroupe, R E Hughes, *J. Am. Chem. Soc.*, **80**, 1768 (1958).

[290] D Shriver, P W Atkins, *Inorganic Chemistry 3rd Ed*, Oxford University Press, 1999.

[291] K H Tan, *Principles of Soil Chemistry*, CRC Press, 1998.

[292] E Stanley, M Litt, *J. Polymer Sci.*, **45**, 453 (1960).

[293] F Danusso, G Moraglio, *Accad. Nazl. Lincei, Rend., Classe. Sci. Fis., Mat. Nat.*, **27**, 381 (1959).

[294] L P Kobets, M A Chubarova, D K Khakimova, N V Polyakova, A S Fialkov, in *4th All-Union Conference on the Mechanics of Polymer and Composite Materials*, Riga, 1980.

[295] H Selig, M Zayat, D Davidov, *J. Fluorine Chem.*, **54**, 130 (1991).

[296] DIN 53 482, *Method of Test for Materials for Electrical Purposes, Measuring of Electrical Resistance of Non-metallic Materials.*

[297] S L Phoenix, H L Taylor, *Adv. Appl. Prob.*, **5**, 200 (1973).

[298] D G Harlow, S L Phoenix, *J. Comp. Mat.*, **12**, 195 (1978).

[299] BS ISO 11566, *Carbon fibre- Determination of the tensile properties of single-filament specimens*, 1996.

[300] W J Weibull, *Applied Mechanics*, **18**, 293 (1951).

[301] H Kawai, *Jpn. J. Appl. Phys.*, **8**, 1975 (1969).

[302] A J Lovinger, in *Developments in Crystalline Polymers*, eds: I D Bassset, Applied Science, London, 1982.

[303] H M G Correia, M M D Ramos, *Comput. Mater. Sci.*, **33**, 224 (2005).

[304] K Nakagawa, Y Ishida, *J. Poly. Sci. Polym. Phys. Ed.*, **11**, 1503 (1973).

[305] R V Price, *US Patent*, **3 742 106** (1973).

[306] L Tang, L Li, X Yi, Z Pan, *Polym Composites*, **18**, 223 (1997).

[307] P Mitschang, M Blinzler, A Wöginger, *Comp. Sci. Tech.*, **63**, 2099 (2003).

[308] A M Vodermayer, J C Kärger, G Hinrichsen, *Composites Manufacturing*, **4**, 233 (1993).

[309] G Hinrichsen, A M Vodermayer, K H Reichert, L Kuhnert, W Linder, G Goldman, *US Patent*, **5 888 580** (1999).

[310] W H Krueger, *US Patent*, **5 085 928** (1992).

[311] L S Penn, in *Handbook of Polymer-Fibre Composites*, ed: F R Jones, Longman Scientific & Technical, 1994.

[312] J X Li, *J. Appl. Polym. Sci.*, **53**, 225 (1994).

[313] P S Chua, M R Piggot, *Comp. Sci. Tech.*, **22**, 107 (1985).

[314] C T Chou, L S Penn, *J. Adhesion*, **35**, 127 (1991).

[315] A Hampe, I Boro, K Schmacher, *Forschung Aktuell der TU Berlin*, **7**, 21 (1990).

[316] C DiFrancia, T C. Ward, R O Claus, *Composites A*, 27, 597 (1996).

[317] ASTM D790-03, *Standard Test Methods for Flexural Properties of Unreinforced and Reinforced Plastics and Electrical Insulating Materials*, 2003.

[318] ASTM D2344-00, *Standard Test Method for Short-Beam Strength of Polymer Matrix Composites and Their Laminates*, 2000.

[319] R E Johnson Jr., R H Dettre, *Adv. Chem Ser.*, **43**, 112 (1963).

[320] R H Dettre, R E Johnson Jr., *Adv. Chem. Ser.*, **43**, 136 (1963).

[321] R J Smiley, W N J Delgass, *J. Mat. Sci.*, **28**, 3601 (1993).

[322] A Pizzi, K L Mittal, *Handbook of Adhesive Technology*, CRC Press, 2003.

[323] P H Serp, J L Figueiredo, P Bertrand, J P Issi, *Carbon*, **36**, 1791 (1998).

[324] J I Paredes, A Martínez-Alonso, J M D Tascón, *Carbon*, **40**, 1101 (2001).

[325] V S Babu, M S Seehra, *Carbon*, **34**, 1259 (1996).

[326] K K C Ho, G Kalinka, M Q Tran, N V Polyakova, A Bismarck, *Comp. Sci. Tech.*, **67**, 2699 (2007).

[327] C Wang, C R Liu, *Polymer*, **40**, 289 (1999).

[328] M Heppenstall-Butler, D J Bannister, R J Young, *Composites A*, **27**, 833 (1996).

[329] N Klein, G Marom, A Pegoretti, C Migliaresi, *Composites*, **26**, 707 (1995).

[330] H Benkhati, T That, M Tan, B J Jungnickel, *J. Polym. Sci., Part B: Polym. Phys.*, **39**, 2130 (2001).

[331] C Auer, G Kalinka, T H Krause, G Hinrichsen, *J. Appl. Polym. Sci.*, **51**, 407 (1994).

[332] S Meretz, W Auersch, S Marotzke, E Schulz, A Hampe, *Comp. Sci. Tech.*, **48**, 285 (1993).

[333] T Ramanathan, A Bismarck, E Schulz, K Subramanian, *Comp. Sci. Tech.*, **61**, 1703 (2001).

[334] J Houghton, *Global Warming*, Cambridge University Press, 1997.

[335] J C Farman, B G Gardiner, J D Shanklin, *Nature*, **315**, 207 (1985).

[336] The Montreal Protocol on Substances that Deplete the Ozone Layer, United Nations Environment Program, Sept 1987.

[337] Refrigeration and Air Conditioning CFC and HCFC Phase Out. In: Advice on Alternatives and Guidelines for Users, Department of Environment Trade Transport (DETR), Department of Trade and Industry (dti), Dec 2000.

[338] J M Hodgkinson, *Mechanical testing of advanced fibre composites*, CRC Press, 2000.

[339] J H G Ashbee, *Fundamental Principles of Fiber Reinforced Composites,* CRC Press, 1993.

[340] JIS K7086. *Testing Methods for Interlaminar Fracture Toughness of Carbon fiber Reinforced Plastics*, Japanese Industry Standards, 1993.

[341] ASTM D5528-94a, *Standard test method for mode I interlaminar fracture toughness of composites*, American Society of Testing and materials, 1997.

[342] T K O'Brien, *NASA Technical memorandum 110280*, NASA Langley Research Centre, Virginia, USA.

[343] E Greenhalgh, S Singh, in *12th International Conference on Composite Materials (ICCM)*, Paris, 1999.

[344] P Robinson, D Q Song, *Comp Sci Tech*, **32**, 217 (1994).

[345] E Greenhalgh, L Asp, S Singh, in *5th International Conference on Deformation and Fracture of Composites*, Manchester, 1997.

[346] E S Greenhalgh, C E Rogers, P Robinson, in *16th International Conference on Composite Materials (ICCM)*, Kyoto, 2007.

Glossary

Symbols

α	Alpha-phase of PVDF chain configuration
β	Beta-phase of PVDF chain configuration
β	Full width at half maximum (°)
γ	Surface tension or energy (mN/m)
γ_l	Surface tension of liquids (mN/m)
γ_l^{AB}	Acid/ base component of the surface tension of liquids (mN/m)
γ_l^{d}	Non-polar or dispersive parameters of a liquid (mN/m)
γ_l^{LW}	Liftshitz/ van der Waals component of the surface tension of liquids (mN/m)
γ_l^{p}	Polar or non-dispersive parameters of a liquid (mN/m)
γ_l^{+}	Acid or electron acceptor parameters of a liquid (mN/m)
γ_l^{-}	Base or electron donor parameters of a liquid (mN/m)
γ_s	Surface free energy of solids (mN/m)
γ_s (AB)	Surface energy of solids determined using the acid-base approach (mN/m)
γ_s^{AB}	Acid/ base component of the surface tension of solids (mN/m)
γ_s^{d}	Non-polar or dispersive parameters of a solid (mN/m)
γ_s (EoS)	Surface energy of solids determined using the Equation-of-State approach (mN/m)
γ_s^{LW}	Liftshitz/ van der Waals component of the surface tension of solids (mN/m)
γ_s^{p}	Polar or non-dispersive parameters of a solid (mN/m)
γ_s^{+}	Acid or electron acceptor parameters of a solid (mN/m)

γ_s^-	Base or electron donor parameters of a solid (mN/m)
γ_{sl}	Interfacial tension of the solid-liquid interface (mN/m)
$\Delta\theta_{1/2}$	Half width at half maximum (°)
ΔH_m	Heat of Melting (J/g)
ΔH_f^0	Heat of fusion of 100% crystalline PVDF (J/g)
ΔL	Change in length (mm)
ζ	Zeta-potential (mV)
θ	Contact angle (°)
θ_a	Advancing contact angle (°)
θ_a(DIM)	Advancing diiodomethane contact angle (°)
θ_a(FA)	Advancing formamide contact angle (°)
θ_a(W)	Advancing water contact angle (°)
θ_r	Receding contact angle (°)
θ_r(DIM)	Receding diiodomethane contact angle (°)
θ_r(FA)	Receding formamide contact angle (°)
θ_r(W)	Receding water contact angle (°)
κ	Specific conductivity (S/cm)
λ	Wavelength of X-ray (cm^{-1})
ρ	Electrical resistivity (mΩcm)
ρ_f	Density of fibre (g/mm^3)
ρ_m	Density of matrix (g/mm^3)
σ	Tensile strength of single carbon fibre (MPa)
σ_o	Weibull scale parameter or characteristic stress (MPa)
$\sigma_{o(l)}$	Tensile strength of a single fibre at a given length *l* (MPa)
σ_f	Flexural strength (MPa)
τ_{IFSS}	Apparent interfacial shear strength (MPa)
A_f	Cross sectional area of carbon fibres (mm^2)

A_s	BET fibre surface area (m^2/g)
b	Specimen width (mm)
D	Central deflection
d	Specimen thickness (mm)
d_f	Diameter of fibres (μm)
D/G ratio	Ratio of degenerate Raman deformation mode and Raman crystallite mode
e^-	Electrons
E_f	Flexual modulus (GPa)
F	Measured tensile force at break (N)
F_{max}	Maximum pull-out force (N)
F^{SBS}	Short beam shear strength (MPa)
g	Acceleration due to gravity: 9.81 (m/s^2)
G_{IC}	Interlaminar fracture toughness of laminated composites under mode I loading (J/m^2)
G_{IIC}	Interlaminar fracture toughness of laminated composites under mode II loading (J/m^2)
h	Planck's constant: $6.626*10^{-34}$ (m^2kg/s)
H_f^0	Heat of fusion (J/g)
I	Current (A)
K	Constant
l	Fibre length (cm)
L	Length of a specimen (mm)
L_c	Crystallite size
L_0	Original length (mm)
m	Mass (g)
m	Gradient of the initial part of the force displacement curve

n	An integer determined by the order given
n_a	Number of gas molecules absorbed
n_m	Specific monolayer absorption capacity of carbon fibres
P	Current vapour pressure (bar)
$P_{f(L)}$	Probability of failure of a fibre of length L
P_{MAX}	Failure load (kN)
P_0	Saturated vapour pressure (bar)
$\frac{P}{P_0}$	Relative pressure: pressure as compared to atmospheric pressure
R	Electrical resistance (Ω)
S/h	Span to thickness ratio
T_m	Melting temperature of a polymer (°C)
T_g	Glass transition temperature (°C)
U	Voltage (V)
w	Shape parameter of Weibull modulus
W_a	Work of adhesion (mN/m)
W_f	Weight of fibre (g)
W_m	Weight of matrix (g)
X_c	Crystallinity (%)

Subscripts

a = absorbed

a = adhesion

a = advancing

c = crystallite

f = failure

f = fibres

f = flexural

g = glass

I = mode I crack opening

II = mode II crack opening

ILSS = interfacial shear strength

l = liquids

l = length

m = matrix

m = melting

max = maximum

r = receding

s = solids

s = surface

sl = solid-liquid

0 = initial

½ = half

Superscripts

AB = acid/ base

d = non-polar or dispersive

LW = Liftshitz/ van der Waals

p = polar or non-dispersive

SBS = short beam shear strength

+ = acid or electron acceptor

- = base or electron donor

Abbreviations

AB	Acid/ base
AC	Alternating current
AP	Atmospheric plasma
APF	Atmospheric plasma fluorination
AS4	HexTow™ AS4 carbon fibres
ASTM	American Society for Testing and Materials
A320	Airbus 320 aircraft
BE	Binding energy
BET	Brunauer-Emmett-Teller
BSI	British Standards Institution
B777	Boeing 777 aircraft
CF	Correction factor
CFCs	Chlorofluorocarbons
CPL	Composite production line
CPS	Counts per second
CRAG	Composites Research Advisory Group
CRT	Cathode-ray tube
DC	Direct current
DCB	Double cantilever beam
DIM	Diiodomethane
DSC	Differential scanning calorimetry
ECT	Edge Crack Torsion
EDL	Electrical double layer
ELS	Equal Load Sharing
ENF	End-Notched Flexure

EOR	Enhanced oil recovery
EoS	Equation-of-State
ETFE	Ethylene tetrafluoroethylene
FA	Formamide
FBE	Fusion bonded epoxy
FEP	Fluorinated ethylene propylene copolymer
FVC	Fibre volume content
GCSG	Gouy-Chapman-Stern-Graham
HCFCs	Hydrochlorofluorocarbons
HFCs	Hydrofluorocarbons
iep	Isoelectric point
IEMP	Inelastic mean free path
IGC	Inverse Gas Chromatography
ILSS	Interlaminar shear strength
ISO	International Organization for Standardization
JIS	Japanese Industry Standards
KE	Kinetic energy
LLS	Local Load Sharing
NEC	National Electrical Code
PAN	Polyacrylonitrile
PCTFE	Polychlorotrifluoroethylene
PE	Polyethylene
PES	Polyethersulfone
PFA	tetrafluoroethylene-perfluoroalkoxy vinyl ether copolymer
PMMA	Polymethyl methacrylate
PTFE	Polytetrafluoroethylene
PVDF	Polyvinylidene fluoride

PVF	Polyvinyl fluoride
RAE	Royal Aircraft Establishment
SEM	Scanning electron microscopy
SBS	Shortbeam shear test
TFE	Tetrafluoroethylene
T0	Original but desized T700 carbon fibres
T1	Atmospheric plasma fluorinated T700 carbon fibres for 1 minute
T2	Atmospheric plasma fluorinated T700 carbon fibres for 2 minute
T4	Atmospheric plasma fluorinated T700 carbon fibres for 4 minute
T8	Atmospheric plasma fluorinated T700 carbon fibres for 8 minute
T700	Torayca T700SC® carbon fibres
UD	Unidirectional
USDA	United States Department of Agriculture
VDF	Vinylidene fluoride
W	Water
XRD	X-ray Diffraction
XPS	X-ray photoelectron spectroscopy

Appendix A

Calculations on determining the fibre diameter using the modified Wilhelmey-method

$$\cos\theta = \frac{mg}{nd\pi\gamma_l} \qquad (A.1)$$

Where the components in Eq A.1 are known:

$g = 9.81\ ms^{-2}$

$\pi = 3.14$

$\gamma_l = 25.53$ mN/m

n (number of fibres) = 5

$\theta = 0$ (i.e. full wetting and therefore when $\theta = 0$, $\cos\theta = 1$)

Rearranging Eq A.1 making *d* the subject:

$$d = \frac{mg}{n\cos\theta\pi\gamma} \qquad (A.2)$$

The only unknown in Eq A.2 are *d* and *m*. *m* can be determined from Fig.3.3.

$m = 0.15 - -0.14 = 0.29$

Therefore by entering all the parameters into Eq A.2:

$$d = \frac{0.29 \times 9.81}{5 \times 1 \times 3.14 \times 25.53 \times 10^{-3}}$$

$$d = \frac{2.84}{0.40}$$

$$d = 7.10\mu m$$

Appendix B

Step by step procedure in how a mixed Gaussian-Lorentzian (G/L ratio of 30:70) is fitted to a typical Raman spectrum:

1) Open the software GRAMS/AI
2) Open file with extension *.spc that was recorded from the LabRam Infinity Analytical Raman Spectrometer
3) Edit current trace limits (Last icon on right in toolbar)
4) Setup limits 800 to 2000
5) Run peak fitting application
6) Press Yes when asked for converting the XY trace

In Peaks Tab

- Set Baseline Function sets to Linear

In Find Tab

- Set Peaks Function sets to Mixed G+L (30:70)
- Peaks Sensitivity sets to Low
- Maximum sets to 3

Approximate the position of the peaks using the right click

Do not forget the small peak adjacent to the large second one for better fitting

Click Estimate within the Find Tab, Press Accept

In the Iterate Tab

Select Estimate Parameters, Press Accept

Iteration Control Maximum # sets to 50

Press Run

Select Peak Parameters to find the values of the peaks.

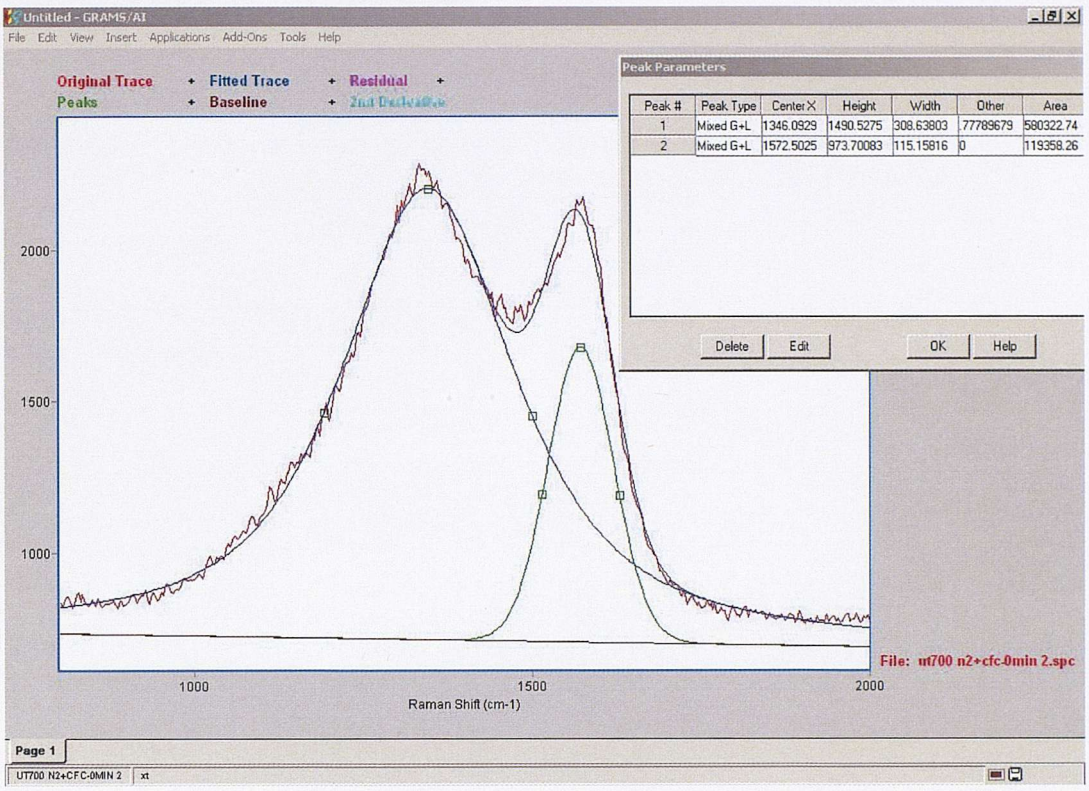


Fig. A.B1: A representative Raman spectrum fitted using a mixed Gaussian-Lorentzian of 30:70

Appendix C

Table A.C1: Dynamic contact angles and contact angle hysteresis of 4 min APF desized T700 carbon fibres against diiodomethane (DIM) and formamide (FA)

Sample	θ_a(DIM) / °	θ_r(DIM) / °	Δθ (DIM)	θ_a(FA) / °	θ_r(FA) / °	Δθ (FA)
original	60.1 ± 3.2	56.7 ± 2.9	3.4	38.0 ± 2.4	28.0 ± 1.6	10.0
N_2	46.4 ± 3.6	33.4 ± 2.6	13.0	33.4 ± 3.5	32.8 ± 3.2	0.6
N_2+SF_6	40.3 ± 5.5	23.8 ± 3.5	16.5	21.8 ± 3.6	20.2 ± 1.2	1.6
N_2 + $CHClF_2$	55.8 ± 3.3	23.8 ± 3.5	32.0	57.2 ± 2.5	32.7 ± 2.3	24.5
N_2 + $CHClF_2$ (After 1 month)	41.0 ± 6.0	29.9 ± 8.1	11.1	28.9 ± 4.9	20.0 ± 1.1	8.9

Table A.C2: Dynamic contact angles and contact angle hysteresis of APF AS4 carbon fibres against diiodomethane (DIM) and formamide (FA)

Fibres treatment	Speed/ m min^{-1}	Retention time/ min	θ_a(DIM) /°	θ_r(DIM) /°	Δθ (DIM)	θ_a(FA) / °	θ_r(FA) / °	Δθ (FA)
Original	0	0	59.7 ± 2.9	58.8 ± 0.7	0.9	46.3 ± 2.6	35.9 ± 0.5	10.4
Batch	0	4	47.6 ± 2.0	47.3 ± 2.7	0.3	45.6 ± 1.4	38.5 ± 2.7	7.11
Continuous single sided	0.15	1.3	46.2 ± 1.8	45.6 ± 1.2	0.6	53.5 ± 5.3	34.8 ± 1.8	18.7
Continuous double sided	0.75	0.8	47.2 ± 1.6	47.0 ± 0.1	0.2	67.7 ± 4.4	48.2 ± 2.2	19.5
	0.33	1.8	50.3 ± 4.0	48.1 ± 1.0	2.2	55.3 ± 3.1	40.7 ± 3.0	14.6
	0.15	4	47.8 ± 1.1	45.6 ± 0.9	2.2	50.3 ± 3.1	34.9 ± 3.1	15.4

Appendix D

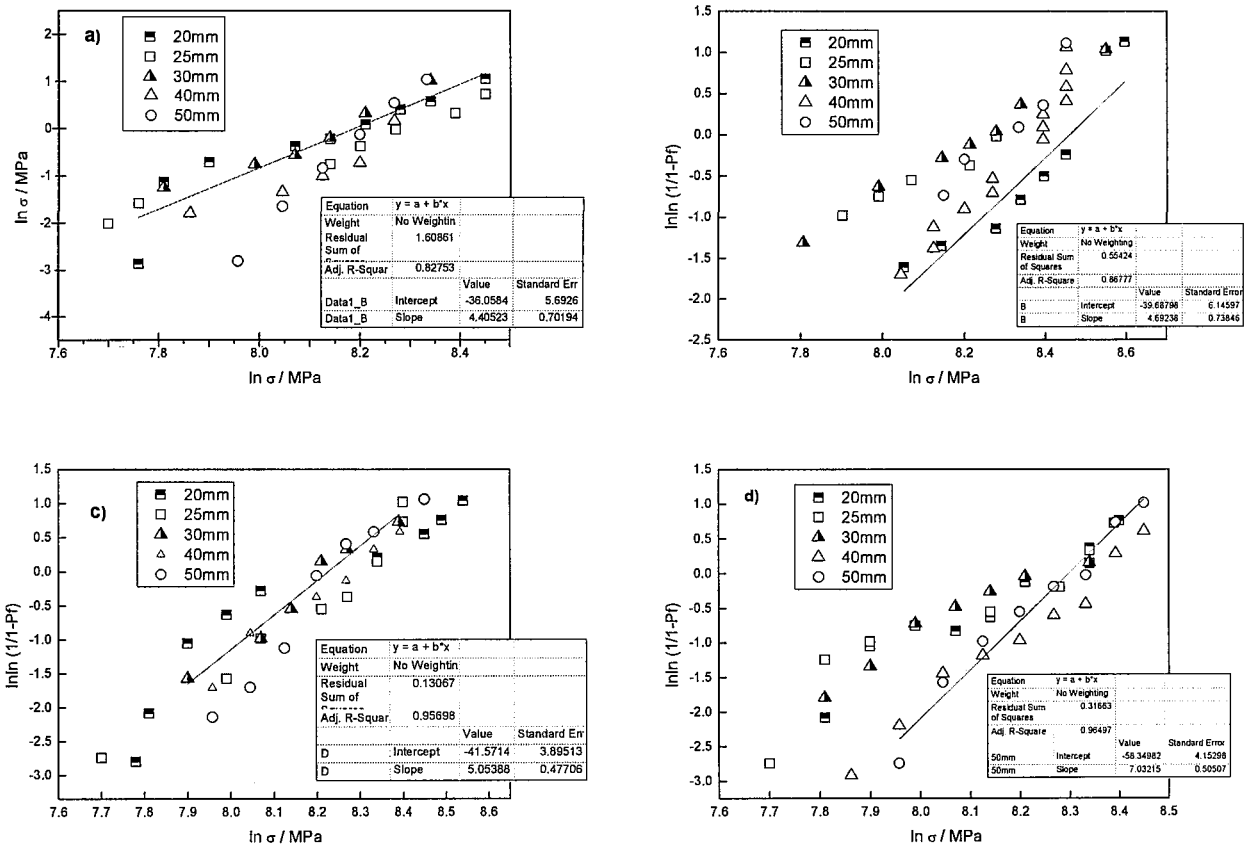


Fig. A.D1: Examples of linear regression analysis of Weibull plots of continuous double sided APF treated AS4 carbon fibres at a) original, b) 0.15 m/min, c) 0.33 m/min and d) 0.75 m/min.

Appendix E

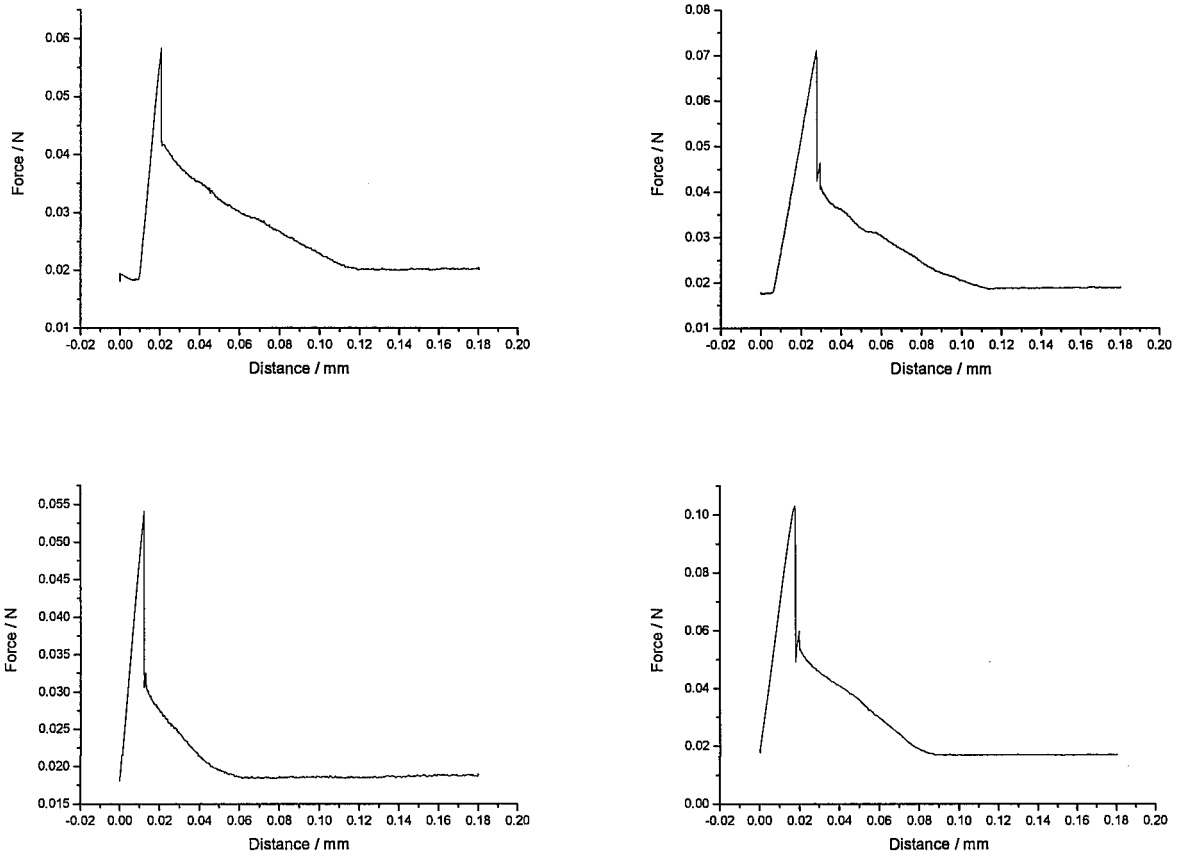


Fig. A.E1: Graphs of pull-out force as a function of displacement obtained from single fibre pull-out tests of desized T700 carbon fibres.